**ESECMaSE**

Enhanced Safety and Efficient Construction of Masonry Structures in Europe

**Project No. Coll – Ct - 2003 - 500291**

**ESECMaSE**

**Enhanced Safety and Efficient Construction of Masonry Structures in Europe**

Horizontal Research Activities Involving SMEs

Collective Research

Work Package N°: 7

# D 7.1c Test results on the behaviour of masonry under static cyclic in plane lateral loads

Guido Magenes, Paolo Morandi, Andrea Penna

Due date of deliverable: 10/03/2007
Actual submission date: 29/02/2008

Start date of project: 10 June 2004 Duration: 36 month

Draft N°: 1

University of Pavia
Department of Structural Mechanics
Via Ferrata, 1
27100 Pavia, Italy

| Project co-funded by the European Commission within the Sixth Framework Programme (2002-2006) | | |
|---|---|---|
| Dissemination level | | |
| PU | Public | X |
| PP | Restricted to other programme participants (including the Commission Services) | |
| RE | Restricted to a group specified by the consortium (including the Commission Services) | |
| CO | Confidential, only for members of the consortium (including the Commission Services) | |

# Contents

# 1.Introduction

The ESECMaSE Project is a research project funded by the European Commission within the Sixth Framework Programme, aiming at improving the knowledge on the lateral in-plane response of masonry walls and the global seismic behaviour of entire buildings. The project is mainly focused on three typologies of blocks produced in Europe for new constructions: hollow clay, calcium silicate and lightweight aggregate concrete blocks.

Within the ESECMaSE framework both numerical simulations and experimental tests are carried out by the project partners.

The activity of the University of Pavia is mainly devoted to the in-plane cyclic testing of masonry piers. A total of 28 large scale walls have been tested.

In order to be able to control the walls boundary conditions (cantilever or double-fixed) and also to speed up the tests, a completely new test setup has been designed; a clear and repeatable procedure has been used for the whole testing campaign.

In this deliverable the results obtained from the tests of the 28 walls are presented. Different failure modes have been observed and the associated force-displacement capacity and energy dissipation properties are reported.

Results of several tests carried out on masonry specimens and hardened mortar, in order to determine the mechanical properties of some of the masonry typologies used in the cyclic shear tests, are also presented.

## 2.Test set-up and instrumentation

The in-plane cyclic tests were carried out in the EUCENTRE Laboratory for Seismic Testing of Large Structures. The installation of the new test setup took advantage of the three-dimensional configuration of the strong floor and the L-shaped strong walls.

The adopted test setup is shown in Figure 1. The walls are built on a 400 mm thick reinforced concrete footing which could be clamped to the strong floor by means of post-tensioned steel bars. A horizontally mounted servohydraulic actuator applies a horizontal shear force to the top of the wall through a composite steel spreader beam. The steel beam is stiffened with steel plates positioned orthogonally to the axis of the beam. The wall is restrained from out-of-plane deflections by a low-friction sliding restrainer system. Two vertical servohydraulic actuators apply the vertical load on the wall, reacting on a steel frame fixed on one of the strong walls of the laboratory.

Figure 2 schematically shows the typical wall instrumentation. The horizontal load was measured by a load cell positioned in the horizontal actuator. Twenty five displacement transducers (linear potentiometers) were installed on each wall. The horizontal displacement at the top of the wall was measured by instruments 15, 16 and 24 (in the case of r.c. beam is placed at the top of tested walls, the potentiometer n. 16 measured the relative sliding displacements between the r.c. beam and the steel beam on which the horizontal actuator is fixed). Wall flexural deformations were monitored by instruments 2-11, whereas shear deformations were monitored by instruments 0 and 1. Relative sliding displacements between the wall and the footing, between the top beam and the wall and between the strong floor and the footing were monitored by instruments 13, 14 and 17 respectively. Control of out-of-plane displacements was monitored by instruments 18 and 19. The flexural deformations of the steel frame placed at the top of the vertical actuators was measured by instruments 20-21 and, finally, the sliding between the steel plates welded at the steel frame at the top of the vertical actuators and the reaction wall was measured by instruments 22-23.

The force of the horizontal actuator and the displacements of the 25 transducers applied to the specimens as a function of the time of the test for all the walls testd are reported in annex B.

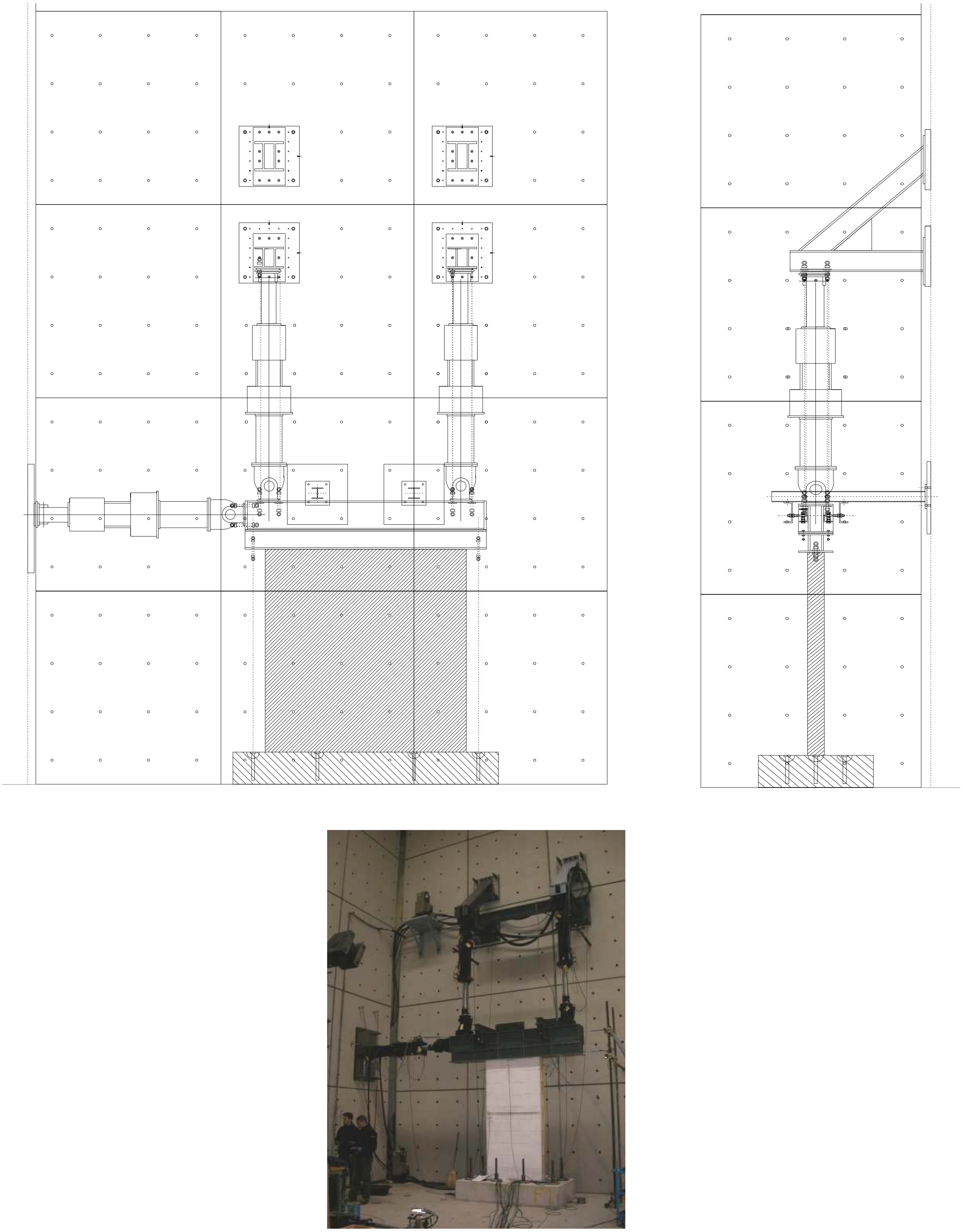

Figure 1. Test set-up

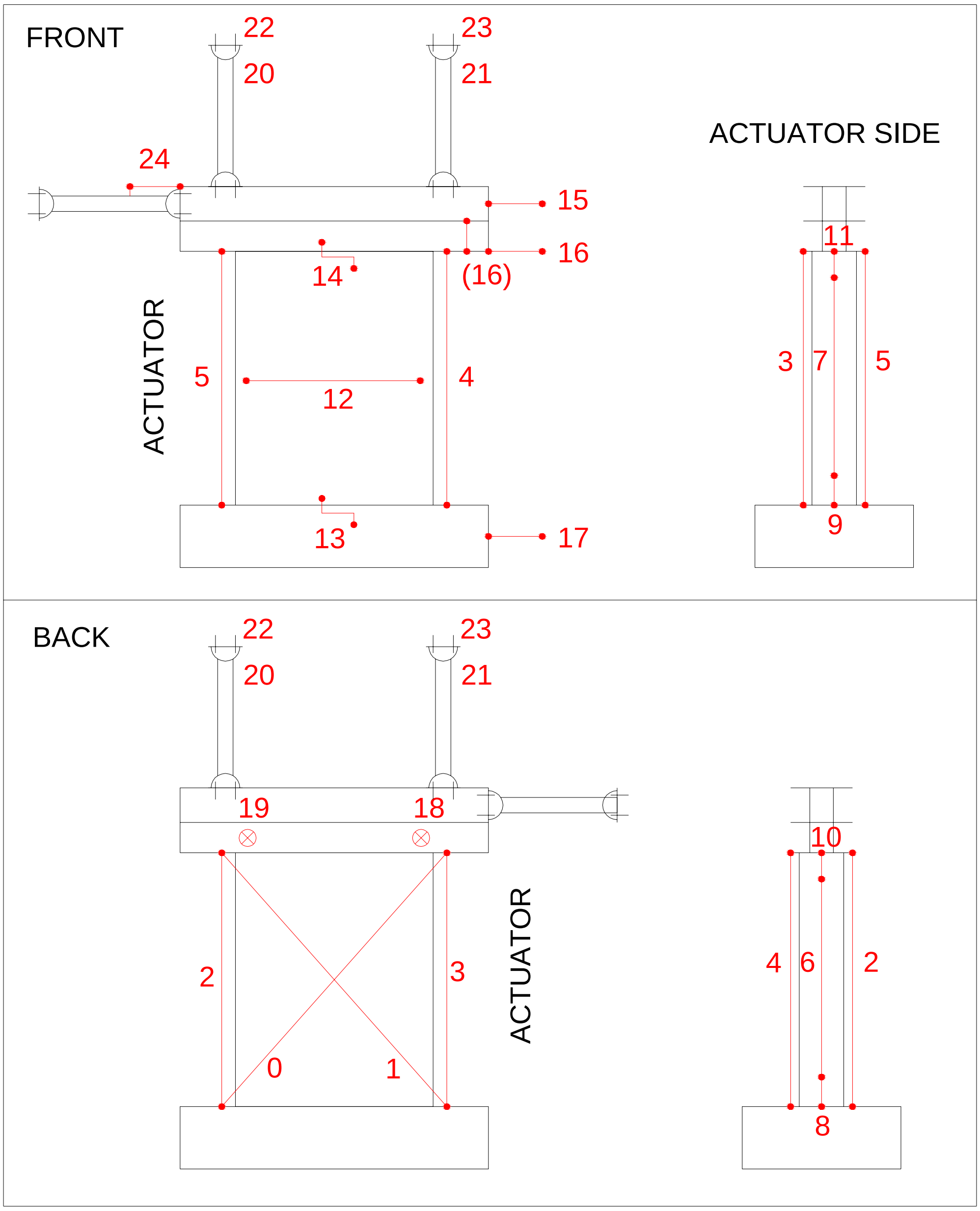


Figure 2. Instrumentation

# 3.Testing procedure

The testing procedure envisaged two different boundary conditions: a "double fixed" system (rotation restrained at the top beam) and a "cantilever" system (free rotation at the top) with a constant vertical load applied at the top with servohydraulic actuators. The horizontal load was applied using a servohydraulic actuator, with an initial force-controlled phase followed by a displacement-controlled loading history, performing three cycles for each target displacement level.

The top steel beam was connected to the wall by a layer of high strength gypsum mortar.

The vertical force imposed by the vertical actuators was initially gradually applied in order to estimate the compressive Young's modulus of masonry.

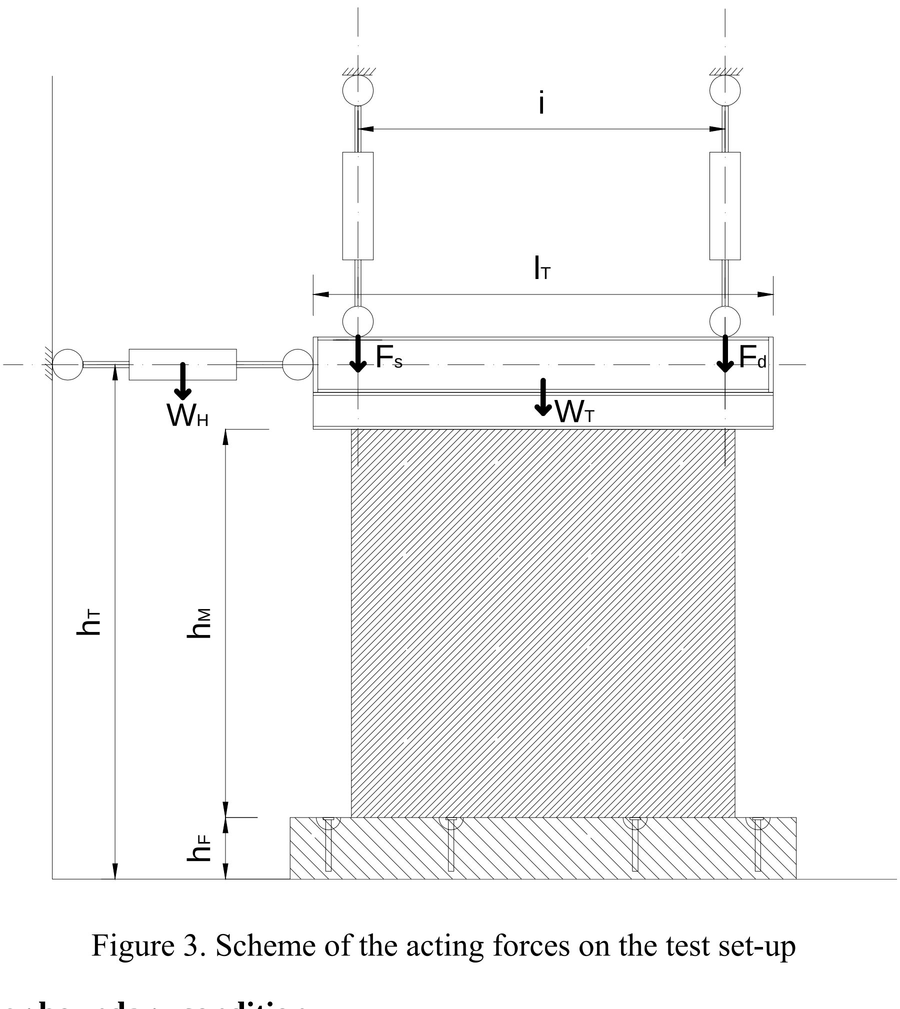


Figure 3. Scheme of the acting forces on the test set-up

## 3.1 Cantilever boundary condition

In case of a cantilever system both the forces of the right and left actuators are kept constant during the test and hence they are not dependent on the horizontal actuator force and displacement. Therefore, the following expressions should be implemented in test procedure (see Figure 3):

$$\begin{cases} F_D + F_S + \dfrac{W_H}{2} + W_T = P \\ F_D \dfrac{i}{2} = F_S \dfrac{i}{2} + \dfrac{W_H l_T}{4} \end{cases}$$

where $F_D$ and $F_S$ are the applied forces of the right and on the left actuator respectively.

$W_H$ is the weight of the horizontal actuator,

$W_T$ is the weight of top beam,

$i$ is the horizontal distance between the 2 vertical actuators,

$l_T$ is the length of the top beam

Therefore, independently from the imposed value of the horizontal displacement $u_H$, the transmitted forces of the vertical actuators are computed with the following expressions:

$$\begin{cases} F_S = \dfrac{P}{2} - \dfrac{W_T}{2} - \dfrac{W_H}{4}\left(1 + \dfrac{l_T}{i}\right) \\ F_D = \dfrac{P}{2} - \dfrac{W_T}{2} - \dfrac{W_H}{4}\left(1 - \dfrac{l_T}{i}\right) \end{cases}.$$

### 3.2 Double fixed boundary condition

The double fixed system can be instead obtained by two alternative settings of the actuator control. The first one is based on a "static" criterion (force control), the second one, adopted for all the tests carried out in the University of Pavia (except for wall CS01), consists of a "kinematic" criterion (mixed control).

#### 3.2.1 "Static criterion" (force control)

The "static criterion" is obtained imposing the condition of zero bending moment at midheight of the wall. Therefore, the following expressions are implemented in the test procedure (see Figure 3):

$$\begin{cases} F_D + F_S + \dfrac{W_H}{2} + W_T = P \\ (F_S - F_D)\dfrac{i}{2} + \dfrac{l_H W_H}{4} = F_H\left(h_H - \dfrac{h_M}{2} - h_F\right) \end{cases},$$

$$\begin{cases} F_D + F_S = P - \dfrac{W_H}{2} - W_T \\ F_S - F_D = F_H \dfrac{2}{i}\left(h_H - \dfrac{h_M}{2} - h_F\right) - \dfrac{l_H W_H}{2i} \end{cases}$$

Finally, the correction should be based on the following expressions:

$$\begin{cases} \Delta F_S = \dfrac{F_H}{i}\left(h_H - \dfrac{h_M}{2} - h_F\right) \\ \Delta F_D = -\Delta F_S \end{cases}$$

where $F_D$ and $F_S$ are the applied vertical forces of the right and on the left actuator respectively.

$F_H$ is the applied horizontal force of the horizontal actuator,

$W_H$ is the weight of the horizontal actuator,

$W_T$ is the weight of top beam,

$i$ is the horizontal distance between the 2 vertical actuators,

$l_T$ is the length of the top beam

$h_H$ is the height of the axis of the horizontal actuator,

$h_M$ is the clear height of the wall,

$h_F$ is the height of the foundation.

### 3.2.2 Double fixed boundary condition (mixed control)

The “kinematic” criterion involves a mixed force-displacement control, imposing both a constant vertical load and a condition of free translation with no rotation of the top beam. Therefore, the following expressions are implemented in the test procedure (see Figure 3):

$$\begin{cases} F_D + F_S + \dfrac{W_H}{2} + W_T = P \\ u_D = u_S \end{cases},$$

where $u_D$ and $u_S$ are the vertical displacements of the right and on the left actuator respectively,

$F_D$ and $F_S$ are the applied forces of the right and on the left actuator respectively.

$W_H$ is the weight of the horizontal actuator,

$W_T$ is the weight of top beam,

$i$ is the horizontal distance between the 2 vertical actuators,

$l_T$ is the length of the top beam

## 3.3 Execution of the test and horizontal loading history

The execution of the test is performed in the following way.

First of all, the horizontal actuator is kept without pressure and vertical load is applied in the vertical actuators with constant velocity (in our case 2 kN/s).

It is necessary to reach the value of the vertical load *P*, acting on the vertical actuators, imposing the forces with the following expressions according to Figure 3:

$$\begin{cases} F_S = \dfrac{P}{2} - \dfrac{W_T}{2} - \dfrac{W_H}{4}\left(1 + \dfrac{l_T}{i}\right) \\ F_D = \dfrac{P}{2} - \dfrac{W_T}{2} - \dfrac{W_H}{4}\left(1 - \dfrac{l_T}{i}\right) \end{cases};$$

The following step is to control the horizontal actuator, zeroing the residual horizontal force which may have been generated while applying the vertical forces.

The horizontal loading history is then applied to the test as follows.

A first repetition of three fully reversed cycles is performed by imposing, in a force-controlled way, a horizontal force equal to one fourth of the maximum estimated strength $F_{max}$ (cycle 1F, see Table 1). Horizontal displacements are recorded.

The procedure is then switched to a displacement-controlled one, in which the target displacements are multiple of the displacement measured in the first force-controlled phase, repeating three cycles for each target displacement (cycles 2F, 3F and 4F). This method aims at obtaining sufficient points describing the ascending branch of the force-displacement envelope curve. Once the specimen approaches its maximum shear strength the further target displacements are then chosen from a predefined sequence of drift-based displacement levels as reported in Table 1 (“S” cycles).

The duration of each cycle is kept constant incrementing the actuator displacement rate proportionally to the cycle target displacement as also done in past experimental campaigns (Tomazevic *et al.*, 1993). The tests are stopped in case of critical damage conditions or at a horizontal top displacement larger than 3.0% drift.

Table 1. Cycles of horizontal displacement imposed to the horizontal actuator ($h_M$ is the clear height of the wall in mm).

| **Cycles** | **Drift ($\delta/h_M$)** | **Target displacement $\delta$ [mm]** | **Velocity v [mm/s]** | **Duration of each single cycle [s]** |
|---|---|---|---|---|
| Cycle 1 F | - | 0.25 $F_{max}$ | 2 kN/s | = 4*0.25 $F_{max}$/2 |
| Cycle 2 F | 2 * cycle 1 | 2 * $\delta_{cycle\ 1}$ | 0.0250 | =4*2*$\delta_{cycle\ 1}$/0.025 |
| Cycle 3 F | 3 * cycle 1 | 3 * $\delta_{cycle\ 1}$ | 0.0250 | =4*3*$\delta_{cycle\ 1}$/0.025 |
| Cycle 4 F | 4 * cycle 1 | 4 * $\delta_{cycle\ 1}$ | 0.0250 | =4*4 *$\delta_{cycle\ 1}$/0.025 |
| Cycle 1 S | 0.050% | =0.050%* $h_M$ | 0.0250 | = 4*(0.050%*$h_M$)/0.025 |
| Cycle 2 S | 0.075% | =0.075%* $h_M$ | 0.0375 | =4*(0.075%* $h_M$)/0.0375 |
| Cycle 3 S | 0.100% | =0.100%* $h_M$ | 0.0500 | =4*(0.100%* $h_M$)/0.0500 |
| Cycle 4 S | 0.150% | =0.150%* $h_M$ | 0.0625 | =4*(0.150%* $h_M$)/0.0625 |
| Cycle 5 S | 0.200% | =0.200%* $h_M$ | 0.0800 | =4*(0.200%* $h_M$)/0.080 |
| Cycle 6 S | 0.250% | =0.250%* $h_M$ | 0.1000 | =4*(0.250%* $h_M$)/0.100 |
| Cycle 7 S | 0.300% | =0.300%* $h_M$ | 0.1200 | =4*(0.300%* $h_M$)/0.120 |
| Cycle 8 S | 0.400% | =0.400%* $h_M$ | 0.1600 | =4*(0.400%* $h_M$)/0.160 |
| Cycle 9 S | 0.500% | =0.500%* $h_M$ | 0.2000 | =4*(0.500%* $h_M$)/0.200 |
| Cycle 10 S | 0.600% | =0.600%* $h_M$ | 0.2400 | =4*(0.600%* $h_M$)/0.240 |
| Cycle 11 S | 0.700% | =0.700%* $h_M$ | 0.2800 | =4*(0.700%* $h_M$)/0.280 |
| Cycle 12 S | 0.800% | =0.800%* $h_M$ | 0.3200 | =4*(0.800%* $h_M$)/0.320 |
| Cycle 13 S | 1.000% | =1.000%* $h_M$ | 0.4000 | =4*(1.000%* $h_M$)/0.400 |
| Cycle 14 S | 1.250% | =1.250%* $h_M$ | 0.5000 | =4*(1.250%* $h_M$)/0.500 |
| Cycle 15 S | 1.500% | =1.500%* $h_M$ | 0.6000 | =4*(1.500%* $h_M$)/0.600 |
| Cycle 16 S | 1.750% | =1.750%* $h_M$ | 0.7000 | =4*(1.750%* $h_M$)/0.700 |
| Cycle 17 S | 2.000% | =2.000%* $h_M$ | 0.8000 | =4*(2.000%* $h_M$)/0.800 |
| Cycle 18 S | 2.500% | =2.500%* $h_M$ | 1.0000 | =4*(2.500%* $h_M$)/1.000 |
| Cycle 19 S | 3.000% | =3.000%* $h_M$ | 1.0000 | =4*(3.000%* $h_M$)/1.000 |

The first cycles in "displacement control" (2F, 3F, 4F) are omitted in the case the corresponding level of displacement in the cycles 2F, 3F, 4F exceeds the target of the first "S" cycles.

# 4.Test specimens and material properties

The in-plane cyclic testing of masonry piers on a total of 28 large scale walls has been carried out. Three typologies of masonry have been considered in the experimental campaign: calcium silicate, hollow clay and lightweight aggregate concrete masonry.

## 4.1 Calcium silicate masonry

A total of fourteen calcium-silicate masonry walls were tested.
The walls have been constructed with two different kind of units:
1) The "optimised" unit;
2) The "Quadro E" unit.

### 4.1.1 Walls made of "optimised" units

Eight walls made up by the calcium-silicate "optimised" units have been tested and the dimensions and the details of these walls are summarized in Table 2.
The units were square 248x248 mm with a thickness of 175 mm (see Figure 4).
The testing campaign included six walls (CS01-C606) with a length of 1.25 m and two walls (CS07 and CS08) with a length of 2.5m. All walls were 2.5 m high and were made with thin layer mortar bedjoints (about 2 mm thick) with unfilled head joints. Only for wall CS05 head joints had been filled by thin layer mortar. The mortar used was thin layer mortar class M10 according to EN 998-2.
Three levels of vertical mean compression stress $\sigma_v$ were applied: 0.5, 1.0 and 2.0 MPa.
All walls were tested with double fixed boundary conditions except walls CS06 and CS08 which were tested as cantilever systems.
The considered experimental configurations are reported in the matrix in Figure 5.
According to the compressive tests carried out at the University of Munich (Grabowski, 2005), the mean compression strength of the units was 26.5 MPa. Three diagonal compression tests on masonry square specimens (1.0 x 1.0 m) with unfilled head joints were carried out in Pavia. The conventional diagonal tensile strength of masonry was computed as $f_t=P/(2{\cdot}t{\cdot}l)$ where P is the maximum diagonal compression load, t and l are the thickness and the length of the specimens respectively. The mean value of the diagonal tensile strength was 0.27 MPa.
All the details of the tests of characterization of the material properties are reported in the annex A.

Figure 4. Type of calcium-silicate "optimised" unit masonry walls
($l$ x $t$ x $h$ =248x175x248 mm)

Table 2. Calcium-silicate masonry piers with "optimised units".

| Wall | l [m] | t [m] | h [m] | $\sigma_v$ [MPa] | Unit size [mm] | Bed joints | Head joints | Bound. Conditions |
|---|---|---|---|---|---|---|---|---|
| CS 01 | 1.25 | 0.175 | 2.5 | 1.0 | 248x175x248 | Thin layer | Unfilled | Double fixed |
| CS 02 | 1.25 | 0.175 | 2.5 | 1.0 | 248x175x248 | Thin layer | Unfilled | Double fixed |
| CS 03 | 1.25 | 0.175 | 2.5 | 0.5 | 248x175x248 | Thin layer | Unfilled | Double fixed |
| CS 04 | 1.25 | 0.175 | 2.5 | 2.0 | 248x175x248 | Thin layer | Unfilled | Double fixed |
| CS 05 | 1.25 | 0.175 | 2.5 | 1.0 | 248x175x248 | Thin layer | Filled (Thin) | Double fixed |
| CS 06 | 1.25 | 0.175 | 2.5 | 1.0 | 248x175x248 | Thin layer | Unfilled | Cantilever |
| CS 07 | 2.50 | 0.175 | 2.5 | 1.0 | 248x175x248 | Thin layer | Unfilled | Double fixed |
| CS 08 | 2.50 | 0.175 | 2.5 | 1.0 | 248x175x248 | Thin layer | Unfilled | Cantilever |

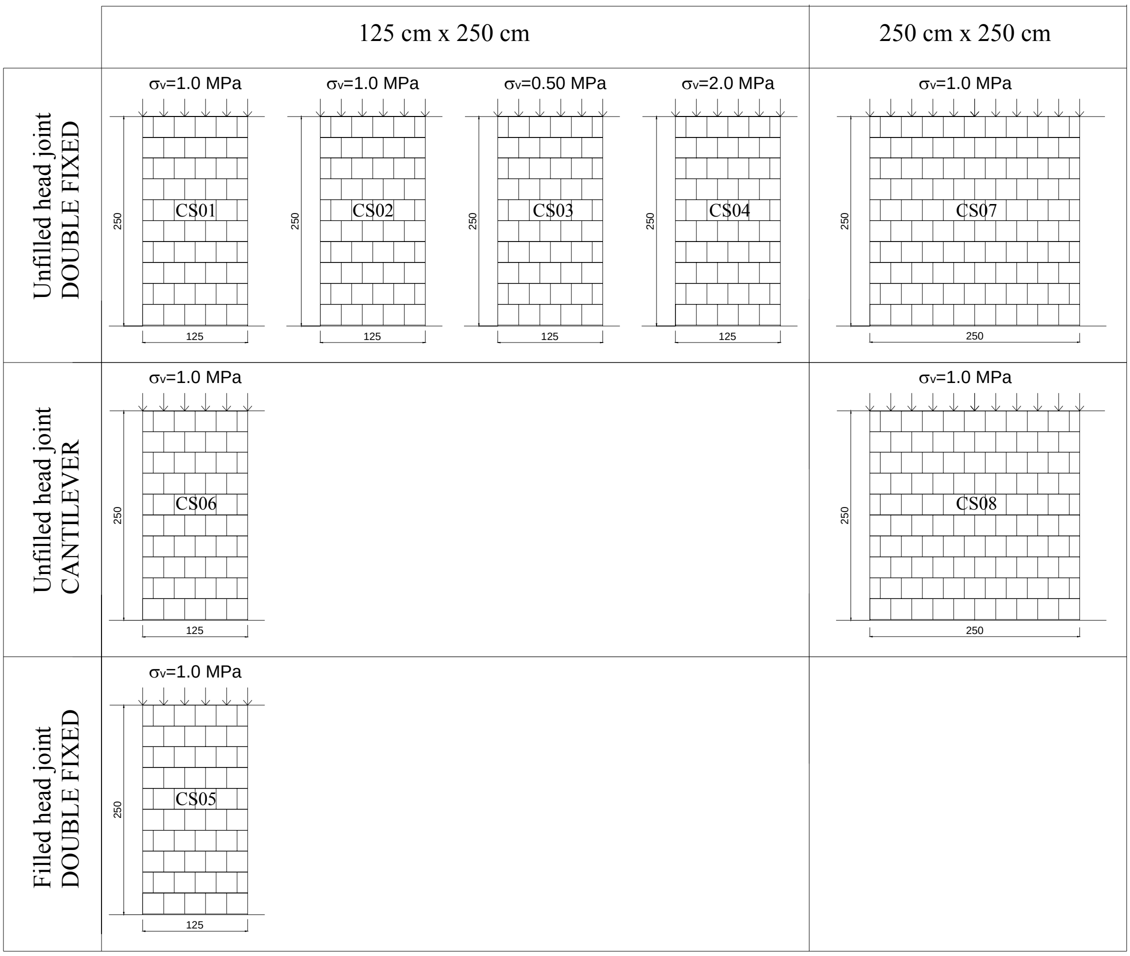


Figure 5. Matrix of the considered experimental scheme. Walls CS01-CS08

### 4.1.2 Walls made of “Quadro E” units

Six walls made up by the calcium-silicate “Quadro E” units have been tested and the dimensions and the details of these walls are summarized in Table 3.

The units were square 498x498 mm with a thickness of 175 mm (see Figure 6).

Four walls were confined with one $\phi$ 16 mm diameter bar at each end of the wall. The holes in the calcium-silicate units having the steel bars inside were grouted with concrete.

The nominal yield strength of the steel of the reinforcement was 500 MPa.

In wall CS14 one 5/8’’ unbonded tendon at each end of the wall was placed and it was post-tensioned with a force of 110 KN in each tendon in order to reach a total vertical stress $\sigma_v$ on the wall of 2 MPa (1 MPa applied through the vertical actuators and 1 MPa through the application of the force in the tendons). The nominal tensile strength of the steel tendons was 1860 MPa.

Finally, wall CS09 was unreinforced.

Except for wall CS13 with a length of 2.5 m, all the other walls had a length of 1.25 m. All walls were 2.5 m high and were made with thin layer mortar bedjoints (about 2 mm thick) with unfilled head joints.

The mortar used was thin layer mortar class M10 according to UNI-EN 998-2.

Three levels of vertical mean compression stress $\sigma_v$ were applied: 0.5, 1.0 and 2.0 MPa.

All walls were tested with double fixed boundary conditions except wall CS14 which was tested as cantilever system.

The considered experimental configurations are reported in the matrix in Figure 7.

Figure 6. Type of calcium-silicate “Quadro E” unit masonry walls
($l$ x $t$ x $h$ =498x175x498 mm)

Table 3. Calcium-silicate masonry piers with “Quadro E” units.

| Wall | l [m] | t [m] | h [m] | $\sigma_v$ [MPa] | Unit size [mm] | Bed joints | Head joints | Bound. Conditions | Reinforcement |
|---|---|---|---|---|---|---|---|---|---|
| CS 09 | 1.25 | 0.175 | 2.5 | 1.0 | 498x175x498 | Thin layer | Unfilled | Double fixed | NO |
| CS 10 | 1.25 | 0.175 | 2.5 | 1.0 | 498x175x498 | Thin layer | Unfilled | Double fixed | Confined (1+1 $\phi$ 16) |
| CS 11 | 1.25 | 0.175 | 2.5 | 0.5 | 498x175x498 | Thin layer | Unfilled | Double fixed | Confined (1+1 $\phi$ 16) |
| CS 12 | 1.25 | 0.175 | 2.5 | 2.0 | 498x175x498 | Thin layer | Unfilled | Double fixed | Confined (1+1 $\phi$ 16) |
| CS 13 | 2.50 | 0.175 | 2.5 | 1.0 | 498x175x498 | Thin layer | Unfilled | Double fixed | Confined (1+1 $\phi$ 16) |
| CS 14 | 1.25 | 0.175 | 2.5 | 1.0+1.0 | 498x175x498 | Thin layer | Unfilled | Cantilever | Post-tensioned (1+1 $\phi$ 5/8’’) |

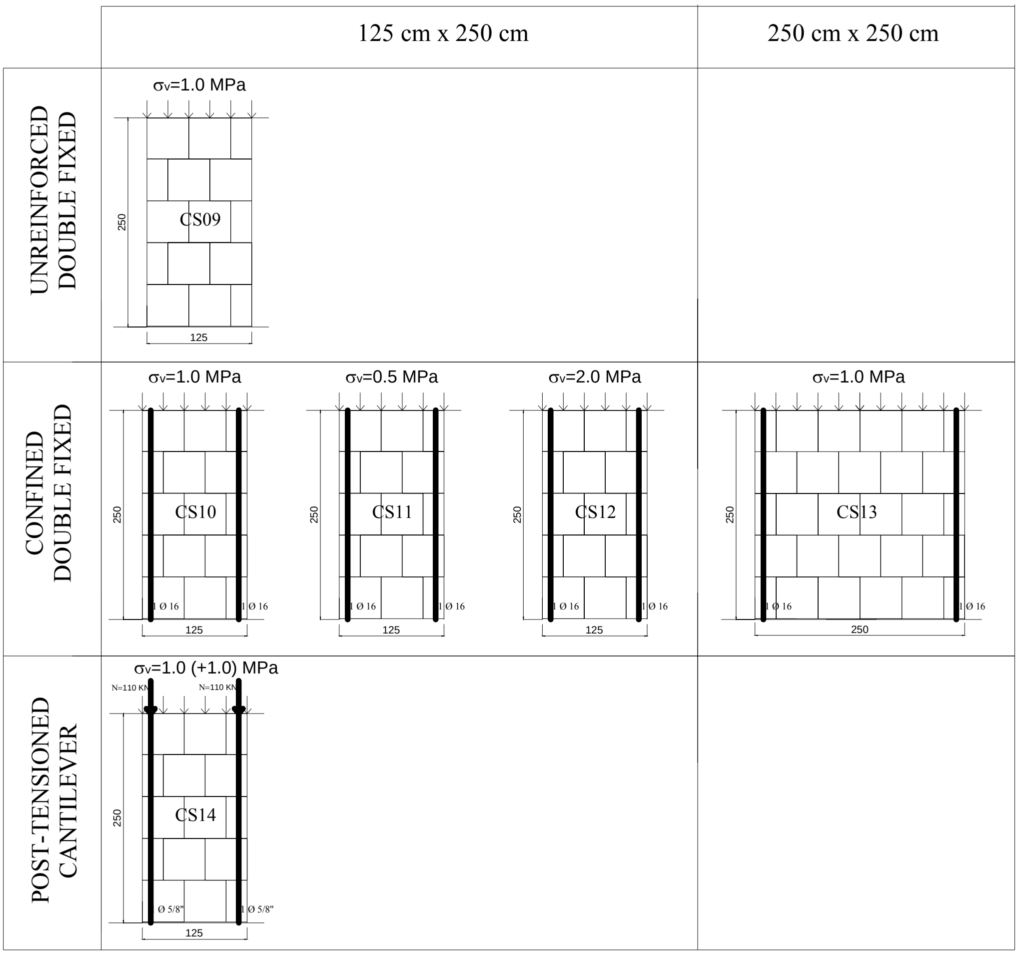


Figure 7. Matrix of the considered experimental scheme. Walls CS09-CS14

## 4.2 Clay masonry

Ten clay masonry walls were tested with different kinds of units and mortar.

The masonry typologies have been divided into two groups:

1) The German clay masonry based on the assemblage of hollow clay units and mortar typical of the German way of construction;

2) The Italian clay masonry based on the Italian types of units and mortar.

### 4.2.1 German clay masonry

Three walls with three different German clay masonry typologies have been subjected to experimental tests.

Wall CL01 was of ureinforced masonry with 175 mm thick hollow Tongue and Groove (T+G) lightweight clay units with thin layer mortar bedjoints and unfilled headjoints. The holes of the units have been completely filled with concrete.

Wall CL02 was a confined wall constituted by a 175 mm thick hollow Tongue and Groove (T+G) lightweight clay units with thin layer mortar bedjoints and unfilled headjoints. The holes of the units have been completely filled with concrete and one $\phi$ 16 mm diameter bar has been placed at each end of the wall.

The length of wall CL01 and CL02 was equal to 1.50 m and the height equal to 2.5 m. The dimensions of the 175 mm thick hollow Tongue and Groove clay unit used for these two walls were 373x175x249 mm ($l$ x $t$ x $h$) with two large holes in the unit (see Figure 8).

Finally, the unreinforced masonry wall CL03 was constructed with 365 mm thick Tongue and Groove (T+G) lightweight clay units with a percentage of holes of 45% with thin layer mortar bedjoints and unfilled headjoints. The length of wall CL03 was equal to 1.00 m and the height equal to 2.5 m. The dimensions of the clay unit used were 247x365x249 mm ($l$ x $t$ x $h$) (see Figure 9).

The mortar used was thin layer mortar class M10 according to UNI-EN 998-2.

Low levels of vertical mean compression stress $\sigma_v$ were applied: 0.31, 0.33 and 0.14 MPa for the walls CL01, CL02 and CL03 respectively, according to the calculated vertical stress in similar walls included in the large scale building subjected to a pseudo-dynamic test carried out at JRC in ISPRA within the ESECMaSE project.

Wall CL01 and CL03 were tested with double fixed boundary conditions, whereas the confined wall CL02 was tested as cantilever system.

Figure 8. 175 mm thick hollow clay unit T+G used in the walls CL01 and CL02
($l$ x $t$ x $h$ =373x175x249 mm)

Figure 9. 365 mm thick hollow clay T+G unit used in the walls CL03
(*l* x *t* x *h* =247x365x249 mm)

Table 4. "German clay" masonry piers

| Wall | l [m] | t [m] | h [m] | $\sigma_v$ [MPa] | Unit size [mm] | Bed joints | Head joints | Bound. Conditions | Reinforcement |
|---|---|---|---|---|---|---|---|---|---|
| CL 01 | 1.50 | 0.175 | 2.5 | 0.31 | 373x175x249 | Thin layer | Unfilled | Double fixed | NO (holes filled by concrete |
| CL 02 | 1.50 | 0.175 | 2.5 | 0.33 | 373x175x249 | Thin layer | Unfilled | Cantilever | Confined (1+1 $\phi$ 16) (holes filled by concrete |
| CL 03 | 1.00 | 0.365 | 2.5 | 0.14 | 247x365x249 | Thin layer | Unfilled | Double fixed | NO |

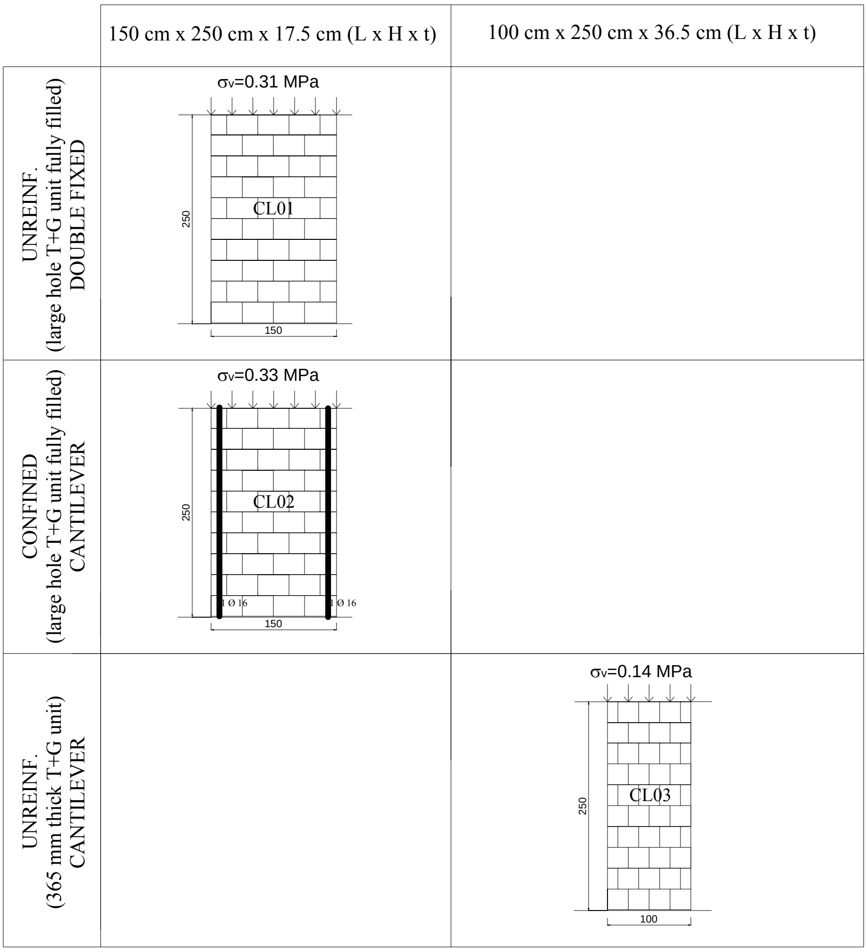


Figure 10. Matrix of the considered experimental scheme. Walls CL01-CL03

### 4.2.2 Italian clay masonry

Seven walls with three different Italian clay masonry typologies have been tested. The properties of such walls are defined in the present paragraph and reported in Table 5.

Three walls (CL04, CL05 and CL06) were built with lightweight hollow clay units with a percentage of holes of 45% with general purpose mortar bedjoints and headjoints (thickness of the mortar joints in the range between 5 and 15 mm). The units are called "ALVEOLATER 45" with dimensions of 250x300x190 mm (*l* x *t* x *h*) as shown in Figure 11.

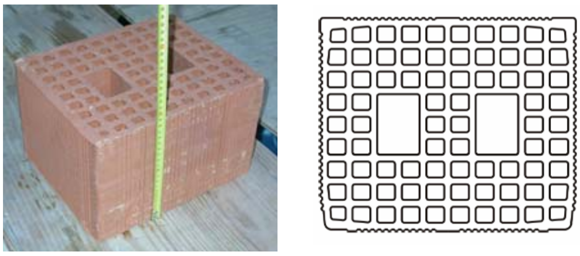

Figure 11. Lightweight hollow clay units used in walls CL04, CL05 and CL06
(*l* x *t* x *h* =250x300x190 mm)

Two walls (CL07 and CL08) were made of masonry with Tongue and Groove (T+G) lightweight clay units with a percentage of holes of 45% with general purpose mortar bedjoints and unfilled headjoints.

Finally, walls CL09 and CL10 were built with Tongue and Groove (T+G) lightweight clay units with a percentage of holes of 45% with thin layer mortar bedjoints and unfilled headjoints. Such clay units were rectified on their surfaces.

The shape of the T+G clay units (perpend joints with mechanical interlocking) is reported in Figure 12. The pockets of the units were ungrouted. The dimensions of the units were 250x300x190 mm (*l* x *t* x *h*) for the walls CL07 and CL08, whereas were 250x300x230 mm (*l* x *t* x *h* ) for walls CL09 and CL10.

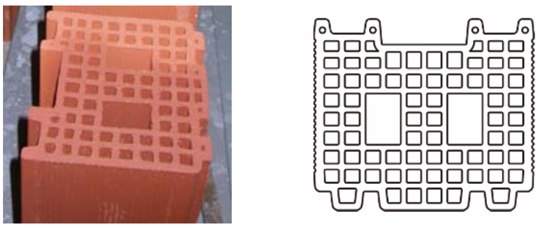

Figure 12. Lightweight hollow clay T+G units used in walls CL07, CL08 (*l* x *t* x *h* =250x300x190 mm) and CL09, CL10 (*l* x *t* x *h* =250x300x230 mm)

The length of walls CL04, CL05, CL08 and CL10 was equal to 2.50 m whereas the length of the walls CL06, CL07 and CL09 was 1.25 m. The height of all Italian clay walls was equal to

2.6 m. Levels of vertical mean compression stress $\sigma_v$ of the most compressed walls in a typical Italian masonry construction were estimated as 0.50 and 0.68 MPa and were applied to the specimens. All walls were tested with double fixed boundary conditions.
The considered experimental configurations are reported in the matrix in Figure 13.

Table 5. "Italian clay" masonry piers

| Wall | l [m] | t [m] | h [m] | $\sigma_v$ [MPa] | Unit size [mm] | Bed joints | Head joints | Bound. Conditions |
|---|---|---|---|---|---|---|---|---|
| CL 04 | 2.50 | 0.300 | 2.6 | 0.50-0.68 | 250x300x190 | General purpose | Filled (G.P.) | Double fixed |
| CL 05 | 2.50 | 0.300 | 2.6 | 0.68 | 250x300x190 | General purpose | Filled (G.P.) | Double fixed |
| CL 06 | 1.25 | 0.300 | 2.6 | 0.50 | 250x300x190 | General purpose | Filled (G.P.) | Double fixed |
| CL 07 | 1.25 | 0.300 | 2.6 | 0.50 | 250x300x190 | General purpose | Unfilled (T+G) | Double fixed |
| CL 08 | 2.50 | 0.300 | 2.6 | 0.68 | 250x300x190 | General purpose | Unfilled (T+G) | Double fixed |
| CL 09 | 1.25 | 0.300 | 2.6 | 0.50 | 250x300x230 | Thin layer | Unfilled (T+G) | Double fixed |
| CL 10 | 2.50 | 0.300 | 2.6 | 0.68 | 250x300x230 | Thin layer | Unfilled (T+G) | Double fixed |

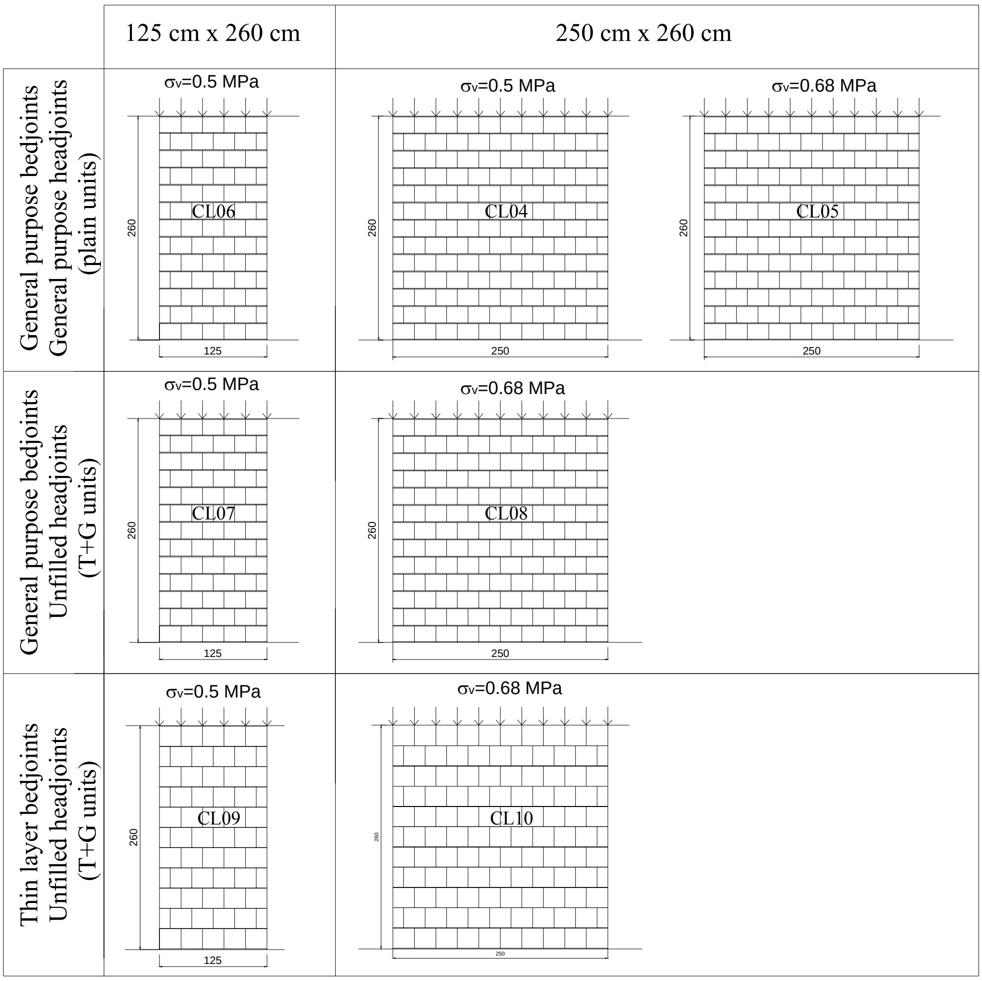


Figure 13. Matrix of the considered experimental scheme. Walls CL04-CL10

Several tests of the characterization of the material properties of the "Italian clay" masonry have been carried out. In particular tests on the mortar and on masonry specimens have been performed.

The general purpose mortar used for the walls CL04, CL05 and CL06 was the M5 pre-mixed mortar according to EN 998-2. The flexural and compressive strength of the hardened mortar has been evaluated carrying out tests according to EN 1015-11. Fifteen specimens of mortar 40x40x160 mm were sampled to evaluate the compression and the flexural strength of the mortar. They were cured in water for 7 days and then cured in air for 21 days before testing. They first were tested in flexure and then the two parts obtained from the bending test were submitted to a compression test. The mean flexural strength was 2.45 MPa, whereas the mean compressive strength was 7.38 MPa.

Another batch of M5 pre-mixed general purpose mortar has been used for the construction of walls CL07 and CL08. Also this mortar has been tested according to EN 1015-11 on 15 specimens. In this case, the mean flexural strength (modulus of rupture) was found equal to 2.53 MPa, whereas the mean compressive strength was 10.64 MPa.

Finally, six specimens of M10 (EN 998-2) thin layer pre-mixed mortar has been tested. The mean flexural strength was 1.49 MPa, whereas the mean compressive strength was 10.23 MPa.

Moreover, several masonry specimens were subjected to simple compression tests and to diagonal compression tests.

In particular, 6 masonry specimens built with lightweight hollow clay units with general purpose mortar bedjoints and headjoints, 6 masonry specimens built with lightweight hollow clay units with general purpose mortar bedjoints with unfilled headjoints (T+G units) and 6 masonry specimens built with lightweight hollow clay units with thin layer mortar bedjoints with unfilled headjoints (T+G units) were subjected to compression tests. The compression strength and the elastic modulus were computed according to EN 1052-1.

The mean compressive strength $f_m$ of the first batch of the specimens was 9.50 MPa and the mean measured elastic modulus (secant at $0.33 \cdot f_m$) was E=5905 MPa, the mean compressive strength $f_m$ of the specimens with T+G units and general purpose mortar was 6.60 MPa and the mean measured elastic modulus was E=3213 MPa and the mean compressive strength $f_m$ of the specimens with T+G units and thin layer mortar was 5.30 MPa and the mean measured elastic modulus was E=3879 MPa.

Finally, three diagonal compression tests were carried out on approximately square panels ($t$ x $l_1$ x $l_2$=300 x 1000 x 980 mm) made up by clay units with general purpose mortar bedjoints and headjoints and "traditional" plain clay units (without tongue and groove). The specimens were placed into a compression testing machine and the loads were applied by means of steel angles. A 5 mm plywood board was placed between the steel angles and the corners of the masonry panels to avoid stress concentrations. Displacement transducers were applied on both sides to measure the deformations along the diagonals. The parameter which is derived by the test is the tensile strength for diagonal cracking which can be used for shear strength calculation in the case the failure mode occurs for diagonal cracking. The mean value of the tensile stress computed as $f_t$=P/[$t$*($l_1$+$l_2$)] was 0.278 MPa where P was the maximum compression force applied to the panel corresponding to the failure for diagonal cracking.
All the details of the tests of characterization of the material properties are reported in the annex A.

### 4.3 Lightweight Aerated Concrete masonry (LAC)

As reported in Table 6, four unreinforced walls constructed with two typologies of Lightweight Aerated Concrete (LAC) unit masonry have been tested. The walls LAC01 and LAC03 were built with Tongue and Groove Lightweight Aerated Concrete units with general purpose mortar bedjoints and unfilled headjoints, whereas the walls LAC02 and LAC04 were constructed with Tongue and Groove Lightweight Aerated Concrete units with thin layer mortar bedjoints and unfilled headjoints.
The units were 175 mm thick and were 247x238 mm ($l$ x $h$) in the case of general purpose mortar and 247x248 mm ($l$ x $h$) in the case of thin layer mortar.
In Figure 14 a LAC unit is shown.
The length and the height of all the LAC walls was equal to 2.5 m and the thickness was equal to 175 mm. The thickness of the general purpose mortar bedjoint was equal to about 10 mm, whereas the thickness of the thin layer bedjoints was about 2 mm. The different height of the units used in the two typologies of masonry produced in the end the same total height for the walls.
The mortar used was general purpose ready mixed mortar class M5 and thin layer mortar class M10 according to UNI-EN 998-2.
Two levels of vertical mean compression stress $\sigma_v$ were applied: 0.5 and 1.0 MPa.
All walls were tested with double fixed boundary conditions.
The considered experimental configurations are reported in the matrix in Figure 15.

Figure 14. Lightweight aerated concrete T+G units used in walls LAC01, LAC03 (*l* x *t* x *h* =247x175x238 mm) and LAC02, LAC04 (*l* x *t* x *h* =247x175x248 mm)

Table 6. Lightweight aerated concrete (LAC) masonry piers

| Wall | l [m] | t [m] | h [m] | $\sigma_v$ [MPa] | Unit size [mm] | Bed joints | Head joints | Bound. Conditions |
|---|---|---|---|---|---|---|---|---|
| LAC01 | 2.50 | 0.175 | 2.5 | 0.50 | 247x175x238 | General purpose | Unfilled (T+G) | Double fixed |
| LAC02 | 2.50 | 0.175 | 2.5 | 0.50 | 247x175x248 | Thin layer | Unfilled (T+G) | Double fixed |
| LAC03 | 2.50 | 0.175 | 2.5 | 1.00 | 247x175x238 | General purpose | Unfilled (T+G) | Double fixed |
| LAC04 | 2.50 | 0.175 | 2.5 | 1.00 | 247x175x248 | Thin layer | Unfilled (T+G) | Double fixed |

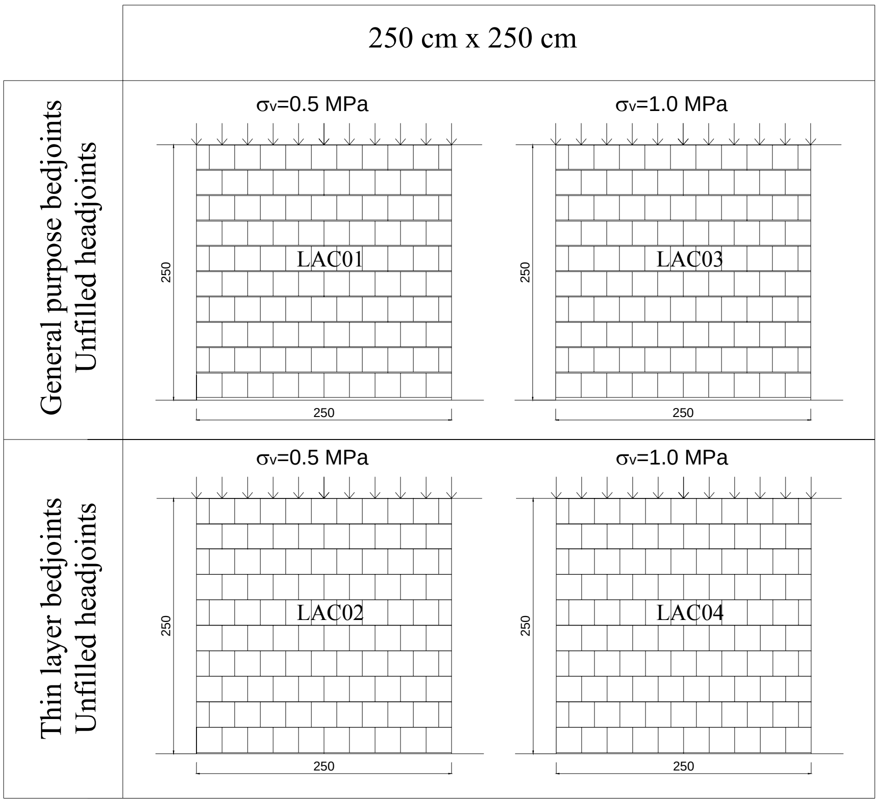


Figure 15. Matrix of the considered experimental scheme. Walls LAC01-LAC04

# 5. Experimental results of the cyclic in-plane shear tests

Ductility, displacement capacity and energy dissipation issues are here discussed with reference to the specific experimental failure mechanisms. The results of the cyclic tests on the twenty eight masonry piers in terms of hysteretic force-displacement curves are presented in Figure 16 to Figure 43.

All the results are shown separately for each different masonry typology:

1) calcium silicate masonry with two different kinds of units: the “optimised” unit and the “Quadro E” unit.
2) hollow clay masonry divided into two groups: the German clay masonry and the Italian clay masonry.
3) lightweight aggregate concrete masonry.

The top displacement δ is measured at the lowest edge of the steel beam. When r.c. beams at the top of the walls are placed, the top displacement δ is measured at the centreline of the steel beam that corresponds to the centre-line of the horizontal actuator.

Pictures of the piers at the end of the tests are also reported.

In annex B the

## 5.1 Force-displacement curves and failure modes of the piers

### 5.1.1 Calcium-silicate masonry with “optimised” units (CS01-CS08)

The double fixed condition on wall CS01 was applied using the “static” criterion described above, i.e. keeping the point of zero moment at mid-height of the pier. The wall failed with a sudden diagonal crack interesting both the joints and the units. Evaluating the data after the test, it appeared clear that keeping constant the point of contra-flexure at mid-height, a very large rotation of the top beam occurred due to inherent unavoidable non-symmetry of the wall, thus resulting in unrealistic kinematic boundary conditions at the top. In addition to that, with such system it was impossible to follow the post-peak branch of the curve, due to loss of control after the formation of the diagonal crack. As a consequence, starting from wall CS02, the tests were carried out with the “kinematic” criterion, i.e. keeping the top beam horizontal.

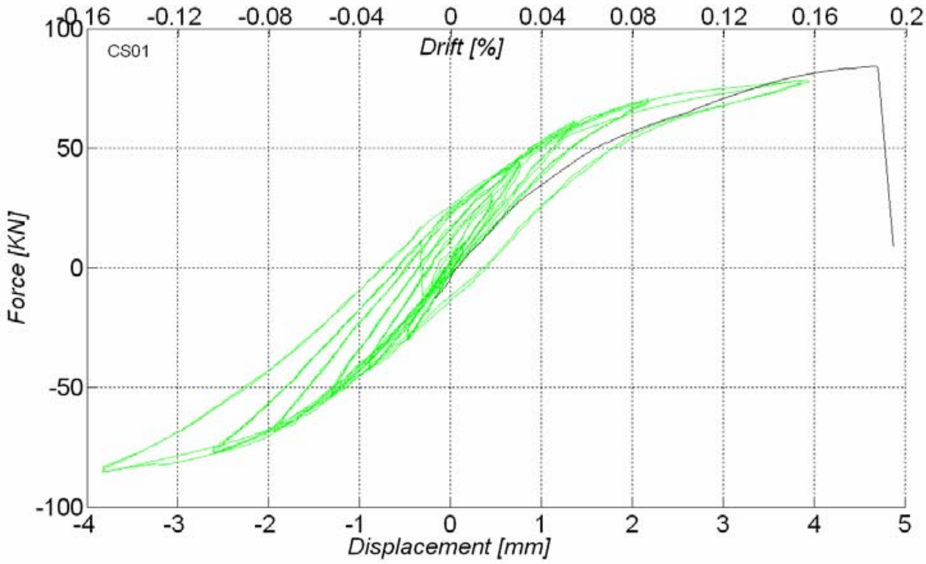


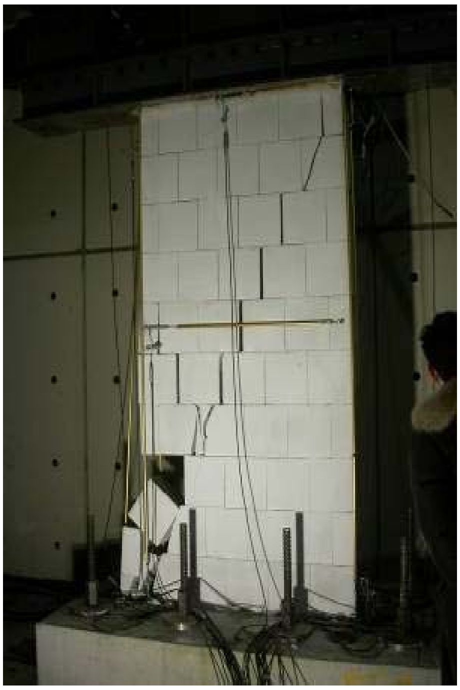

Figure 16 Wall CS01. Double fixed, l=1.25 m, $\sigma_v$=1.0 MPa

The failure of wall CS02 was characterized by corner-to-corner diagonal shear cracks. The cracks developed in the units and in the mortar bedjoints. The units at the top right and top left corner of the wall rotated producing a concentrated compression load that caused diagonal cracks at the units below. Spalling of the units at the centre of the pier occurred and the development of many wide diagonal cracks in the units at the centre of the panel caused the brittle collapse of the wall, with a sudden drop of the shear force.

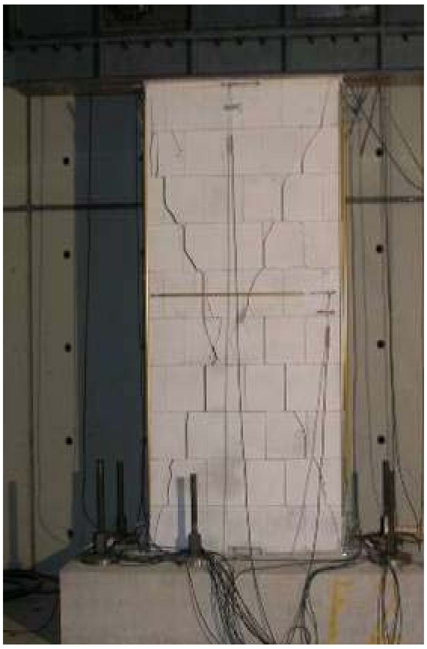

Figure 17 Wall CS02. Double fixed, l=1.25 m, $\sigma_v$=1.0 MPa

Wall CS03 was characterized by the opening of the unfilled head joints which became evident at the top displacement $\delta = \pm$ 10mm. The head- and bed-joint cracks formed a pattern of stepped diagonal cracks along the height of the wall. These cracks closed during unloading. Increasing the top displacement the cracks became rather wide and no further increase of shear was possible. When the top displacement exceeded 15 mm, cracks developed in the units at the centre of the panel, producing large strength degradation and collapse of the wall.

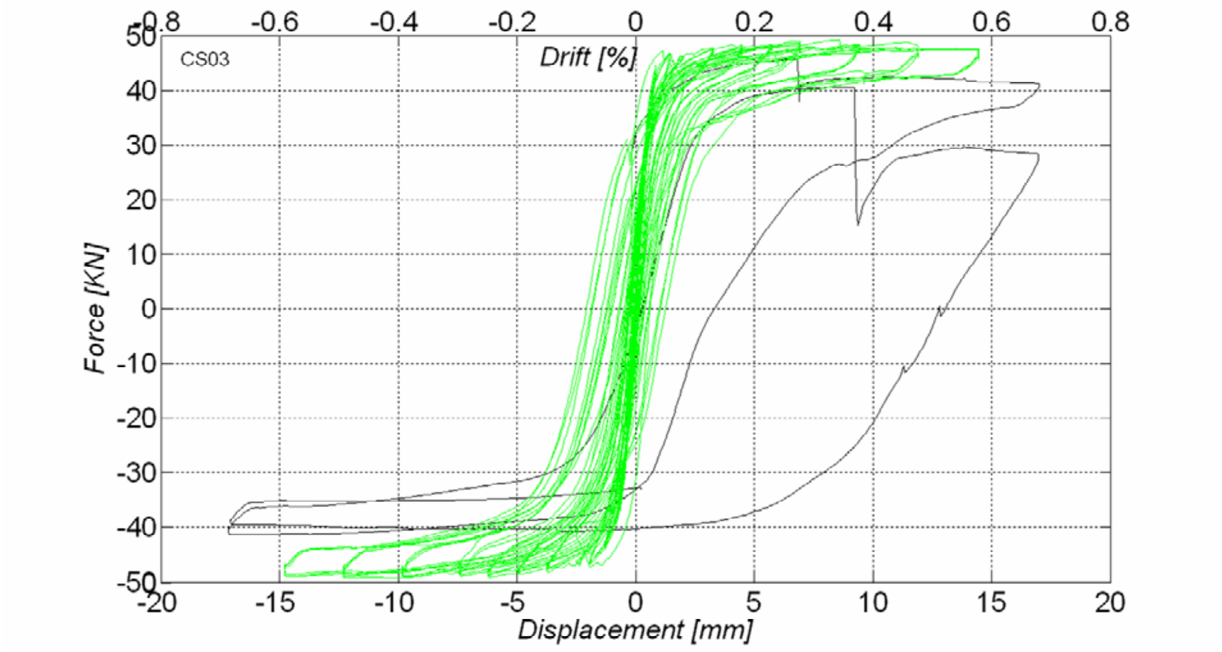


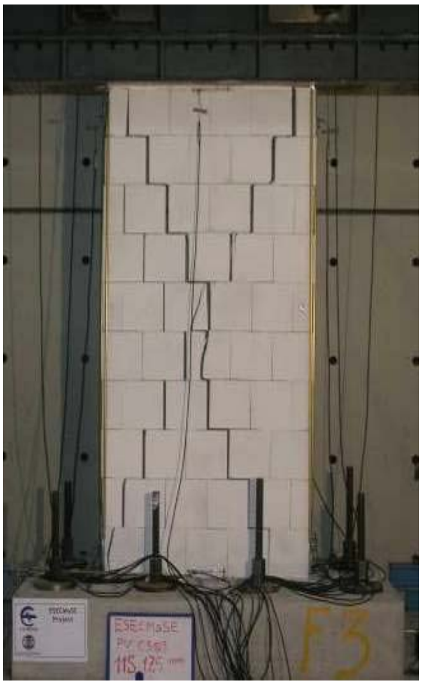

Figure 18 Wall CS03. Double fixed, l=1.25 m, $\sigma_v$=0.5 MPa

In wall CS04, a higher vertical load ($\sigma_v$=2 MPa) was applied, and the wall failed with diagonal shear cracks in the masonry units from corner to corner of the wall, at very small top displacement (just beyond 4.0 mm). Spalling of some units at the centre of the wall also occurred. Large strength and stiffness degradation occurred after diagonal cracking. Before attaining this displacement level no evident damage was present, therefore it is possible to state that this wall behaved almost similar to an elastic-brittle system.

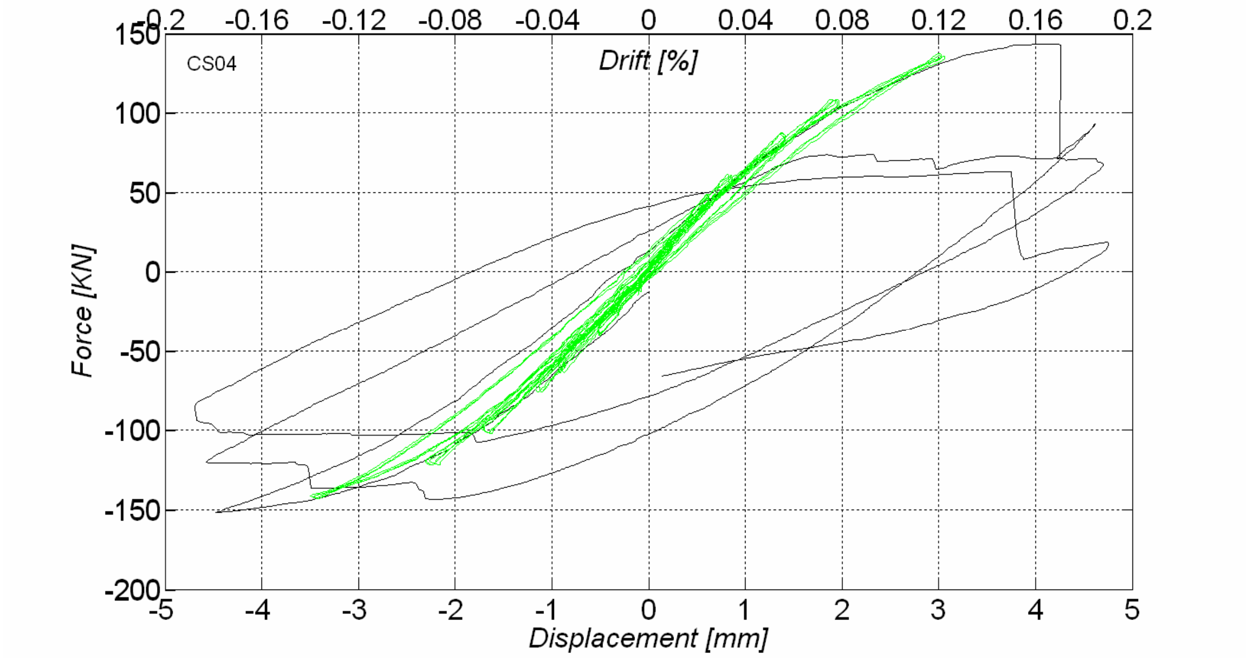


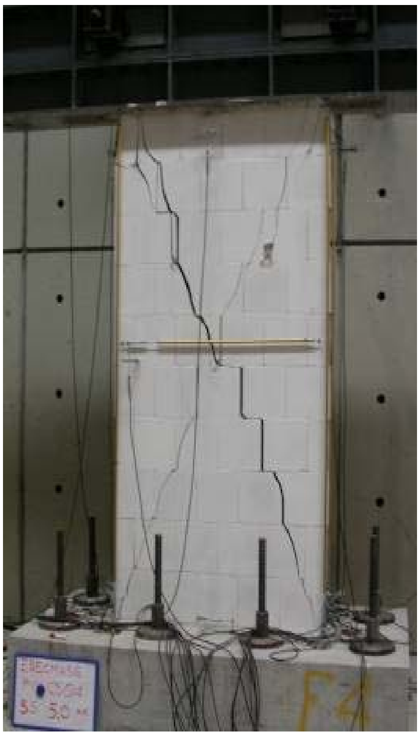

Figure 19 Wall CS04. Double fixed, l=1.25 m, $\sigma_v$=2.0 MPa

Wall CS05 remained undamaged, with the exception of some tension cracks in bedjoints, up to a horizontal top displacement of 35 mm. When this displacement level was exceeded, the wall failed suddenly in shear with the development of a diagonal crack formed in the mortar bedjoints and in the units. Before this damage, the force-displacement curve presented "S-shaped" cycles with low energy dissipation, similar to a typical rocking behaviour.

Although wall CS05 was constructed and tested with the same characteristics of wall CS01 and wall CS02, head joints filled by mortar allowed to attain a larger displacement capacity in comparison with the displacements found in the tests on wall CS01 and wall CS02.

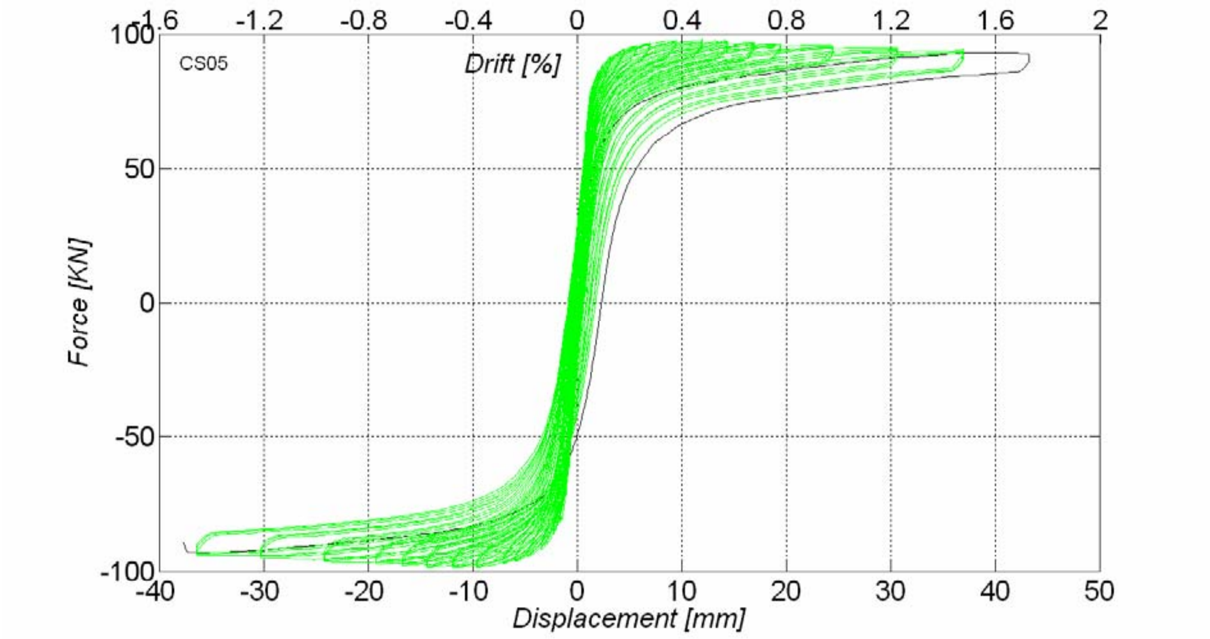


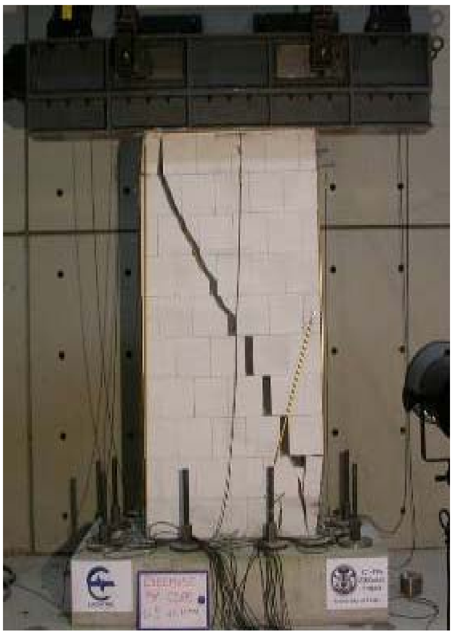

Figure 20 Wall CS05. Double fixed, l=1.25 m, $\sigma_V$=1.0 MPa, filled head joints

Wall CS06 was tested as a cantilever system. No diagonal cracks occurred during the test and the wall displayed a typical rocking behaviour without any significant strength degradation or relevant energy dissipation. With a top displacement larger than 40 mm (corresponding to a drift of 1.6 %) a wide horizontal crack was clearly visible in the bottom right corner of the panel due to tension stresses. The test was interrupted when the top displacement attained about 50 mm (2% drift) for reasons due to the stroke limits of the transducers; at that stage the wall was substantially undamaged (except for the horizontal crack) and probably it would have been still possible to further increase the displacement demand.

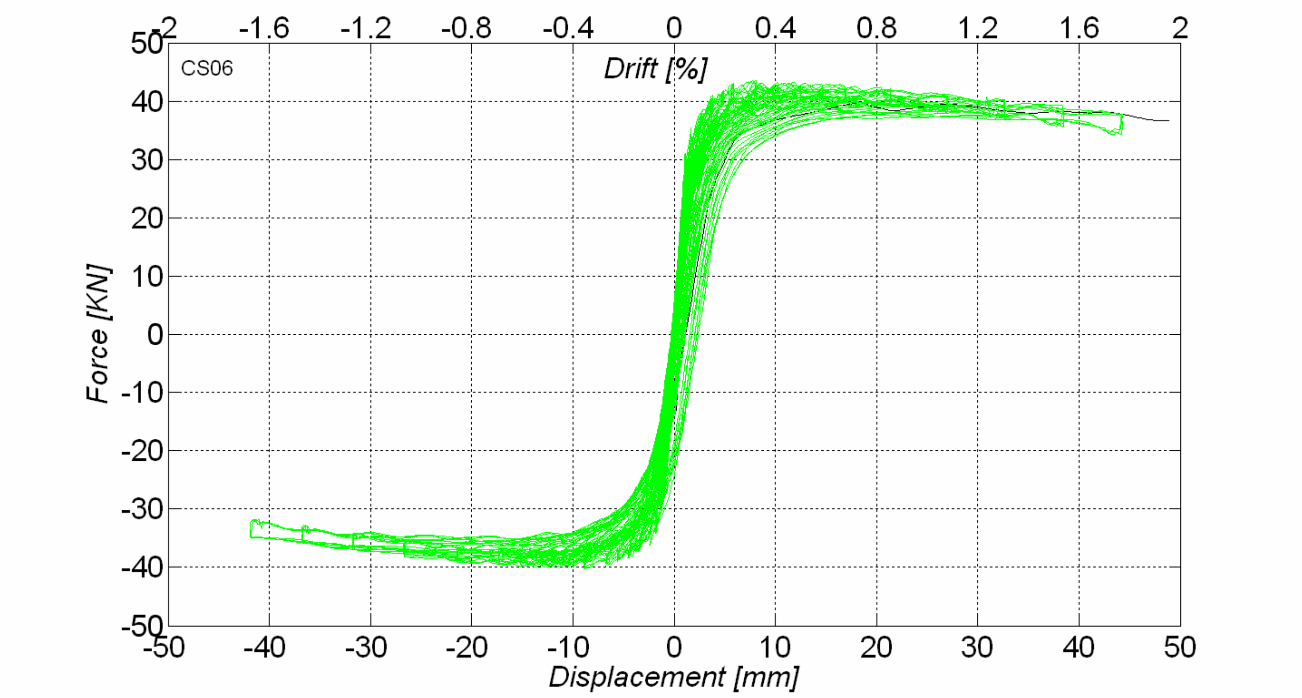


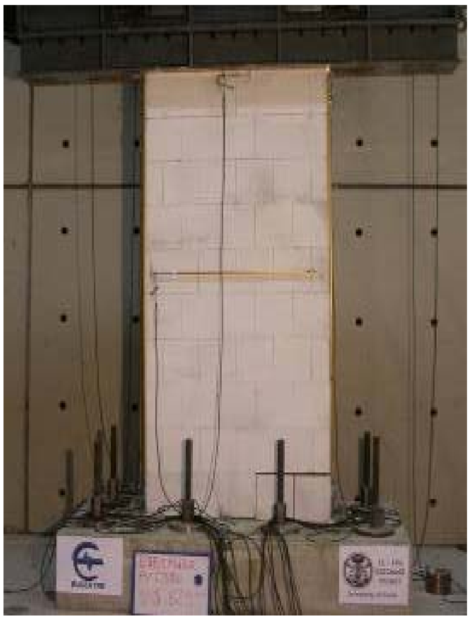

Figure 21 Wall CS06. Cantilever, l=1.25 m, $\sigma_v$=1.0 MPa

Wall CS07 was characterized by a force-displacement response typical of rocking failure (s-shape, low dissipation), nevertheless at a horizontal displacement of about ± 17 mm the opening of the unfilled head joints was very evident, indicating that a "gaping" failure mode was governing the response. Cracking of bedjoints concurred to form a system of stepped diagonal cracks along the wall. These cracks closed during unloading. The hysteresis cycles showed very low energy dissipation and no strength degradation since no cracks in the units or sliding in bedjoints occurred. The test was interrupted when the top displacement was 30 mm (1.2% drift) because wide vertical cracks in the joints had developed and separation of a large wedge of masonry took place, with the danger of a partial collapse of the wedge itself.

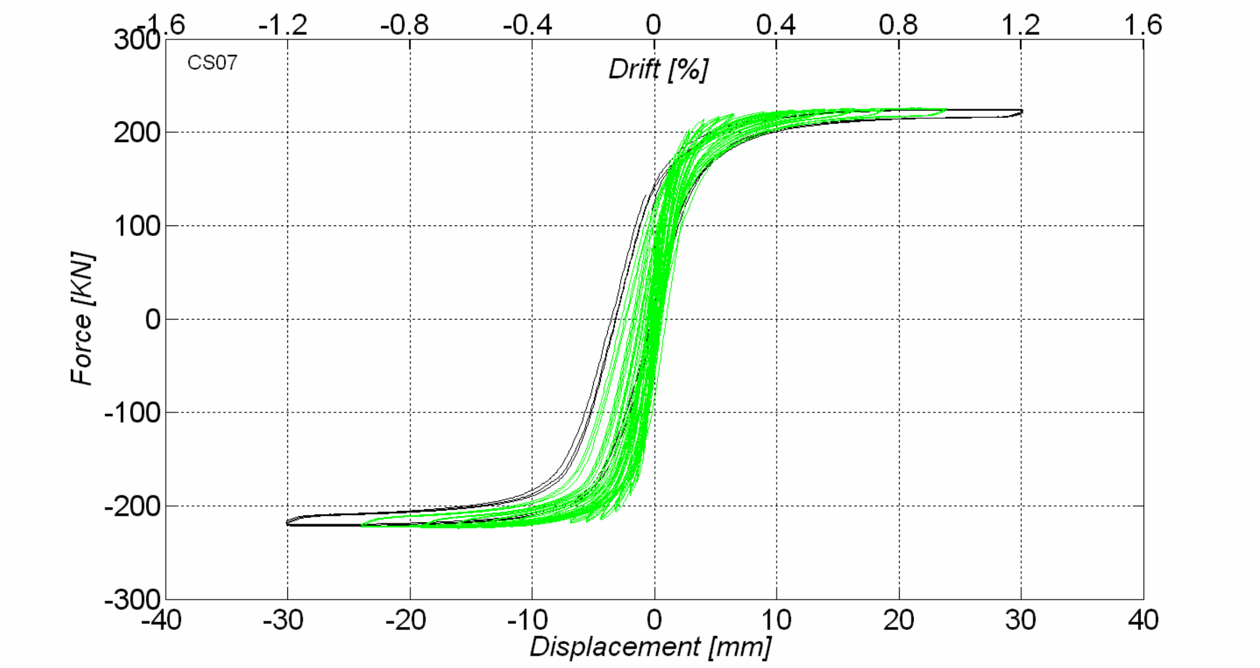


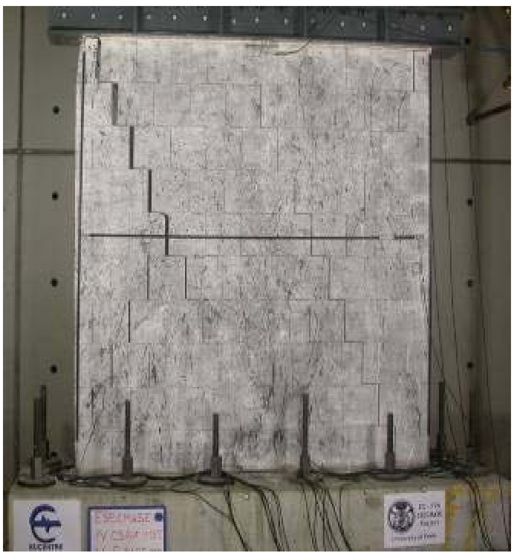

Figure 22 Wall CS07. Double fixed, l=2.50 m, $\sigma_v$=1.0 MPa

Wall CS08 had same geometric characteristic and same vertical load of wall CS07 but it was tested as a cantilever system. At a horizontal displacement of about ± 12 mm opening of the unfilled head joints became visible to form stepped inclined cracks along the height of the wall. Low energy dissipation and no strength degradation occurred. Cracks closed during unloading. Rocking/gaping-type response of the wall was displayed. Beyond a top displacement of 20 mm several diagonal cracks in the units of the right bottom half part of the wall developed and in these last cycles a slightly higher energy dissipation was displayed.

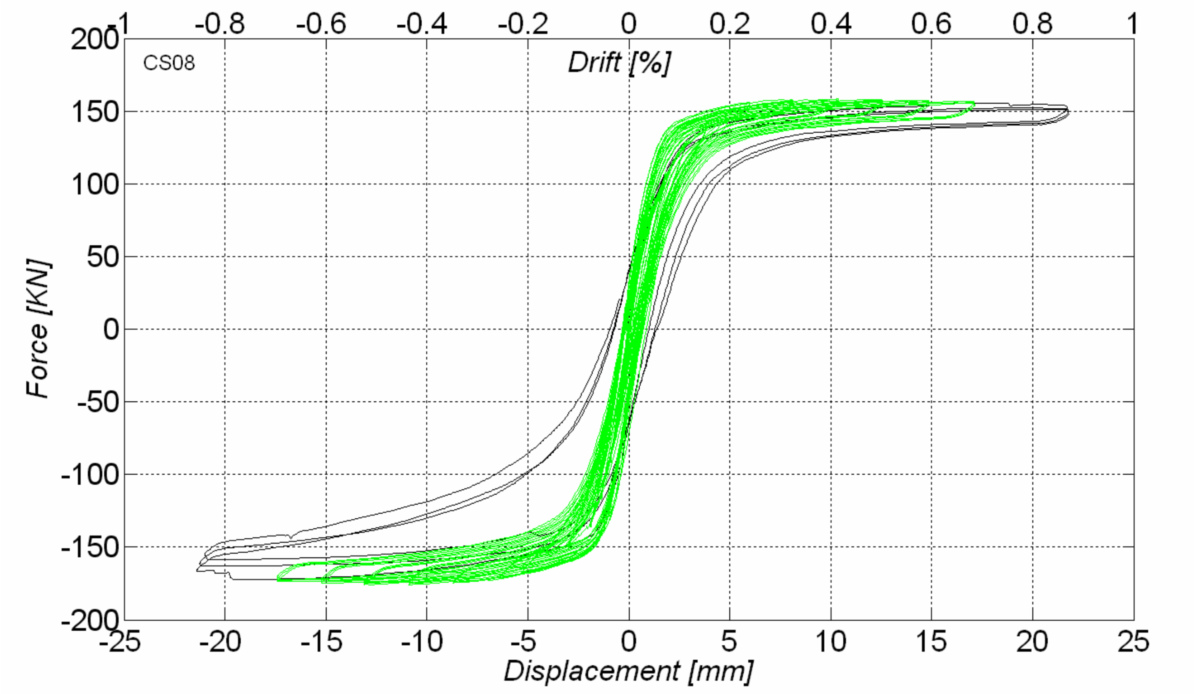


Figure 23 Wall CS08. Cantilever, l=2.50 m, $\sigma_v$=1.0 MPa

### 5.1.2 Calcium-silicate masonry with "Quadro E" units (CS09-CS14)

Wall CS09 was the only unreinforced wall constructed with "Quadro E" units. The wall has been subjected to a first visible damage at a drift of about 0.10%. At that stage a diagonal crack in the top left unit occurred from the top corner of the wall. Horizontal sliding at the centre of the panel was shown and a diagonal crack at the bottom left unit also occurred. Strength degradation due to cracks in the units is evident in the force-displacement curve. The head- and bed-joint cracks formed a pattern of stepped diagonal cracks along the height of the wall. These cracks closed during unloading. The test was interrupted when the width of the opening of the unfilled head joints at the centre of the panel became large (at the end of the test reached more than 20 mm).

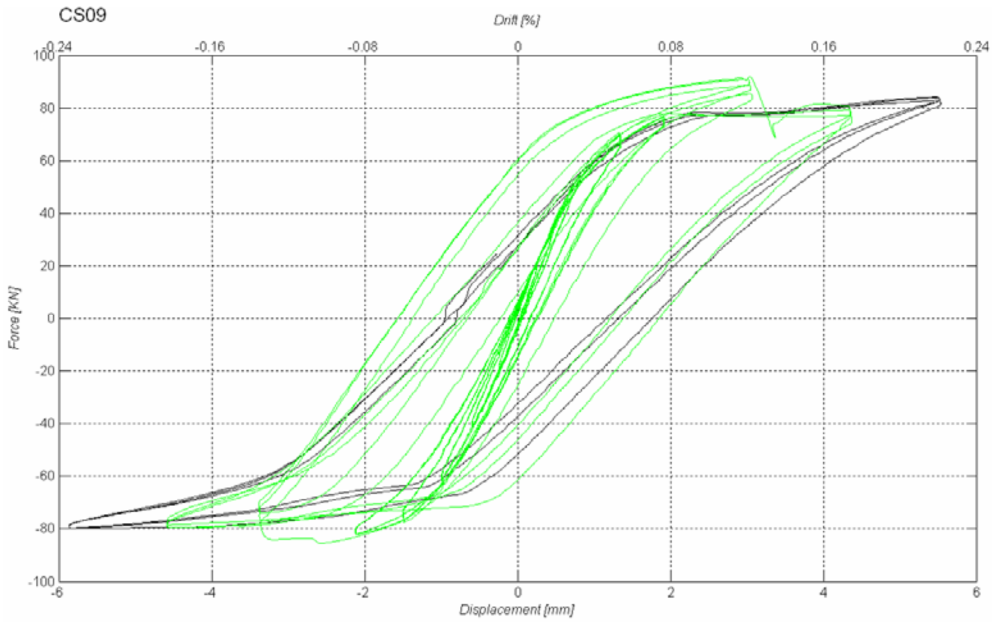


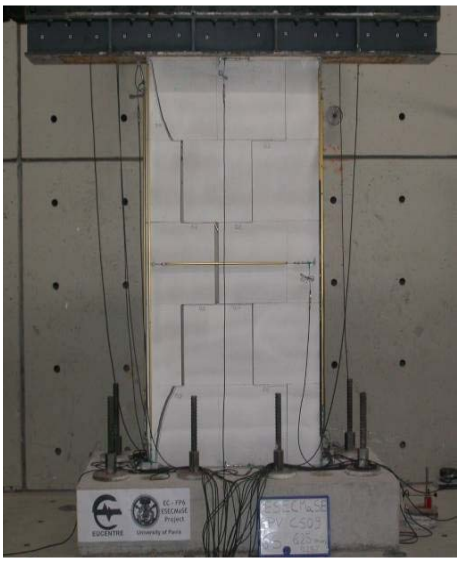

Figure 24 Wall CS09. Unreinforced, double fixed, l=1.25 m, $\sigma_v$=1.0 MPa

The walls CS10, CS11, CS12 and CS13 were confined with 1 $\phi$ 16 at each end of the wall. The opening of the vertical headjoints occurred at low levels of horizontal drift (0.05%) but no stiffness degradation was evident in the F-D hysteresis. In the cycles at a drift of 0.15%, diagonal cracks in the corner units of the right side of the wall appeared. The collapse of the wall happened when cracks in the corner units of the left part of the wall formed (0.4% drift). At this point very wide vertical cracks in the headjoints were also evident.

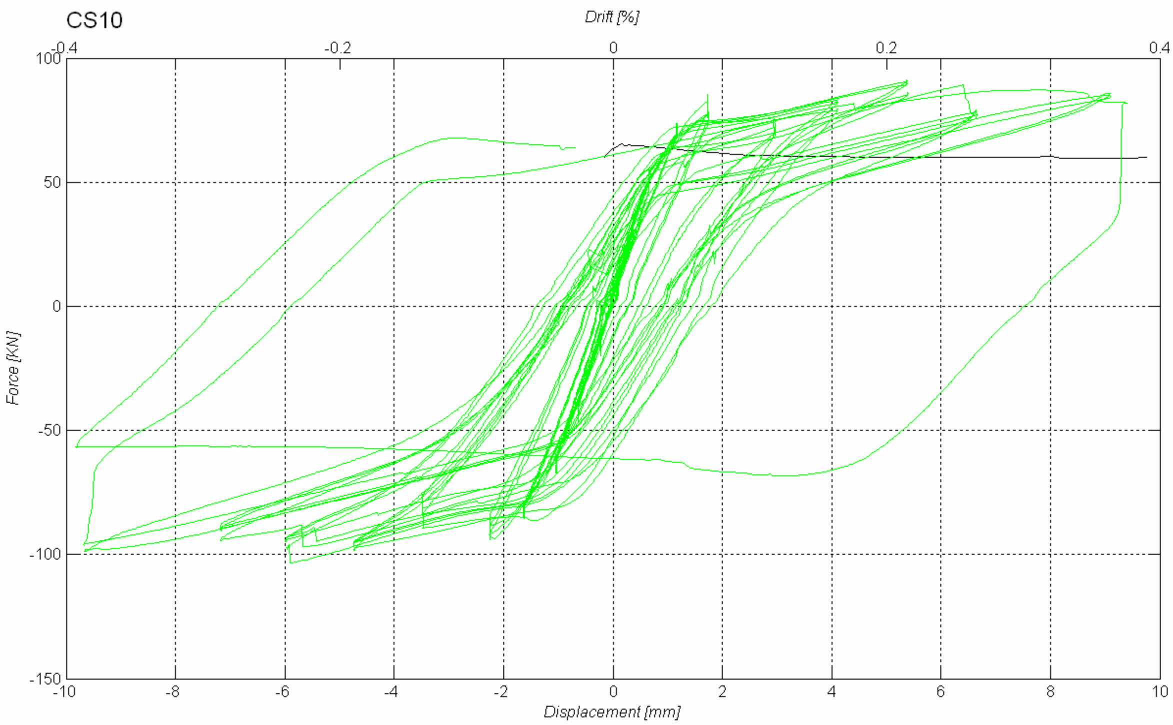


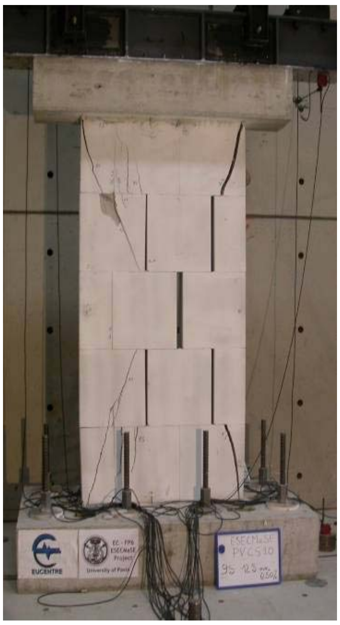

Figure 25 Wall CS10. Confined (1+1$\phi$16), double fixed, l=1.25 m, $\sigma_v$=1.0 MPa

A lower level of vertical stress was applied (0.5 MPa) on wall CS11 with respect to wall CS10. At low levels of horizontal drift (0.10%) small cracks in the units formed. Horizontal and vertical cracks in the joints concurred to form a system of stepped diagonal cracks along the wall; these cracks closed during unloading without any loss of strength or stiffness. In the cycles at a drift of 0.15%, the opening of two large diagonal cracks in the corner units of the left side of the wall appeared. In the following cycle the diagonal crack in the lower unit propagated up to the base of the unit. The wall presented an uncracked behaviour up to the occurrence of these latter diagonal cracks in the calcium silicate units. The collapse of the wall was reached when a wide diagonal crack in the bottom corner unit of the right part of the wall formed (0.6% drift). A slightly higher displacement capacity was reached in comparison with wall CS10.

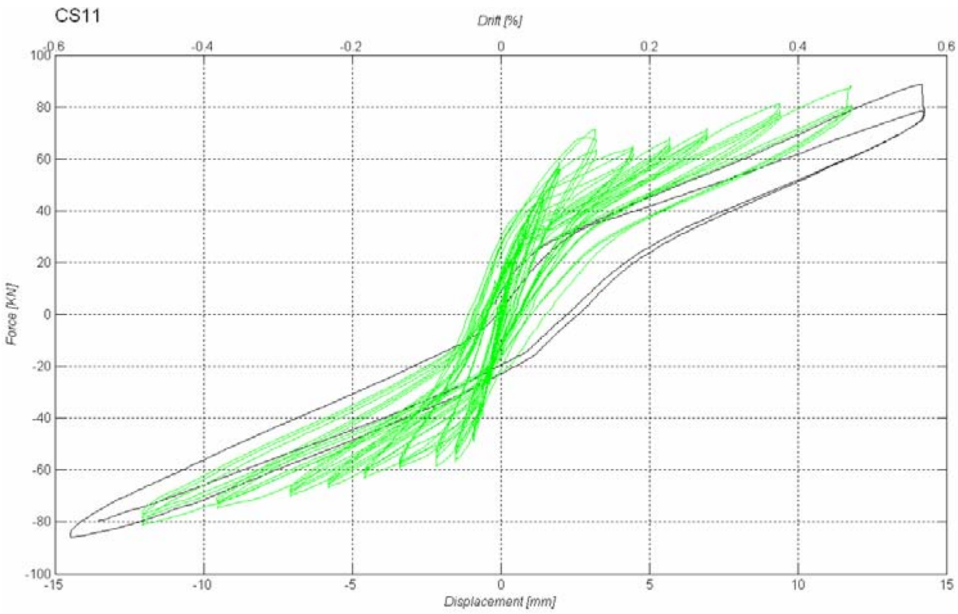


Figure 26 Wall CS11. Confined (1+1$\phi$16), double fixed, l=1.25 m, $\sigma_v$=0.5 MPa

A large vertical stress (2 MPa) was applied on wall CS12. The wall remained substantially uncracked up to a top displacement of about 3 mm when several small diagonal cracks in the units formed, after which strength degradation was shown. In the following cycles these cracks propagated and diffused throughout the pier. In the cycle correspondent to a drift of 0.3 % a large diagonal crack in the center of the panel appeared and, as a consequence, strength degradation happened. Spalling of some units in the center of the wall also occurred. The collapse of the wall was reached when the horizontal displacement was slightly less of 10 mm, the diagonal cracks in the wall became very wide and the wall lost any capacity of resisting the horizontal forces.

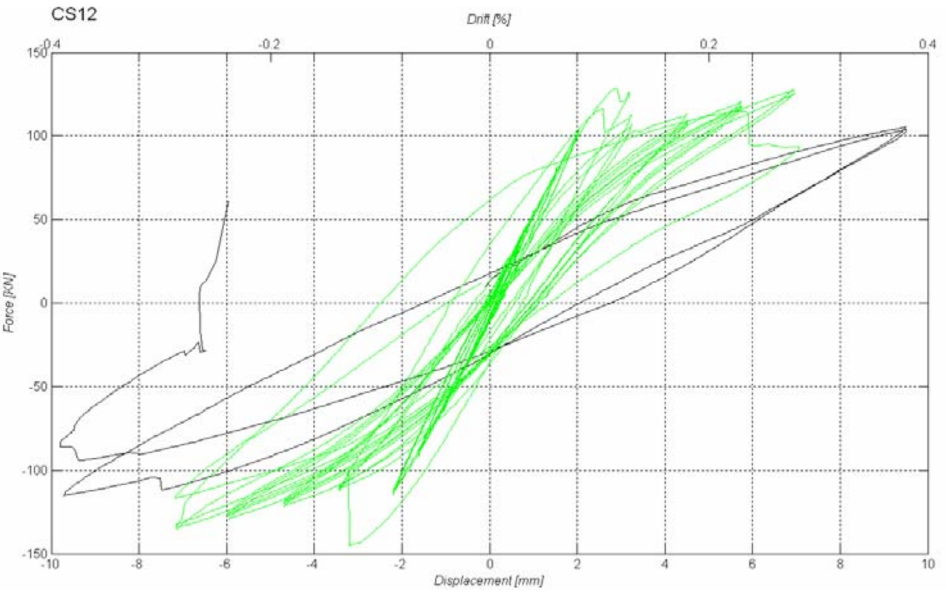


Figure 27 Wall CS12. Confined (1+1$\phi$16), double fixed, l=1.25 m, $\sigma_v$=2.0 MPa

The confined wall CS13 was 2.5 m long with a vertical stress of 1 MPa. The wall remained undamaged up to a top displacement of about 3 mm. Horizontal and vertical cracks in the joints concurred to form a system of stepped diagonal cracks along the wall; these cracks closed during unloading without any loss of strength or stiffness. In the cycles at a drift of 0.6%, the opening of a diagonal crack in the unit at the center of the wall appeared. In the following cycle several diagonal cracks formed in the units propagated down to the base of the wall. Both the stepped diagonal cracks and the cracks in the units became very wide and separation of large masonry wedges at both sides of the wall took place at a drift of 1.2%. The spalling of the masonry units and the separation of the masonry wedges exposed the steel rebars. At this level of horizontal displacement a significant loss of strength occurred and the wall collapsed. In this test a very large value of shear strength was reached.

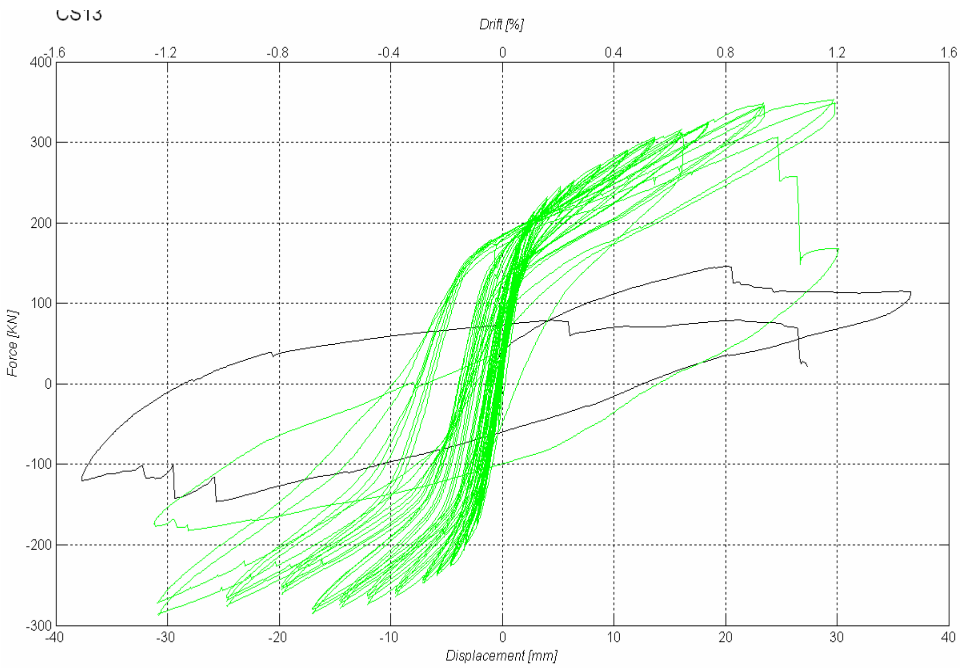


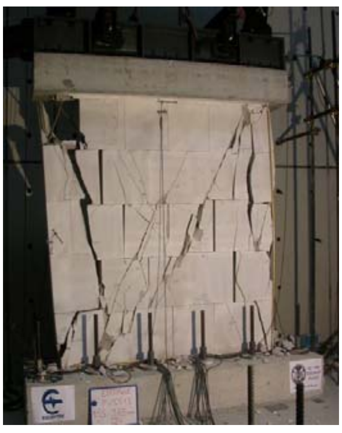

Figure 28 Wall CS13. Confined (1+1ϕ16), double fixed, l=2.50 m, $\sigma_v$=1.0 MPa

The wall CS14 was post tensioned before the beginning of the test with an application of a vertical force of 110 KN at each tendon in order to get a total vertical stress in the wall of 2 MPa (1 MPa given by the vertical actuator and 1 MPa from the vertical forces in the tendons). In order to avoid possible sliding between the r.c. top beam and the steel beam on which the horizontal actuator was fixed, a cantilever system was envisaged for this test.

No appreciable damage was evident up to drift equal to 0.4-0.5% and the shape of the hysteresis curve was similar to that of a rocking response. After this level of displacement small diagonal cracks occurred in the units and the hysteresis curve became slightly fatter without, however, reduction in the strength. At a horizontal displacement of about 24 mm (slightly less than 1 % drift), large strength degradation occurred for the failure of the anchorage in the r.c. foundation of the tendon of the right side. The r.c. foundation was cast with concrete having a compressive strength on cube of 30 MPa (C25/30 according to EN 206).

In Figure 29 it is possible to see the damage in the wall and in the foundation.

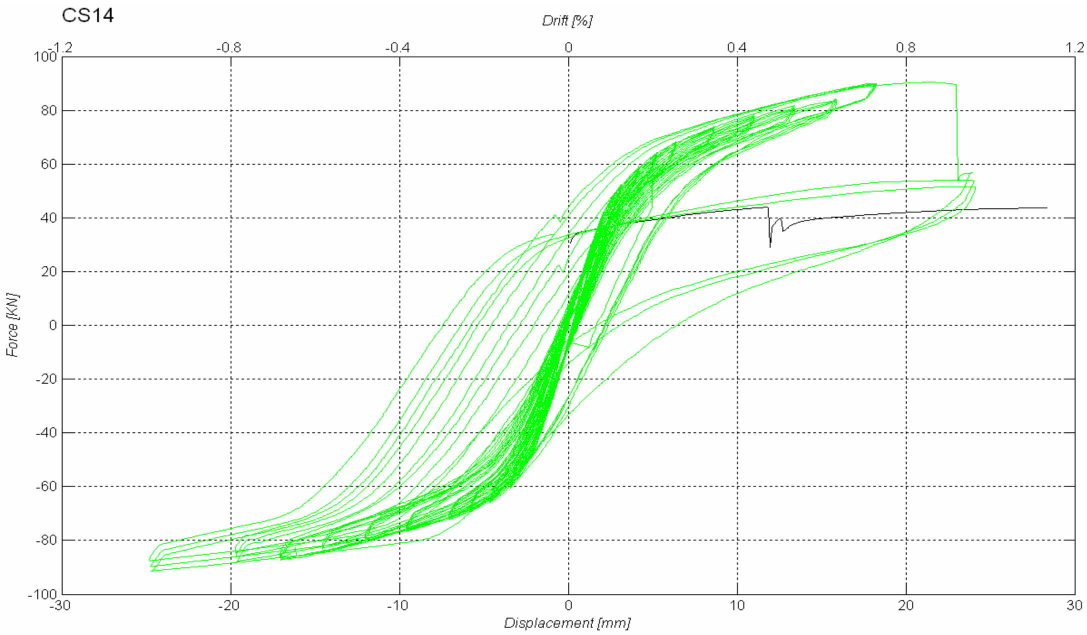


Figure 29 Wall CS14. Post-tensioned, cantilever, l=1.25 m, $\sigma_v$=1.0 (+1.0) MPa

### 5.1.3 Hollow clay masonry: German typologies (CL01-CL03)

The unreinforced wall CL01 was tested as a double fixed system. No diagonal cracks occurred during the test and the wall displayed a typical rocking behaviour without any significant strength degradation or relevant energy dissipation. With a top displacement larger than 50 mm (corresponding to a drift of 2.0 %) a wide horizontal crack was clearly visible in the top and bottom corners of the panels due to tension stresses. The test was interrupted when the top displacement attained about 70 mm due to the stroke limits of the transducers; at that stage the wall was substantially undamaged (except for the horizontal crack).

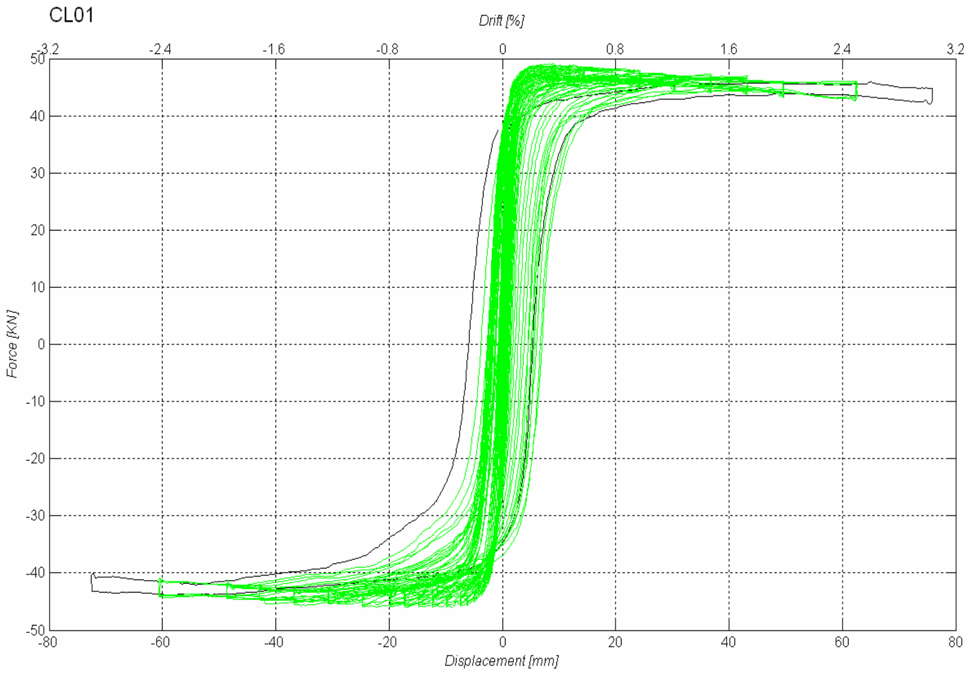


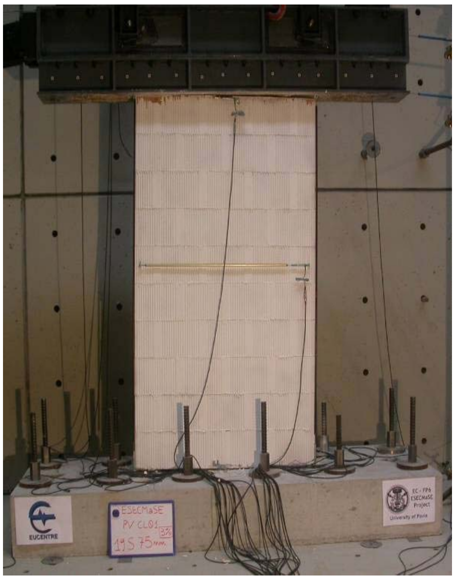

Figure 30 Wall CL01. Unreinforced, double fixed, l=1.50 m, $\sigma_v$=0.31 MPa

The wall CL02 was confined with 1 $\phi$ 16 bar at each end. The wall was tested as cantilever system. This wall has some similarity with a concrete wall with concentrated vertical bars at the ends since the large holes of the clay units were completely filled by concrete. No diagonal cracks occurred during the test. Energy dissipation was due to the yielding of the rebars. At a top displacement larger than 10 mm two vertical parallel cracks at the edges of the walls close to the position of the bars occurred, isolating two r.c. columns at the ends of the walls. Strength degradation after the attainment of peak strength was accompanied also by damage at the compressed corner. The test was interrupted when the top displacement attained more than 70 mm for reasons due to the stroke limits of the transducers and also for quite appreciable strength degradation.

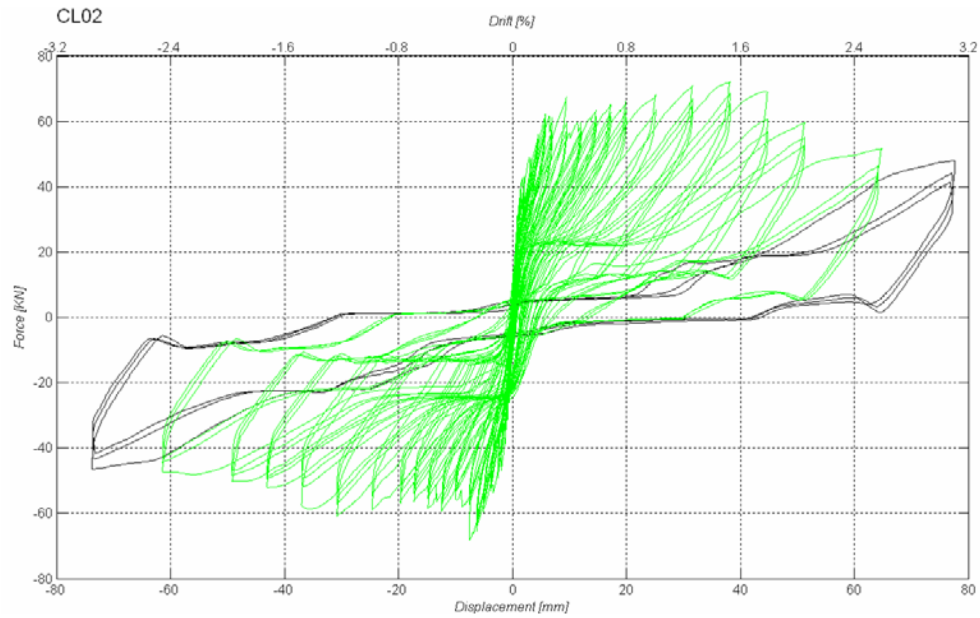


Figure 31 Wall CL02. Confined (1+1$\phi$16), cantilever, l=1.50 m, $\sigma_v$=0.33 MPa

The unreinforced masonry wall CL03 was tested with double fixed boundary condition. The level of the vertical stress was very low (0.14 MPa). No diagonal cracks in the units occurred during the test and the wall displayed a rocking behaviour without any significant strength degradation or relevant energy dissipation. With a drift larger than 1.0 %, horizontal and vertical cracks in the joints concurred to form a system of stepped diagonal cracks along the wall; these cracks closed during unloading without any loss of strength or stiffness. Moreover, wide horizontal cracks were clearly visible in the top corners of the panel due to tension stresses. At the bottom of the wall the horizontal crack due to tension stresses formed at the bedjoints between the first and the second course of the masonry units. The test was interrupted when the top displacement attained about 37 mm for the large damage in the wall.

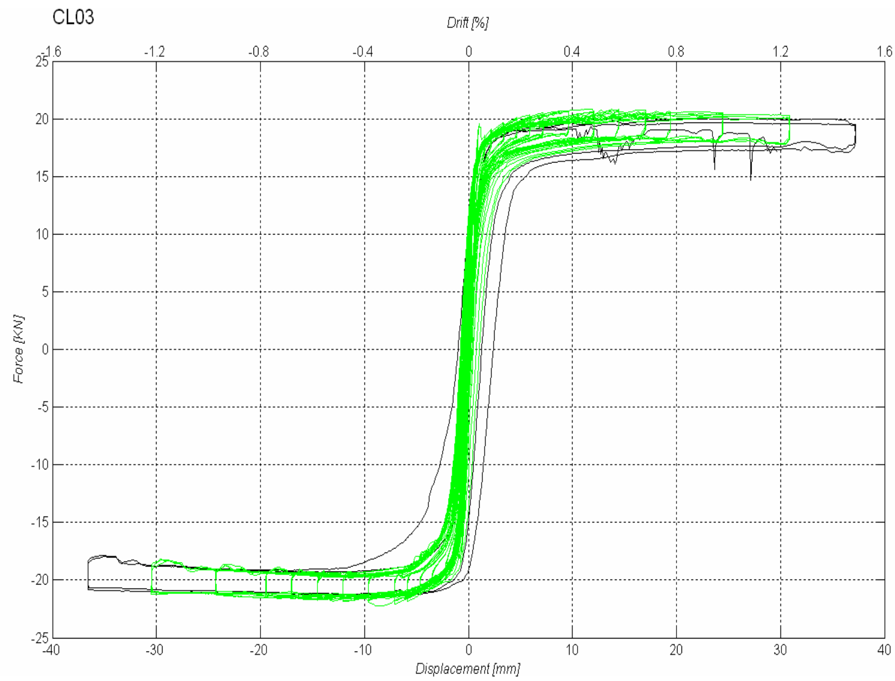


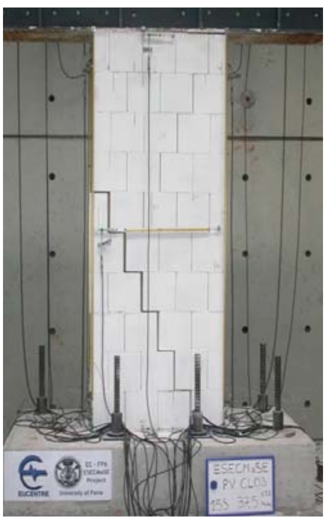


Figure 32 Wall CL03. Unreinforced, double fixed, l=1.00 m, $\sigma_v$=0.14 MPa

### 5.1.4 Hollow clay masonry: Italian typologies (CL04-CL10)

The vertical stress applied on the wall CL04 was initially equal to 0.50 MPa. Nevertheless, significant sliding along the joint between the steel beam at the top and the wall itself was shown after 7 cycles. It was then decided to increment the vertical stress up to 0.68 MPa. At this higher level of compression the wall developed a diagonal cracking failure. Still, the displacement measured at the top beam was found to have a significant component due to sliding. For this reason the hysteresis loops show a large dissipation that was not only associated to cracking in the panel but to a large extent by sliding.

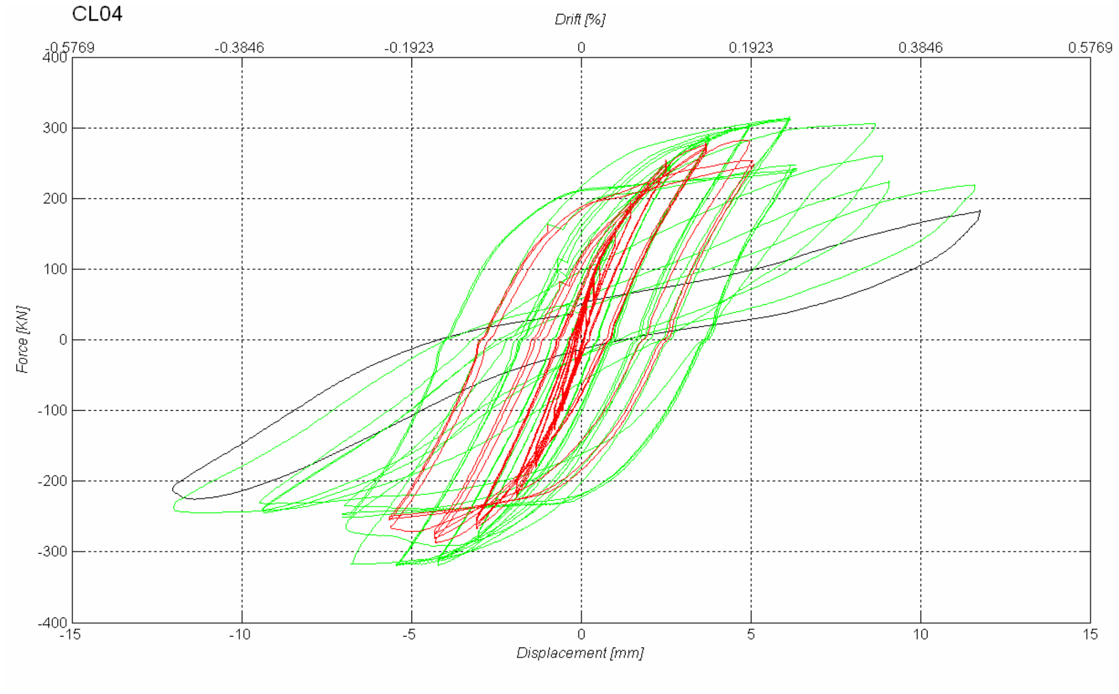


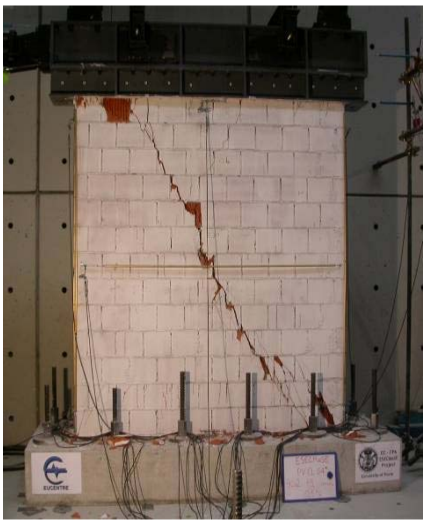

Figure 33 Wall CL04. Traditional unit, G.P. bedjoints and headjoints l=2.50 m.
The cycles with $\sigma_v$=0.50 MPa are shown in red, whereas the cycles with $\sigma_v$=0.68 MPa are shown in green.

Wall CL06 failed with diagonal shear cracks in the masonry units from corner to corner of the wall, at rather small top displacement (just beyond 0.25% drift). Spalling of some units also occurred. Large strength and stiffness degradation occurred after diagonal cracking. Before attaining this displacement level no evident damage was present except for small diagonal cracks in the units.

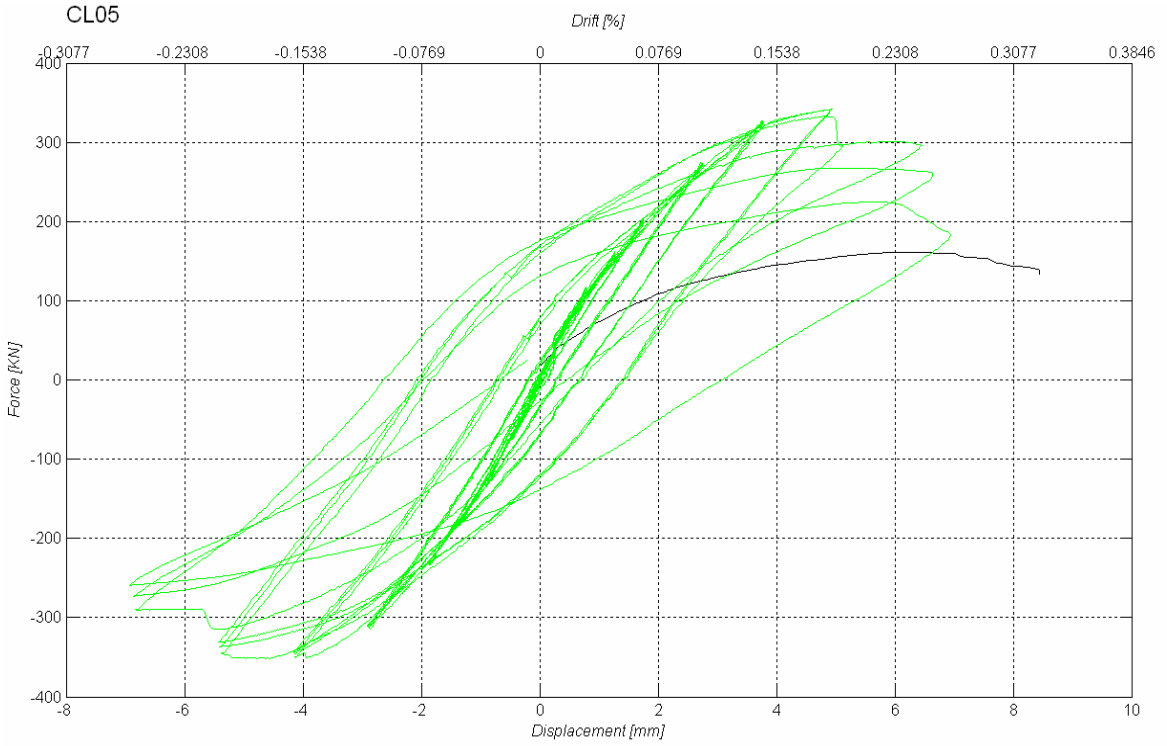


Figure 34 Wall CL05. Traditional unit, G.P. bedjoints and headjoints l=2.50 m, $\sigma_v$=0.68 MPa

In the wall CL06 no diagonal cracks occurred during the test and the wall displayed a typical rocking behaviour with low energy dissipation. Strength degradation after the peak occurred since the resultant of the compression moved towards the centre of the panel for the concentration of the damage in the compressed corners. A wide horizontal crack was clearly visible in the top corners of the panel due to tension stresses. The test was interrupted when the top displacement attained about 50 mm (slightly less than 2% drift) after a conspicuous strength degradation although displacement capacity reserves were probably still present..

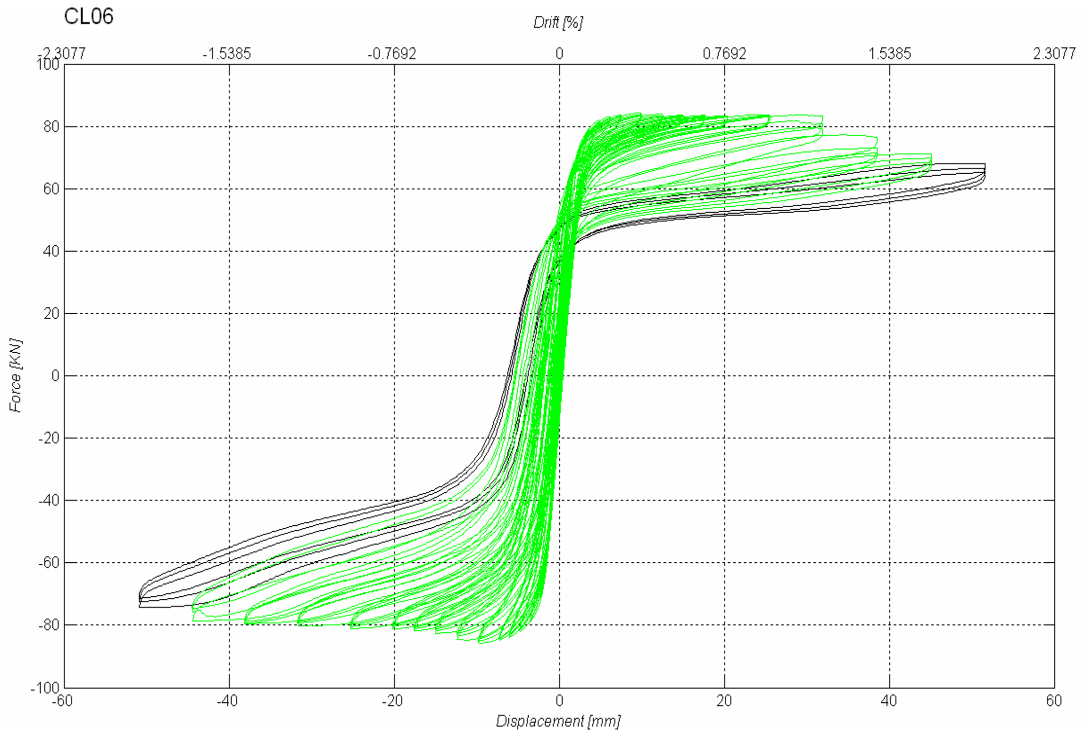


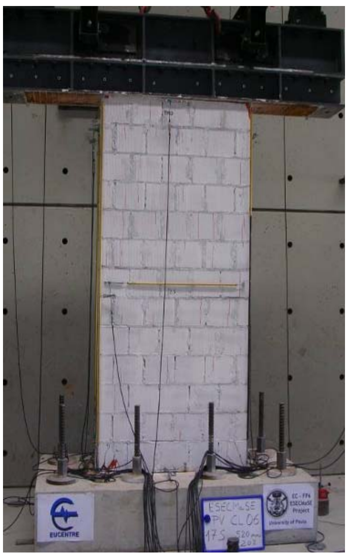

Figure 35 Wall CL06. Traditional unit, G.P. bedjoints and headjoints l=1.25 m, $\sigma_v$=0.50 MPa

Wall CL07 was constructed with T+G clay units and general purpose mortar. The wall failed with two diagonal shear cracks in the masonry units from corner to corner of the wall, at a rather small top displacement (just below 0.2% drift). Spalling of some units at the centre of the panel also occurred. Large strength and stiffness degradation occurred after diagonal cracking. Before attaining this displacement level no evident damage was present, therefore this wall displayed a rather brittle behaviour.

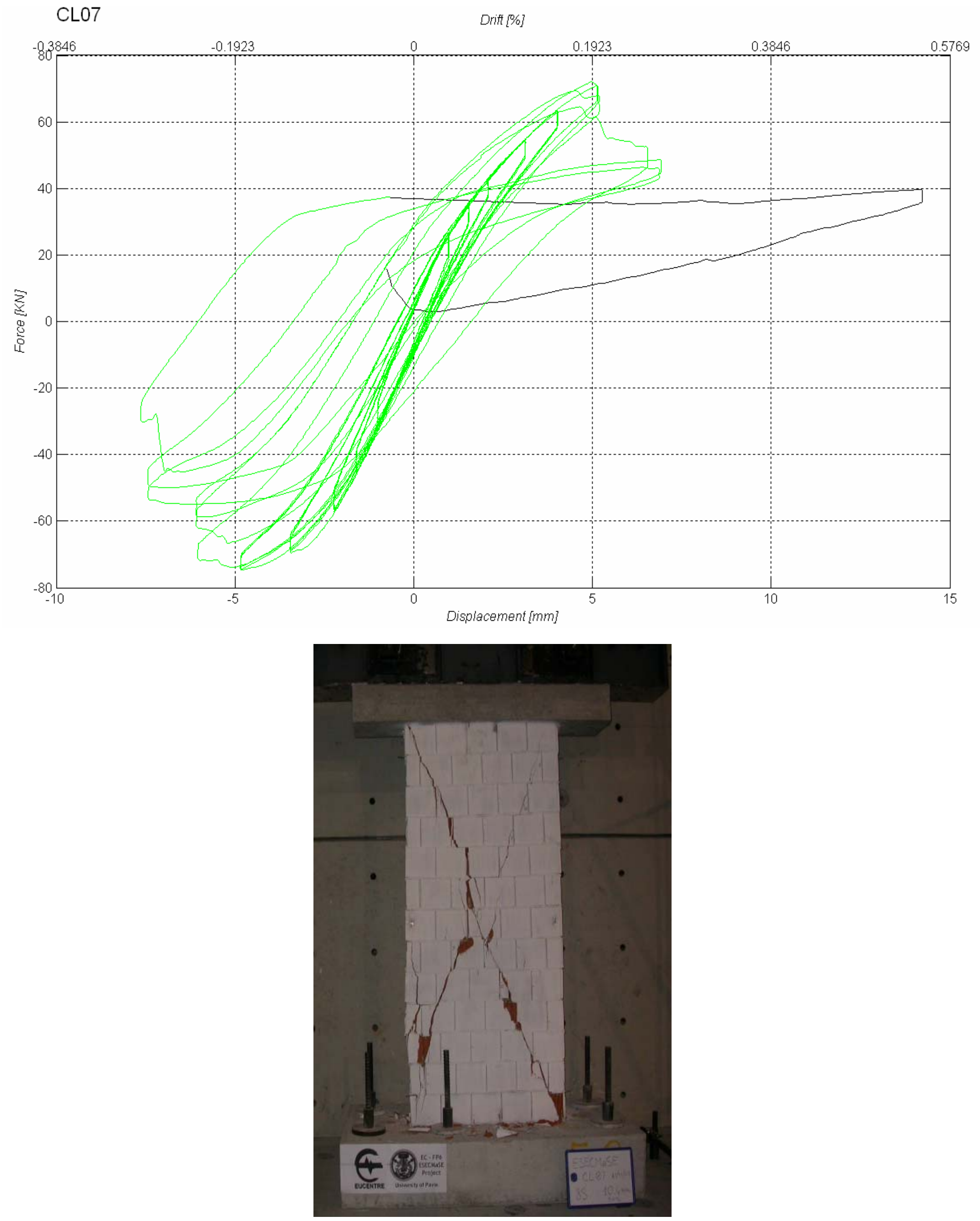


Figure 36 Wall CL07. T+G unit, G.P. bedjoints, unfilled headjoints l=1.25 m, $\sigma_v$=0.50 MPa

Wall CL08 was of the same typology of wall CL07 but with a length of 2.5 m. The wall failed by shear cracking with the occurrence of two diagonal cracks in the masonry units from corner to corner of the wall. This damage started to appear at a drift of 0.2-0.25% and the cracks developed in the panel up to a drift of 0.4 % when strength degradation occurred. Spalling of some units at the centre of the panel also was evident. The test was stopped for diffused damage and large strength degradation.

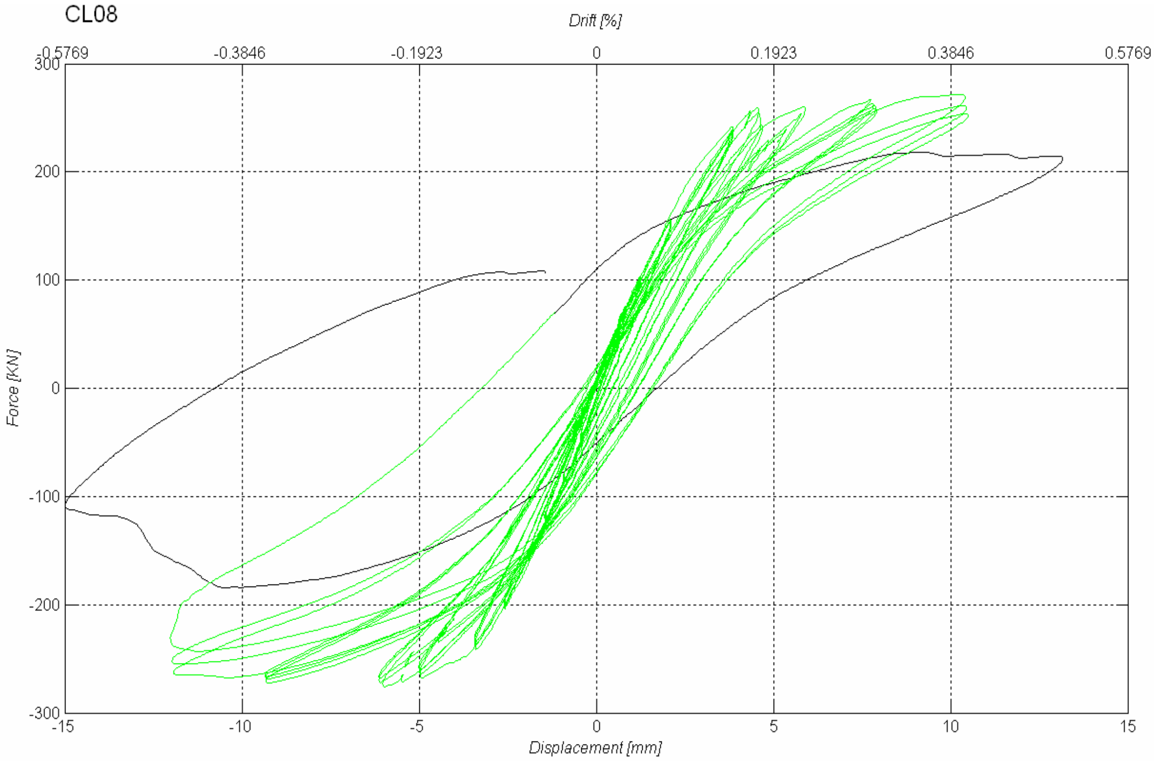


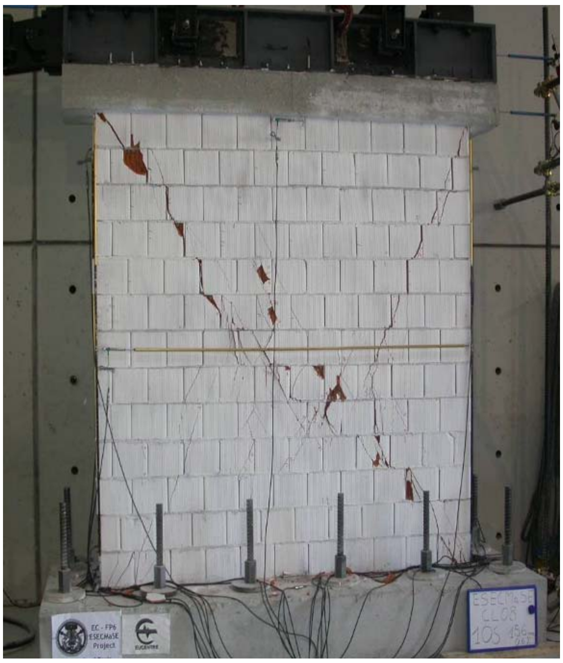

Figure 37 Wall CL08. T+G unit, G.P. bedjoints, unfilled headjoints l=2.50 m, $\sigma_v$=0.68 MPa

Wall CL09 had the same characteristics of wall CL07 but the bedjoints were made up with thin layer mortar instead of general purpose mortar. The failure mode of this wall was very similar to failure of wall CL07 both for the cracking pattern and for the maximum displacement capacity. The wall failed with two diagonal shear cracks in the masonry units from corner to corner of the wall, at rather small top displacement (below 0.25% drift). Strength degradation occurred after diagonal cracking.

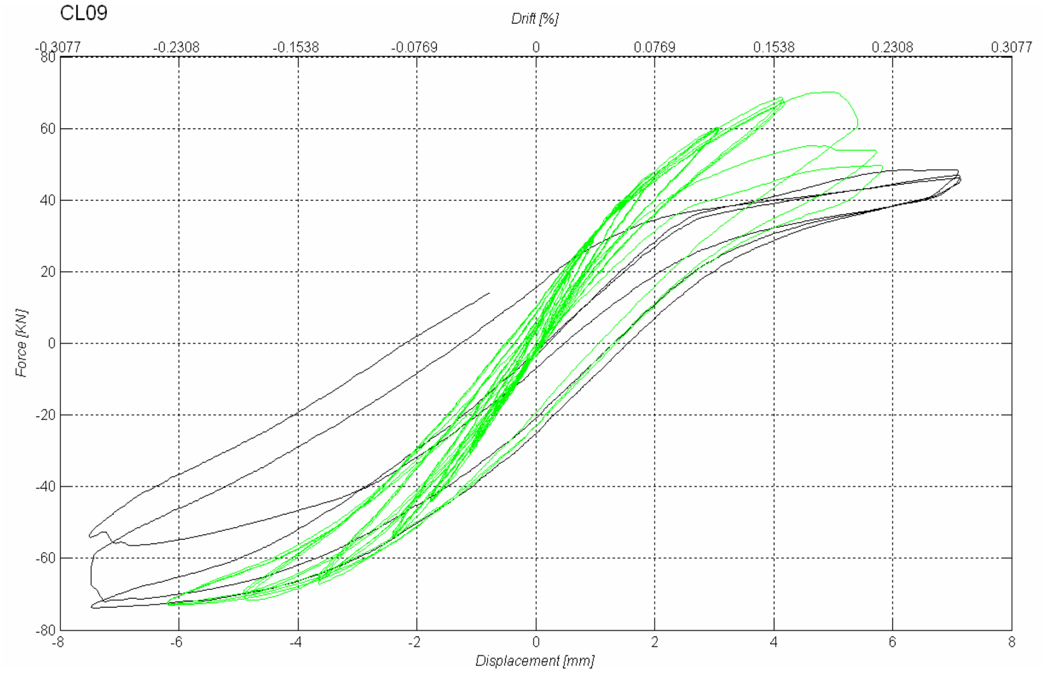


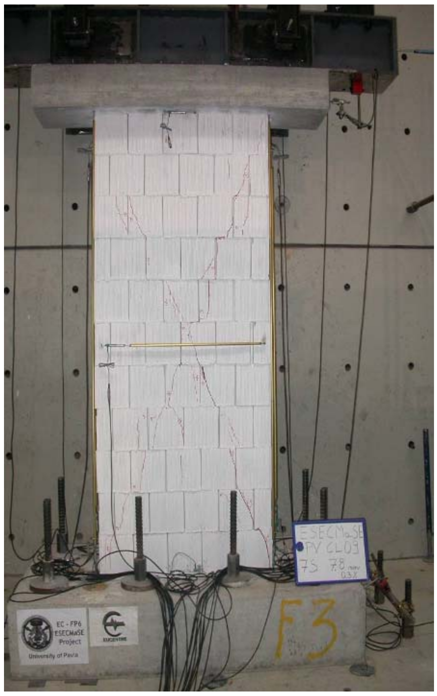


Figure 38 Wall CL09. T+G unit, Thin layer bedjoints, unfilled headjoints l=1.25 m, $\sigma_v$=0.50 MPa

Wall CL10 and wall CL08 showed similar failure modes since the two specimens had the same characteristics in terms of dimensions, vertical load applied and boundary condition. The only difference as respect to wall CL08 were the thin layer bedjoints. Diagonal cracks in the units started to be visible at a drift of about 0.20 %. The wall failed with two diagonal shear cracks in the masonry units from corner to corner of the wall, at small top displacement corresponding to about 0.45% drift. The wall collapsed when strength degradation occurred after the corner to corner diagonal cracking.

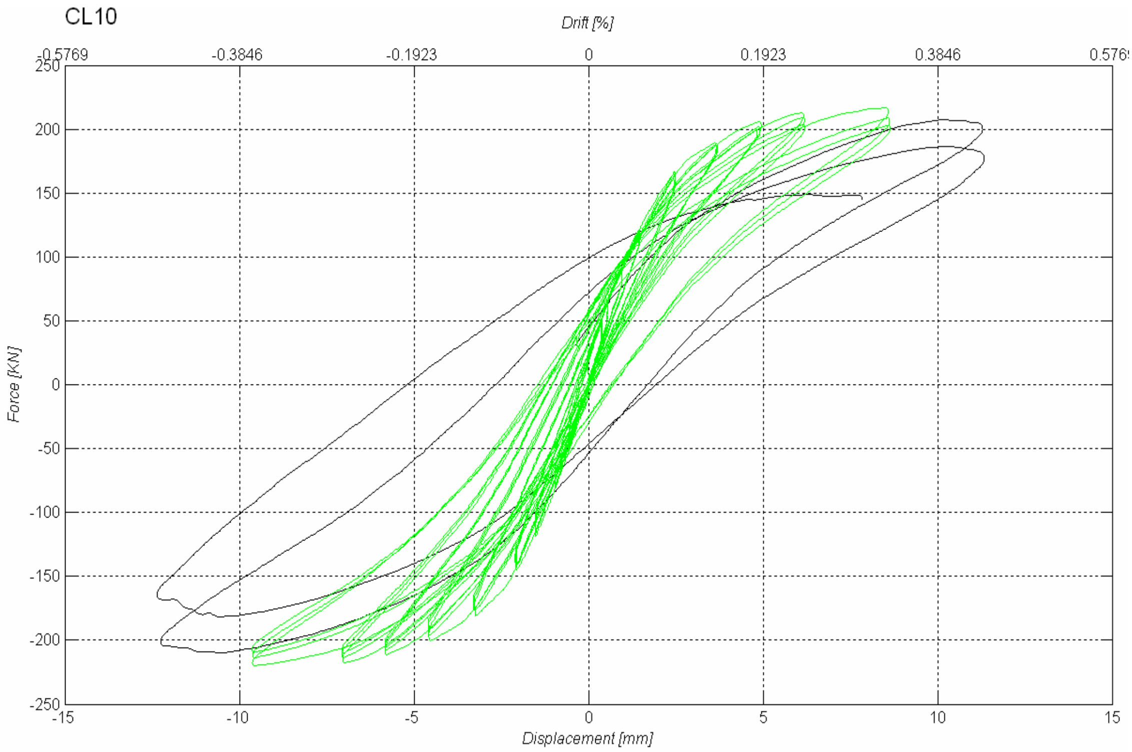


Figure 39 Wall CL10. T+G unit, Thin layer bedjoints, unfilled headjoints l=2.50 m, $\sigma_v$=0.68 MPa

### 5.1.5 Lightweight aerated concrete masonry (LAC01-LAC04)

Wall LAC01 was characterized by a force-displacement response typical of rocking/gaping failure. At a horizontal displacement of about ± 12.5 mm the opening of the unfilled head joints was very evident. Cracking of bedjoints concurred to form a system of stepped diagonal cracks along the wall. These cracks closed during unloading. The hysteresis cycles showed very low energy dissipation without an appreciable strength degradation since no cracks in the units or sliding in bedjoints occurred up to 1% drift when a large horizontal crack at joint under the top steel beam occurred and energy dissipation was developed. The test was interrupted at a drift of 1.25% since large damage occurred in particular because a separation of a masonry wedge was close to happen.

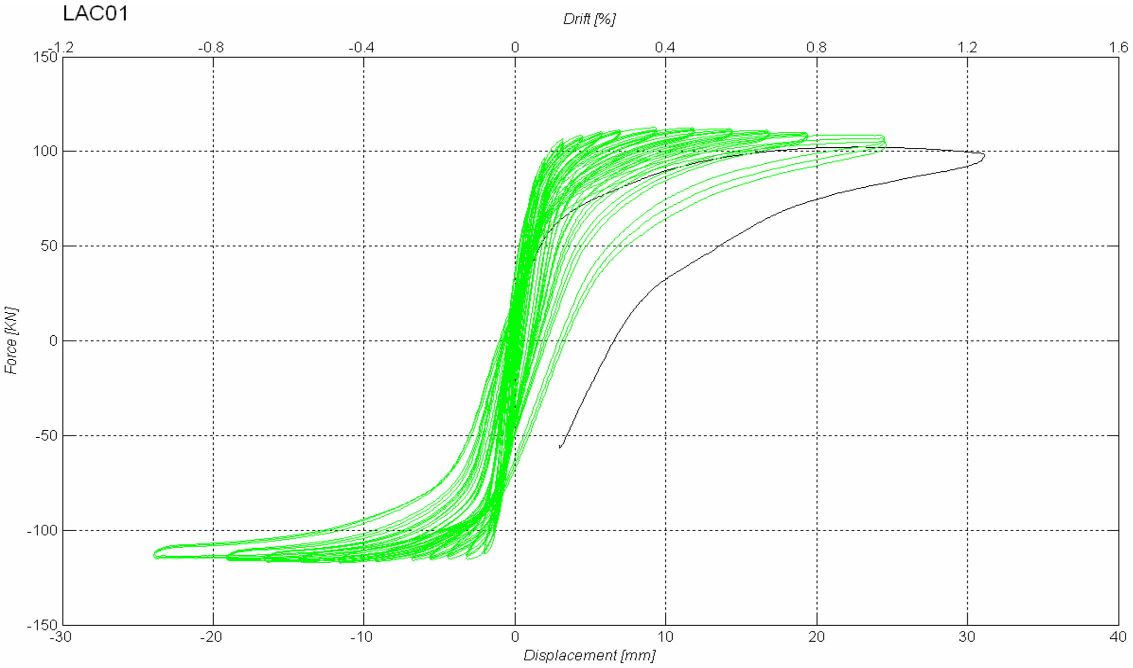


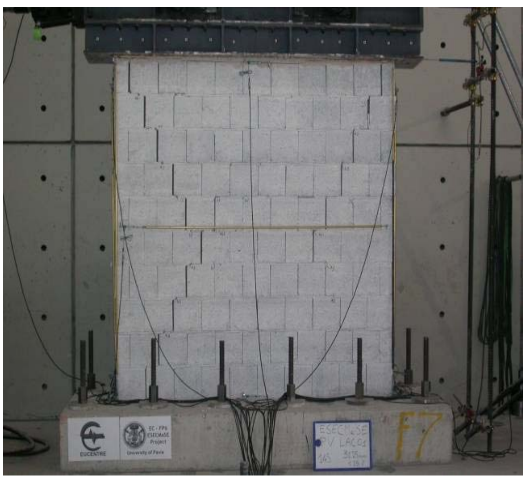

Figure 40 Wall LAC01. G.P. bedjoints, unfilled headjoints, l=2.50 m, $\sigma_v$=0.50 MPa

Wall LAC02 had the same characteristics of wall LAC01 with thin layer mortar bedjoints. At a horizontal displacement of about ± 12.5 mm the opening of the unfilled head joints was evident. Cracking of bedjoints concurred to form a system of stepped diagonal cracks along the wall. These cracks closed during unloading. The hysteresis cycles showed low energy dissipation. Small cracks in the units caused, at small level of drift (less than 0.2%), a slight strength degradation. The test was interrupted at a drift of 1.50% since large damage occurred in particular because very wide cracks occurred in the vertical joints.

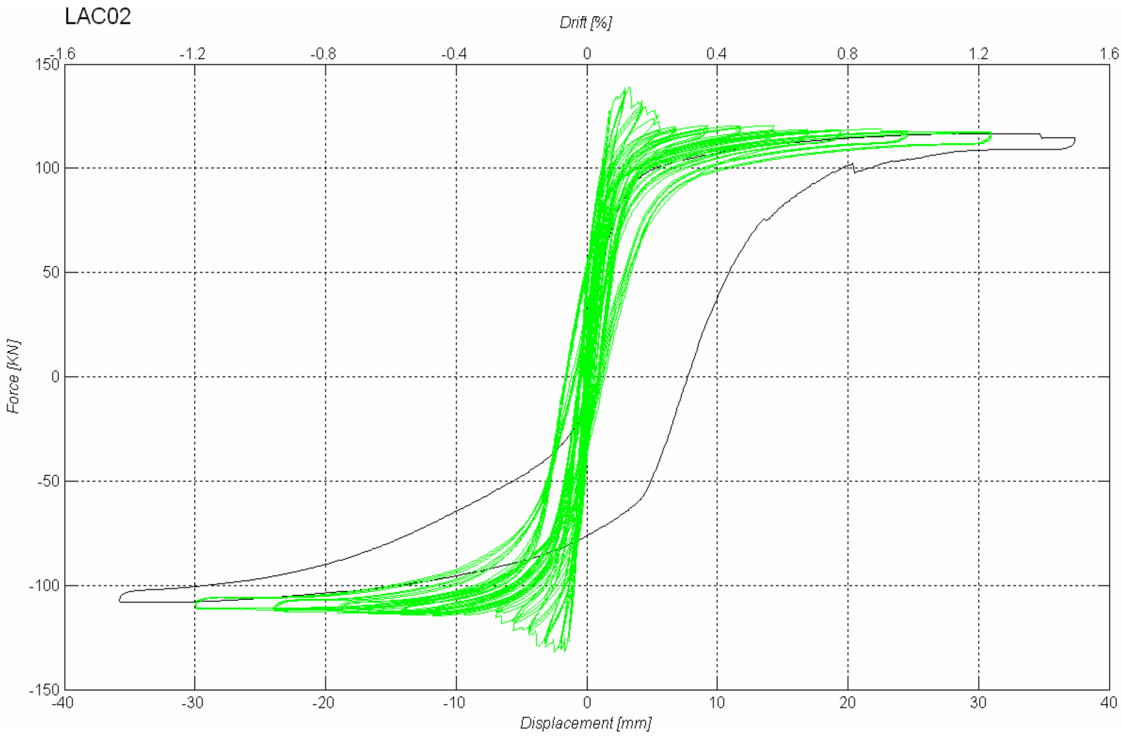


Figure 41 Wall LAC02. Thin layer bedjoints, unfilled headjoints, l=2.50 m, $\sigma_v$=0.50 MPa

Wall LAC03 had the same characteristics of wall LAC01 with higher vertical stress (1.0 MPa). Cracking of bedjoints concurred to form a system of stepped diagonal cracks along the wall. These cracks closed during unloading. The hysteresis cycles showed low energy dissipation up to a drift level of 0.5% when the failure of the two bottom corner units occurred and energy dissipation was developed. However, no strength degradation was evident. The test was interrupted at about 19 mm since large damage occurred.

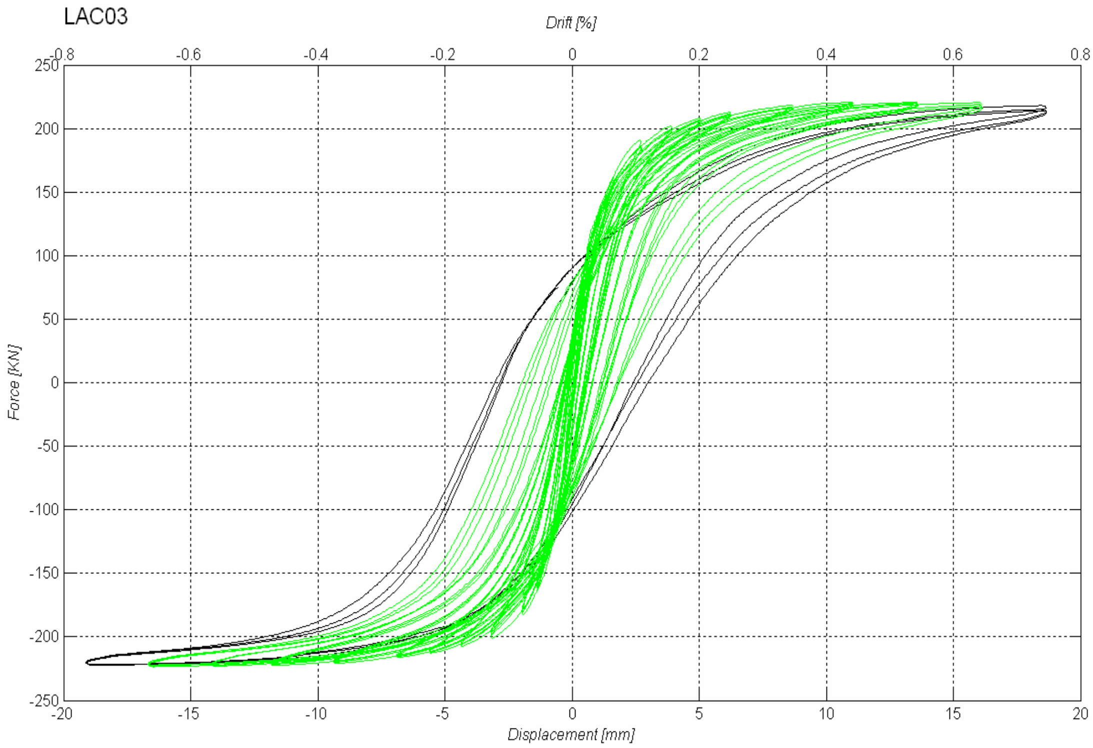


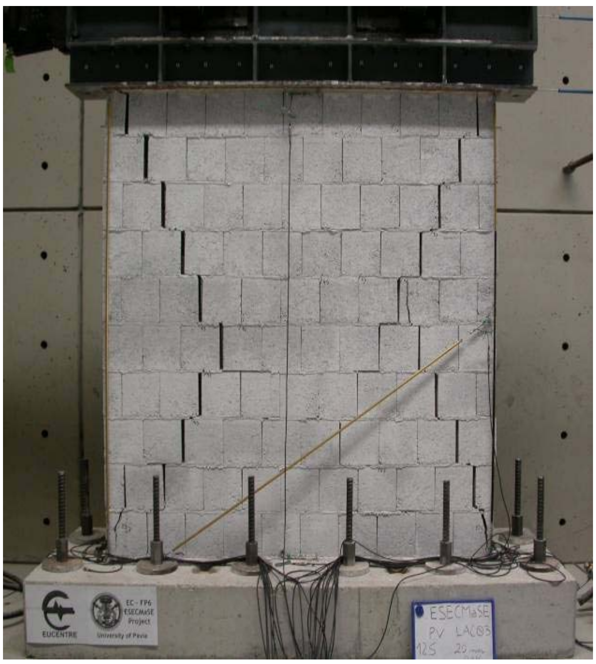

Figure 42 Wall LAC03. G.P. bedjoints, unfilled headjoints, l=2.50 m, $\sigma_v$=1.00 MPa

In wall LAC04 cracking of bedjoints and headjoint concurred to form a system of stepped diagonal cracks along the wall. These cracks closed during unloading. The hysteresis cycles showed low energy dissipation up to a drift level of 0.6% when diagonal cracks of the two bottom corner units occurred and energy dissipation was developed. No strength degradation was evident. As in the wall LAC03, the test was interrupted at about 19 mm since large damage occurred.

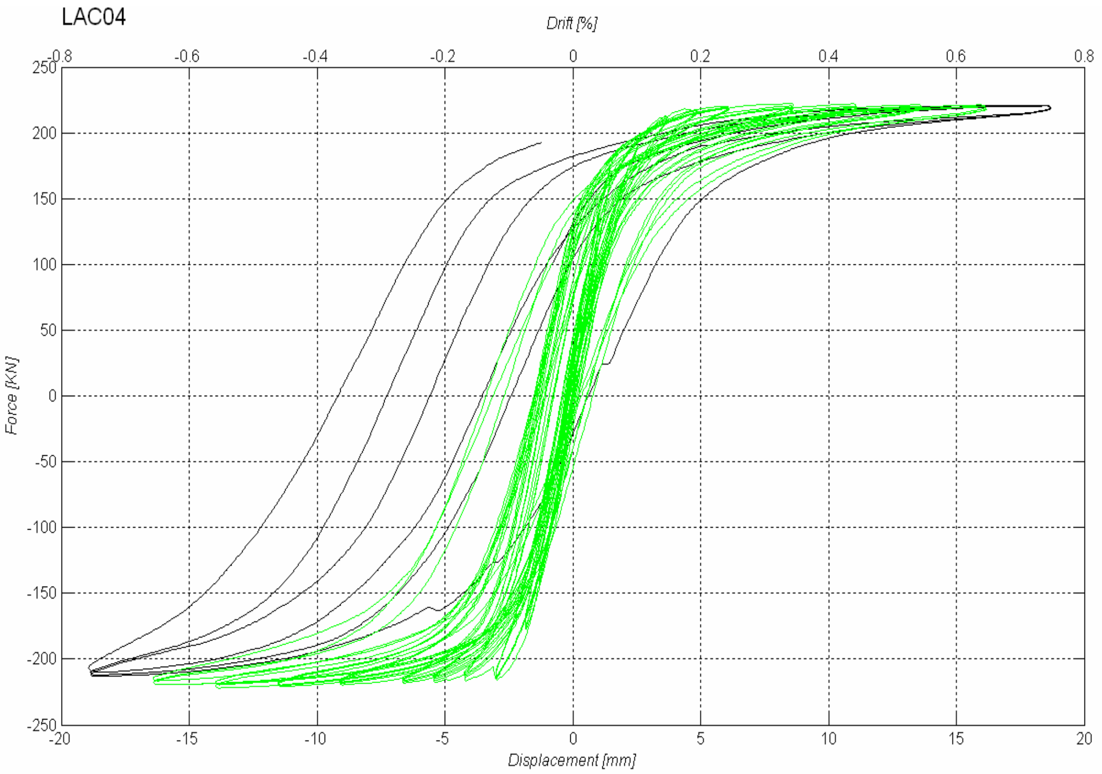


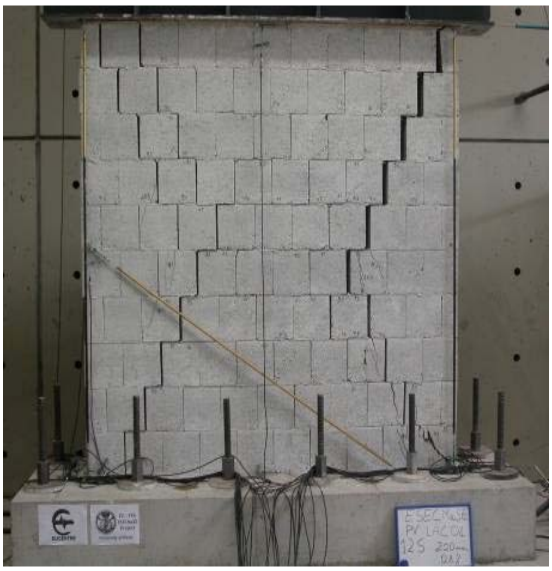

Figure 43 Wall LAC04. Thin layer bedjoints, unfilled headjoints, l=2.50 m, $\sigma_v$=1.00 MPa

### 5.2 Elastic stiffness, ductility and deformation capacity

A common approach to interpret the in-plane response of masonry walls is to idealize the cyclic envelope of the hysteresis loop with a bilinear envelope.

In Figure 44 a possible definition of the parameters of the bilinear curve is given. The elastic stiffness $k_{el}$ is obtained by drawing the secant to the experimental envelope at $0.70V_{max}$, where $V_{max}$ is the maximum shear of the envelope. The ultimate displacement $\delta_u$ can be evaluated as the displacement corresponding to strength degradation equal to 20% of $V_{max}$. The value of the shear $V_u$ corresponding to the horizontal branch of the bilinear curve can be found by ensuring that the areas below the cyclic envelope curve and below the equivalent bilinear curve are equal. Knowing the elastic stiffness $k_{el}$ and the value of $V_u$ it is possible to evaluate the elastic displacement $\delta_e$ as $V_u/k_{el}$. The ultimate ductility is defined as $\mu_u=\delta_u/\delta_e$.

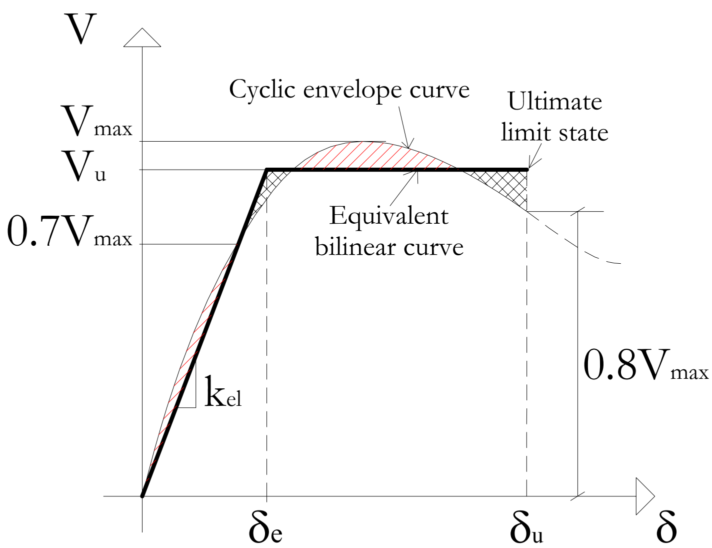


Figure 44. Hysteresis envelope and its bilinear idealization.

In Figure 45 a second definition of the parameters of the bilinear curve is given, as per Magenes & Calvi, 1997. The elastic stiffness is obtained by drawing the secant to the experimental envelope at $0.75V_u$, where $V_u = 0.9 \cdot V_{max}$. The ultimate ductility is defined as $\mu_u=\delta_u/\delta_e$ where the ultimate displacement $\delta_u$ corresponds to a strength degradation equal to 20% of $V_u$.

In the paper by Magenes et al. (2008) this second procedure has been used for the definition of the parameters of the bilinear curve for calcium-silicate walls CS01-CS08. In this document, instead, the procedure defined in Figure 44 has been applied. However, no appreciable differences have been found in the results applying the two different methods, as it was possible to verify comparing the results for walls CS01-CS08. The procedure followed in this report is however considered to be conceptually sounder.

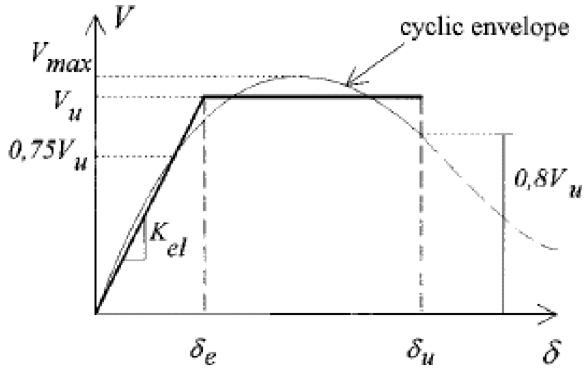


Figure 45. Hysteresis envelope and its bilinear idealization [Magenes and Calvi, 1997].

Ductility and displacement capacity were calculated for each wall considering the first, the second and third cycle envelope both for the positive and for the negative shear displacement envelope. The three positive and negative envelopes and the three positive and negative equivalent bilinear curves of all the tested walls are reported in annex B.

To ease the discussion of the results, in the following tables, for the different masonry typologies, selected values of the elastic stiffness $k_{el}$, the elastic displacement $\delta_e$, the ultimate displacement $\delta_u$, the ultimate ductility $\mu_u$, the ultimate drift $\delta_u/H$ and the failure mechanism are reported. The values in these tables were taken from the envelope (first cycle, second cycle or third cycle) which has been considered as more representative of the results of the test on the specific wall with regard to ultimate displacement capacity. It is, however, possible to evaluate the parameters of the idealised curves for all the three cycles of the experimental tests looking at the bi-linear curves reported in annex B.

The superscripts $^+$ and $^-$ refer to the positive and negative shear-displacement envelope. H is the height of the piers.

The superscript $^i$ after the name of the wall mean that the reported results in terms of ultimate displacement are relevant to the i-th cycle (for example $CL01^1$ means that the ultimate displacement was attained during the first of the three cycles programmed for a given target displacement).

### 5.2.1 Calcium-silicate masonry with "Optimised" units (CS01-CS08)

In the following table the parameters of the idealized curves of the cyclic envelopes of the cyclic tests carried out on the calcium silicate walls with "optimised" units are presented.

Table 7. Elastic stiffness, ultimate ductility and ultimate displacement. Walls CS01-CS08

| Test | $k_{el}^+$ [KN/mm] | $k_{el}^-$ [KN/mm] | $\delta_e^+$ [mm] | $\delta_e^-$ [mm] | $\delta_u^+$ [mm] | $\delta_u^-$ [mm] | $\mu_u^+$ | $\mu_u^-$ | $\mu_{u,min}$ | $\delta_u^+/H$ | $\delta_u^-/H$ | $(\delta_u/H)_{min}$ | Fail. Mech. |
|---|---|---|---|---|---|---|---|---|---|---|---|---|---|
| CS01[1] | 45 | 38 | 1.7 | 1.6 | 4.7 | 3.8 | 2.8 | 2.4 | 2.4 | 0.0019 | 0.0015 | 0.0015 | SHEAR |
| CS02[1] | 47 | 56 | 1.7 | 1.5 | 7.2 | 7.3 | 4.2 | 4.9 | 4.2 | 0.0029 | 0.0029 | 0.0029 | SHEAR |
| CS03[3] | 75 | 60 | 0.6 | 0.8 | 14.5 | 14.7 | 24.6 | 19.5 | 19.5 | 0.0058 | 0.0059 | 0.0058 | SHEAR |
| CS04[1] | 61 | 61 | 2.0 | 2.4 | 4.6 | 4.5 | 2.3 | 1.8 | 1.8 | 0.0018 | 0.0018 | 0.0018 | SHEAR |
| CS05[1] | 72 | 70 | 1.3 | 1.4 | 43.2 | 37.3 | 32.7 | 27.3 | 27.3 | 0.0173 | 0.0149 | 0.0149 | HYBRID |
| CS06[3] | 25 | 26 | 1.6 | 1.5 | 44.2 | 41.9 | 27.6 | 28.9 | 27.6 | 0.0177 | 0.0168 | 0.0168 | FLEXURE |
| CS07[3] | 146 | 144 | 1.5 | 1.5 | 30.1 | 30.1 | 19.8 | 19.8 | 19.8 | 0.0120 | 0.0120 | 0.0120 | HYBRID (GAPING) |
| CS08[3] | 55 | 81 | 2.8 | 2.1 | 21.6 | 21.0 | 7.7 | 10.0 | 7.7 | 0.0087 | 0.0084 | 0.0084 | HYBRID (GAPING) |

High ductility values were found for almost all walls including some of those failing in shear. The lower values were reported for wall CS01 and CS04 for which a sudden drop in the strength was due to brittle diagonal shear crack (CS01 was affected also by loss of control once the diagonal crack developed), whereas walls CS02 despite failing with diagonal cracking, displayed a slightly higher ductility and drift capacity. Wall CS03, characterized by progressive damage propagation for opening and closing of the vertical unfilled head joints attained a remarkable ductility and drift. Wall CS05 characterized by the presence of head joints filled by mortar was able to largely exceed 1% drift with a flexure-dominated response before the occurrence of a diagonal shear crack.

Very high values of ductility and drift capacity were found for walls CS06, CS07 and CS08. The behaviour of wall CS06 is typical of rocking-flexure failure. Walls CS07 and CS08 displayed however the coexistence of a force-displacement response typical of rocking systems with the presence of stepped inclined cracks interesting bed- and headjoints (gaping mechanism) and could be considered a sort of hybrid mechanism. The maximum displacement attained for such walls was more related to the experimental set-up displacement capacity or to the local damage more than significant shear strength degradation. Wall CS08, tested as a cantilever, attained unexpectedly a lower drift and ductility than its double fixed counterpart (CS07), although the drift capacity is quite high compared to the walls failing in shear.

In the case of walls failing by shear, the drift capacities were very low, especially in the case of high values of axial load. Wall CS04 attained a value of drift less than 0.14%.

The failure mechanism of walls CS05, has been classified conventionally as "hybrid" due to the coexistence of a force-displacement response typical of rocking systems, attaining large drifts, which at some point comes to an abrupt failure due to the development of a stepped diagonal crack.

It is interesting to note that similar elastic stiffness $k_{el}$ (as defined in Figure 44) was found for walls having same dimensions and same boundary conditions independently from the axial load.

### 5.2.2 Calcium-silicate masonry with "Quadro E" units (CS09-CS14)

In the following table the parameters of the bilinear curves of the cyclic envelopes of the cyclic tests carried out on the calcium silicate walls with "Quadro E" units are presented.

Table 8. Elastic stiffness, ultimate ductility and ultimate displacement. Walls CS09-CS14

| Test | $k_{el}^+$ [KN/mm] | $k_{el}^-$ [KN/mm] | $\delta_e^+$ [mm] | $\delta_e^-$ [mm] | $\delta_u^+$ [mm] | $\delta_u^-$ [mm] | $\mu_u^+$ | $\mu_u^-$ | $\mu_{u,min}$ | $\delta_u^+/H$ | $\delta_u^-/H$ | $(\delta_u/H)_{min}$ | Fail. Mech. |
|---|---|---|---|---|---|---|---|---|---|---|---|---|---|
| CS09[3] | 57 | 63 | 1.5 | 1.3 | 5.5 | 5.8 | 3.7 | 4.6 | 3.7 | 0.0022 | 0.0023 | 0.0022 | SHEAR |
| CS10[3] | 75 | 64 | 1.1 | 1.3 | 9.4 | 9.8 | 8.8 | 7.4 | 7.4 | 0.0038 | 0.0039 | 0.0038 | SHEAR |
| CS11[1] | 25 | 17 | 3.1 | 5.0 | 14.2 | 14.5 | 4.5 | 2.9 | 2.9 | 0.0057 | 0.0058 | 0.0057 | SHEAR |
| CS12[1] | 52 | 55 | 2.3 | 2.4 | 9.5 | 9.7 | 4.1 | 4.0 | 4.0 | 0.0038 | 0.0039 | 0.0038 | SHEAR |
| CS13[1] | 44 | 62 | 7.5 | 4.3 | 30.2 | 31.1 | 4.0 | 7.2 | 4.0 | 0.0121 | 0.0124 | 0.0121 | SHEAR |
| CS14[2] | 12 | 16 | 6.6 | 5.1 | 24.1 | 24.8 | 3.7 | 4.9 | 3.7 | 0.0097 | 0.0099 | 0.0097 | ANCHOR. |

The unreinforced wall CS09 failed in shear with the occurrence of stepped diagonal cracks along the height of the wall. This wall experienced a minimum ultimate ductility equal to 3.7 and very low drift capacity (0.22%). The elastic stiffness was found very similar to the stiffness computed for the walls constructed with "optimised" units.

The ductility of the slender confined walls CS10, CS11 and CS12 was found to be variable from 2.9 (in the case of vertical stress of 0.5 MPa) to 7.4 (vertical stress equal to 1 MPa). Since these walls failed by shear, the drift capacities were low (0.38%). A higher value of displacement capacity was evaluated in the case of wall CS11 on which the lower value of axial load was applied (0.5 MPa). However, even for wall CS11 the ultimate drift was less than 0.6%. Quite similar elastic stiffness $k_{el}$ was found for walls CS10 and CS12 independently from the axial load.

For the tested slender confined walls it appears that the contribution of the vertical reinforcement does not increase significatively the deformation capacity neither the shear strength of the walls.

Values of ductility higher than the majority of the other confined walls was estimated for wall CS13. The damage pattern occurred to the wall appeared to be a typical shear failure mechanism even if a rather high value of displacement capacity was found (ultimate drift =1.21 %) before a significant loss of strength. The elastic stiffness of the confined wall CS13 is quite similar to the elastic stiffness of the unreinforced wall CS08.

A high value of displacement capacity (drift equal to about 1%) was found for wall CS14 (post-tensioned wall). Large strength degradation occurred for the failure of the anchorage in the r.c. foundation of the tendon on the right side. If no failure in the anchorage had occurred, the ultimate ductility and the ultimate displacement would probably have been higher.

### 5.2.3 Hollow clay masonry: "German" typologies (CL01-CL03)

In the following table the parameters of the bilinear curves of the cyclic envelopes of the cyclic tests carried out on the German hollow clay unit walls are defined.

Table 9. Ultimate ductility and ultimate displacement. Walls CL01-CL03

| Test | $k_{el}^+$ [KN/mm] | $k_{el}^-$ [KN/mm] | $\delta_e^+$ [mm] | $\delta_e^-$ [mm] | $\delta_u^+$ [mm] | $\delta_u^-$ [mm] | $\mu_u^+$ | $\mu_u^-$ | $\mu_{u,min}$ | $\delta_u^+/H$ | $\delta_u^-/H$ | $(\delta_u/H)_{min}$ | Fail. Mech. |
|---|---|---|---|---|---|---|---|---|---|---|---|---|---|
| CL01[1] | 59 | 38 | 0.8 | 1.2 | 75.9 | 72.6 | 95.7 | 60.6 | 60.6 | 0.0304 | 0.0290 | 0.0290 | FLEX. |
| CL02[3] | 16 | 22 | 3.9 | 2.6 | 51.9 | 35.5 | 13.3 | 13.8 | 13.3 | 0.0208 | 0.0142 | 0.0142 | FLEX. |
| CL03[1] | 27 | 35 | 0.8 | 0.6 | 37.2 | 36.6 | 48.5 | 59.6 | 48.5 | 0.0149 | 0.0146 | 0.0146 | FLEX. |

Very high values of ductility and drift capacity were found for walls CL01 and CL03. This behaviour is typical of rocking-flexure failure. The maximum displacement attained for such walls was more related to the experimental set-up displacement capacity or to the local damage more than significant shear strength degradation.

The confined wall CL02, tested as a cantilever, failed by flexure. High values of ductility were found although the maximum displacement was associated to significant shear strength degradation due to the damage at the compressed corner.

### 5.2.4 Hollow clay masonry: "Italian" typologies (CL04-CL10)

In the following table the parameters of the bilinear curves of the cyclic envelopes of the cyclic tests carried out on the Italian hollow clay unit walls are defined.
The values associated to wall CL04 have been omitted because of the way in which the wall was tested (test carried out in two phases with two different levels of axial force).

Table 10. Ultimate ductility and ultimate displacement. Walls CL04-CL10

| Test | $k_{el}^+$ [KN/mm] | $k_{el}^-$ [KN/mm] | $\delta_e^+$ [mm] | $\delta_e^-$ [mm] | $\delta_u^+$ [mm] | $\delta_u^-$ [mm] | $\mu_u^+$ | $\mu_u^-$ | $\mu_{u,min}$ | $\delta_u^+/H$ | $\delta_u^-/H$ | $(\delta_u/H)_{min}$ | Fail. Mech. |
|---|---|---|---|---|---|---|---|---|---|---|---|---|---|
| CL05[1] | 106 | 123 | 3.2 | 2.8 | 6.5 | 6.8 | 2.0 | 2.5 | 2.0 | 0.0025 | 0.0026 | 0.0025 | SHEAR |
| CL06[1] | 40 | 40 | 2.0 | 2.0 | 51.5 | 50.8 | 25.9 | 25.3 | 25.3 | 0.0198 | 0.0195 | 0.0195 | FLEXURE |
| CL07[3] | 19 | 26 | 3.9 | 3.3 | 5.9 | 6.5 | 1.5 | 2.0 | 1.5 | 0.0023 | 0.0025 | 0.0023 | SHEAR |
| CL08[1] | 68 | 80 | 3.8 | 3.4 | 13.1 | 12.8 | 3.4 | 3.8 | 3.4 | 0.0050 | 0.0049 | 0.0049 | SHEAR |
| CL09[3] | 24 | 23 | 2.7 | 3.1 | 5.4 | 7.2 | 2.0 | 2.3 | 2.0 | 0.0021 | 0.0028 | 0.0021 | SHEAR |
| CL10[1] | 71 | 66 | 3.0 | 3.3 | 11.3 | 12.3 | 3.8 | 3.8 | 3.8 | 0.0043 | 0.0047 | 0.0043 | SHEAR |

In the wall CL06 no diagonal cracks occurred during the test and the wall displayed a typical rocking behaviour without any relevant energy dissipation. Strength degradation after the peak occurred since the resultant of the compression moved towards the centre of the panel for the concentration of the damage in the compressed corners. However, very high values of ductility and displacement capacity (a maximum drift of about 2%) were found.
Small values of ductility and ultimate displacement were instead found for the walls failing in shear.
For all the masonry typologies, the maximum drift for the walls failing in shear (all walls except wall CL06) did not exceed 0.5 %, in some cases barely attaining 0.2%.
The 2.5 m long wall constructed with general purpose mortar bedjoints and headjoints (CL05) attained a very small value of ductility and deformation capacity.
Walls CL08 and CL10, constructed with T+G units with unfilled headjoints, having the same dimensions and the same vertical loads of wall CL05, were less resistant but attained a higher displacement capacity, approaching 0.4% drift.
No evident differences in terms of ductility and in terms of displacement capacity were found for the walls with T+G units between different types of mortar bedjoints. The slender wall CL07 with general purpose mortar bedjoints and the slender wall CL09 with thin layer mortar bedjoints showed very similar values of ultimate ductility (1.5 and 2) and of ultimate drift (0.23% and 0.21%). Same conclusions can be drawn for walls CL08 and CL10. In fact the

ultimate ductility and the ultimate drift for wall CL08 were 3.4 and 0.49%, whereas for wall CL10 were 3.8 and 4.3% respectively.

Very similar values of elastic stiffness were also found for the walls with T+G units between the two different types of mortar bedjoints.

### 5.2.5 Lightweight aerated concrete masonry (LAC01-LAC04)

Finally, in the following table the parameters of the bilinear curves of the cyclic envelopes of the cyclic tests carried out on lightweight aerated concrete masonry walls are reported.

Table 11. Ultimate ductility and ultimate displacement. Walls LAC01-LAC04

| Test | $k_{el}^+$ [KN/mm] | $k_{el}^-$ [KN/mm] | $\delta_e^+$ [mm] | $\delta_e^-$ [mm] | $\delta_u^+$ [mm] | $\delta_u^-$ [mm] | $\mu_u^+$ | $\mu_u^-$ | $\mu_{u,min}$ | $\delta_u^+/H$ | $\delta_u^-/H$ | $(\delta_u/H)_{min}$ | Fail. Mech. |
|---|---|---|---|---|---|---|---|---|---|---|---|---|---|
| LAC01[3] | 68 | 84 | 1.6 | 1.4 | 24.3 | 23.7 | 15.2 | 17.3 | 15.2 | 0.0097 | 0.0095 | 0.0095 | HYBRID (GAPING) |
| LAC02[1] | 83 | 110 | 1.4 | 1.0 | 37.4 | 35.7 | 25.9 | 34.1 | 25.9 | 0.0149 | 0.0143 | 0.0143 | HYBRID (GAPING) |
| LAC03[3] | 105 | 122 | 2.0 | 1.8 | 18.7 | 19.1 | 9.2 | 10.8 | 9.2 | 0.0075 | 0.0076 | 0.0075 | HYBRID (GAPING) |
| LAC04[3] | 128 | 103 | 1.7 | 2.1 | 18.7 | 18.9 | 11.0 | 9.0 | 9.0 | 0.0075 | 0.0076 | 0.0075 | HYBRID (GAPING) |

The failure mechanism of all the lightweight aerated concrete masonry walls has been classified conventionally as “hybrid” due to the coexistence of a force-displacement response typical of rocking systems with the presence of stepped inclined cracks interesting bed- and headjoints (gaping failure mechanism). All the walls were able to exceed 0.75% drift before the occurrence of a diagonal shear crack.

Very high values of ultimate ductility and drift were attained for the wall LAC02 (wall constructed with thin layer mortar bedjoints and vertical stress of 0.5 MPa).

As for the clay masonry with tongue and groove units, no main differences in terms of the elastic stiffness were evident between the walls with the two different types of mortar bedjoints.

## 5.3 Energy dissipation capacity

The dissipated hysteretic energy was examined in terms of equivalent viscous damping, which, given a single load–displacement cycle can be expressed as a function of the dissipated energy $W_d$ and the elastic energy at peak displacement $W_e$: $\xi_{eq}=W_d/2\pi(W_e^{+}+W_e^{-})$.

### 5.3.1 Calcium-silicate masonry with "optimised" units (CS01-CS08)

For calcium-silicate masonry with "optimised" units, the results of the calculated equivalent viscous damping $\xi_{eq}$ are plotted in Figure 46 as a function of the displacement ductility ($\delta/\delta_e$) and of the drift ($\delta$/H) of each cycle and considering the first, the second and the third cycle at each target displacement.

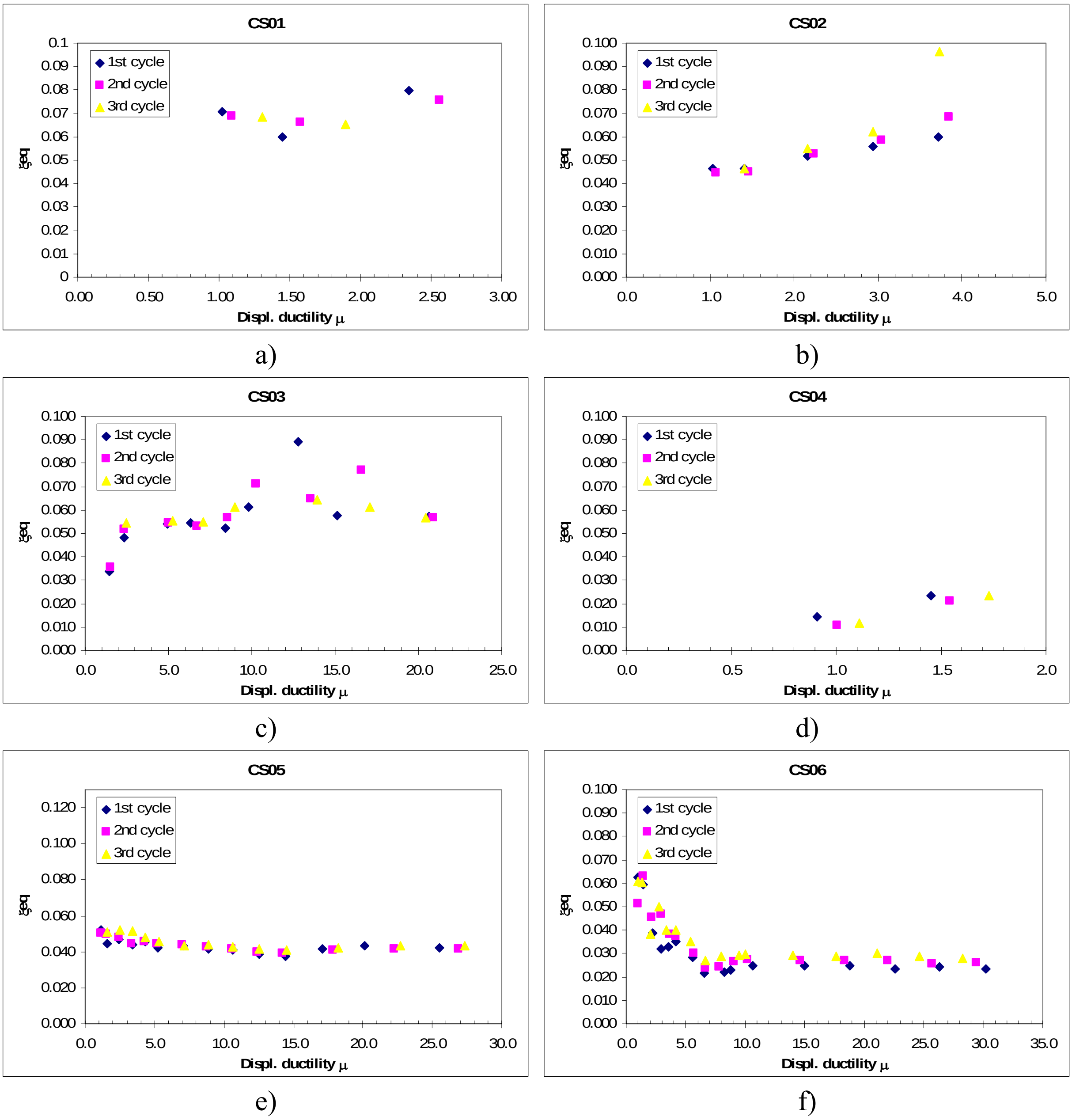

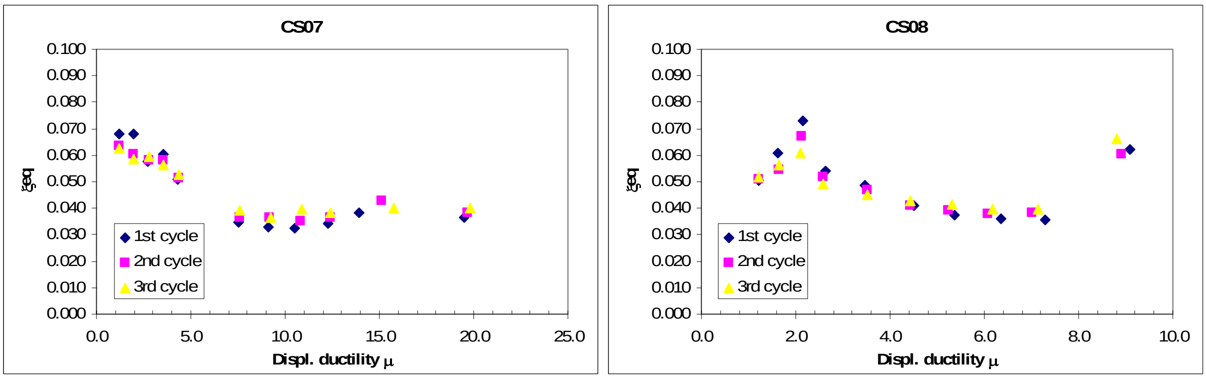


g) h)

Figure 46. Equivalent viscous damping ratio calculated from the hysteresis loop as a function of ductility ($\mu=\delta/\delta_e$), where $\delta$ is the maximum displacement of the cycle. Walls CS01-CS08

Except for wall CS07, the equivalent viscous damping $\xi_{eq}$ associated to the cycles corresponding to failure (ultimate) was not plotted.

It may be observed that the cycles have moderate dissipativity both for shear failures and for flexural failures. The equivalent viscous damping $\xi_{eq}$ was found to be less than 7-8% for almost all cycles, most often around 4%. In wall CS04 very small dissipation occurred, since the wall, before shear failure, behaved essentially in the elastic range. No clear distinction between flexural and shear failure can be noticed looking at the $\xi_{eq}$-$\mu$ plots.

### 5.3.2 Calcium-silicate masonry with "Quadro E" units (CS09-CS14)

For calcium-silicate masonry with "Quadro E" units, the results of the calculated equivalent viscous damping $\xi_{eq}$ are plotted in the following figure as a function of the displacement ductility ($\delta/\delta_e$) and of the drift ($\delta/H$) of each cycle and considering the first, the second and the third cycle at each target displacement.

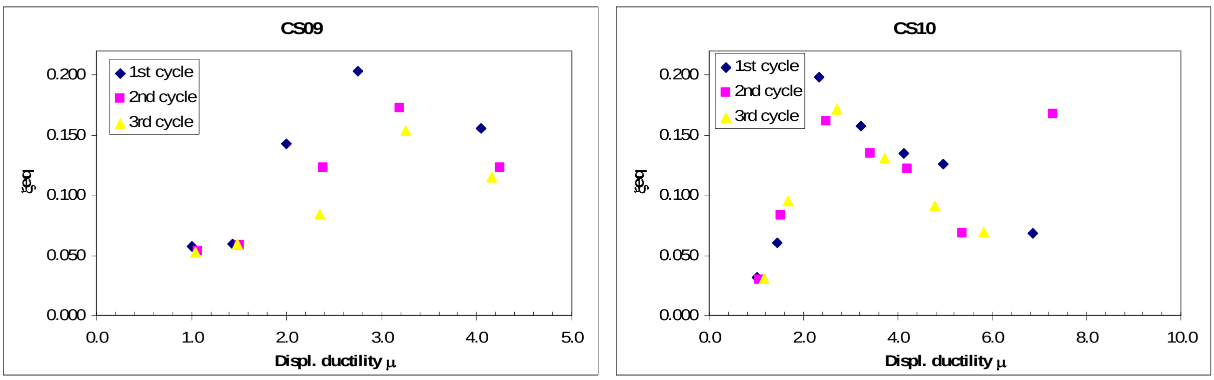


a) b)

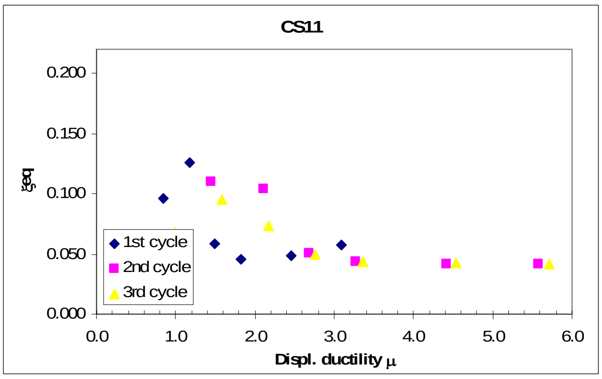


c)

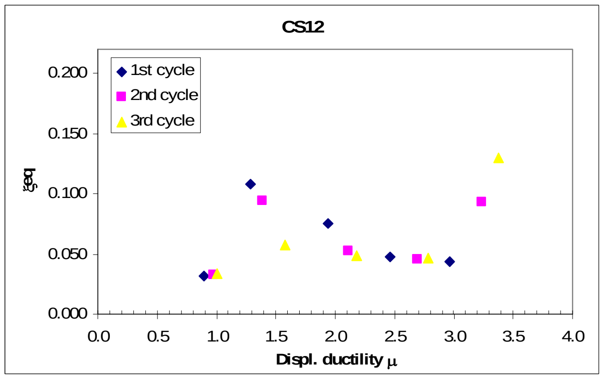


d)

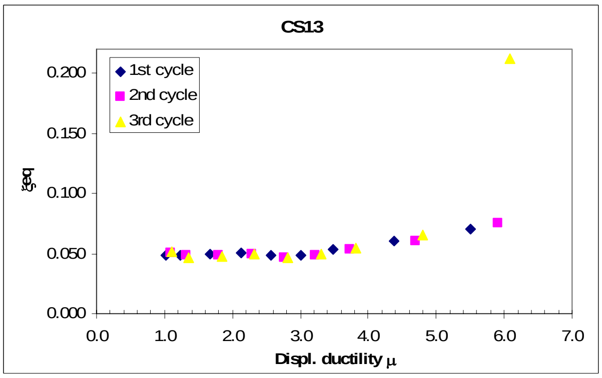


e)

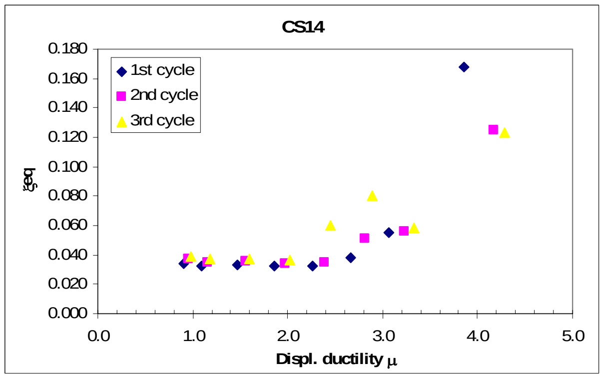


f)

Figure 47. Equivalent viscous damping ratio calculated from the hysteresis loop as a function of ductility. Walls CS09-CS14

The equivalent viscous damping $\xi_{eq}$ was found to be higher than 10 % for some cycles of walls that failed by shear (CS09 to CS12) but a unique trend as a function of the ductility was not found. When diagonal cracks occurred in the units, an increase of the value of the damping was observed. The opening and the closing of the cracks in the bedjoints and in the headjoints did not produce cycles with high energy dissipation.

The trend of the equivalent damping was found to be more regular for walls CS13 and CS14 where the energy dissipation increased as the ductility increased. In these walls the mean value of the damping was around 5% with peaks higher than 15 % when major cracks occurred and the collapse of the walls was imminent.

### 5.3.3 Hollow clay masonry: "German" typologies (CL01-CL03)

For "German" hollow clay masonry, the results of the calculated equivalent viscous damping $\xi_{eq}$ are plotted in the following figure as a function of the displacement ductility ($\delta/\delta_e$) and of the drift ($\delta/H$) of each cycle and considering the first, the second and the third cycle at each target displacement.

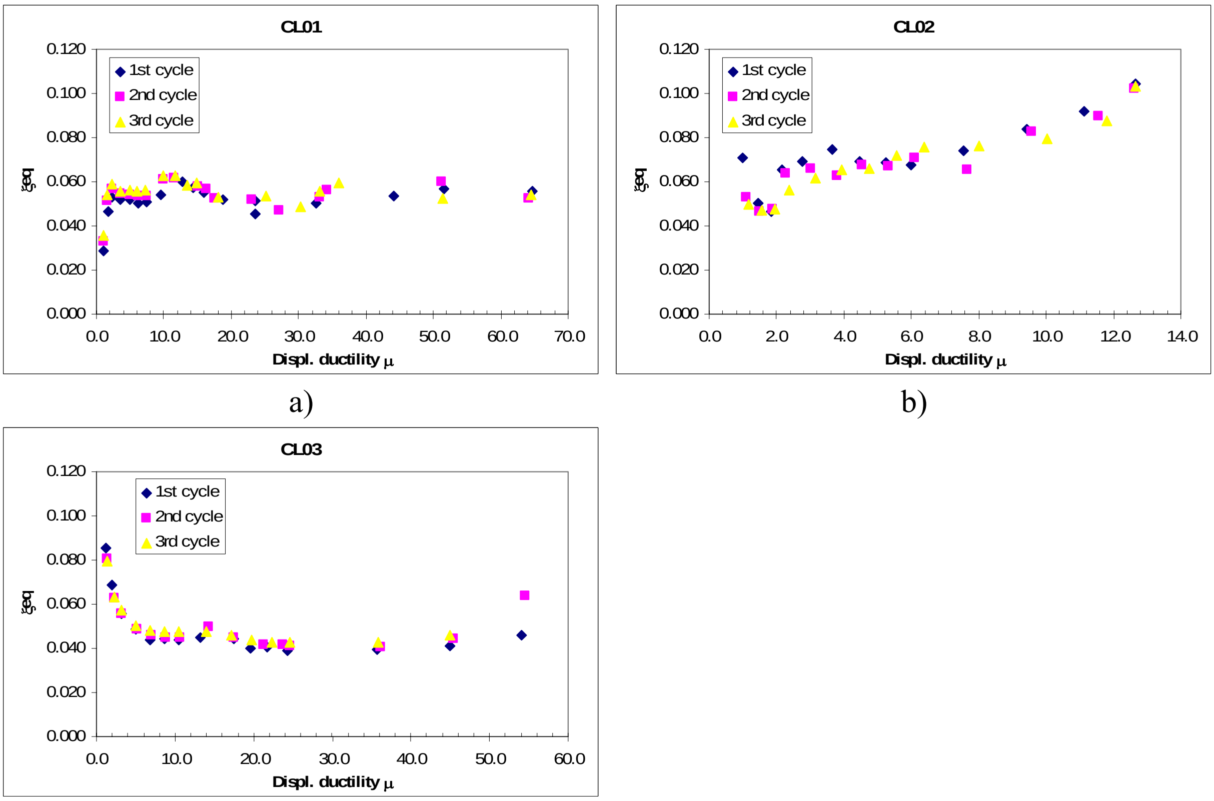


a) b) c)

Figure 48. Equivalent viscous damping ratio calculated from the hysteresis loop as a function of ductility. Walls CL01-CL03

The cycles of these walls have low dissipativity. All these walls failed in flexure.

The equivalent viscous damping $\xi_{eq}$ for unreinforced walls CL01 and CL03 was found to be around 5% and almost constant for all cycles. In the confined wall CL02 higher dissipation occurred because of the yielding of the vertical bars; the equivalent viscous damping increased linearly as a function of the ductility from 5 to 10%.

### 5.3.4 Hollow clay masonry: "Italian" typologies (CL04-CL10)

For "Italian" hollow clay masonry, the results of the calculated equivalent viscous damping $\xi_{eq}$ are plotted in the following figure as a function of the displacement ductility ($\delta/\delta_e$) and of the drift ($\delta$/H) of each cycle and considering the first, the second and the third cycle at each target displacement.

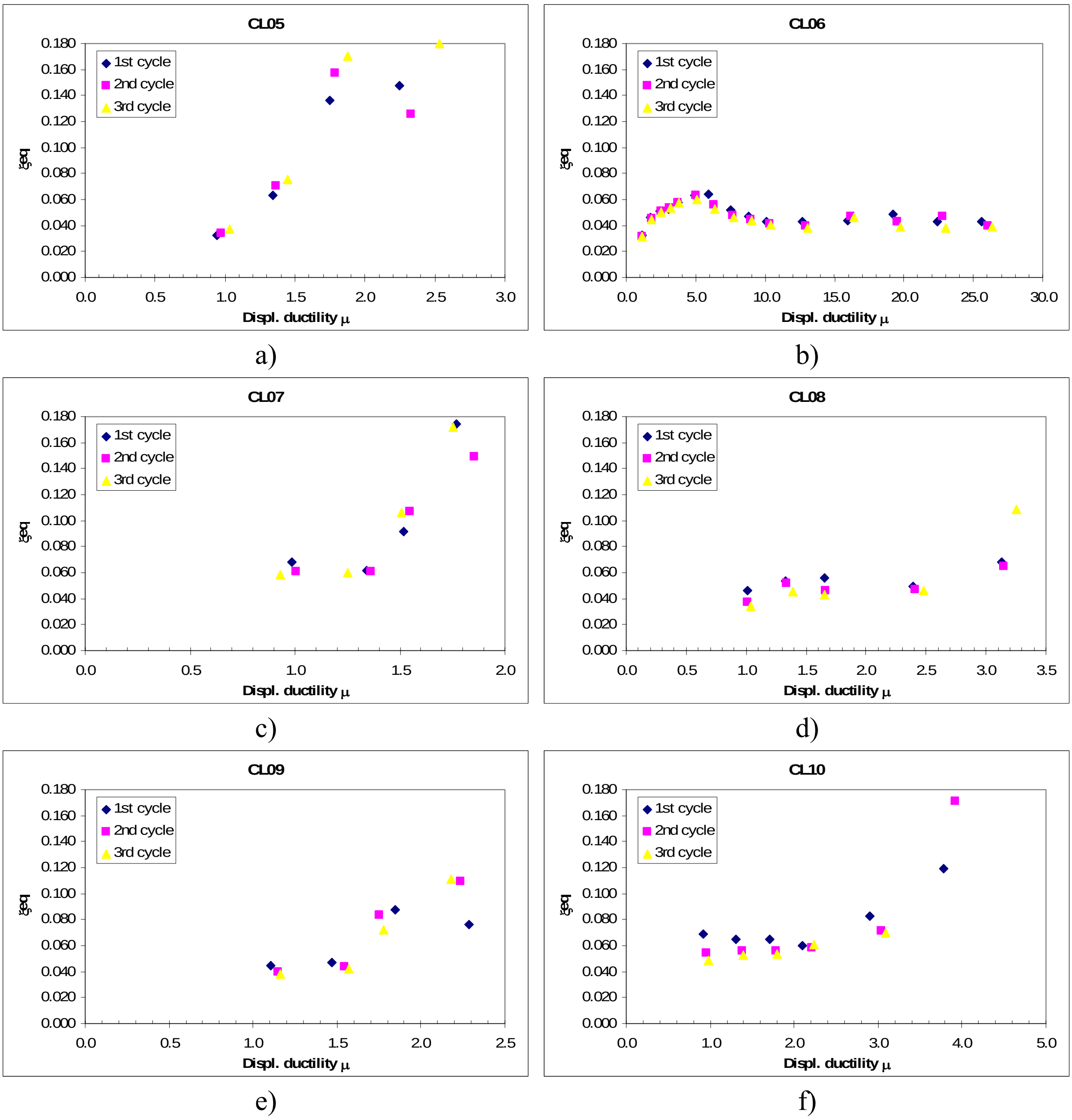


Figure 49. Equivalent viscous damping ratio calculated from the hysteresis loop as a function of ductility. Walls CL05-CL10

The trend of the equivalent viscous damping was similar for all the walls that failed in shear. The damping increased as the ductility increased from 5 % up to values higher than 10 %.

It may be observed that the cycles of the wall that failed for flexure (CL06) have low dissipation. The damping was found to be around 5% and almost constant for all cycles.

A clear distinction between shear and flexural failure can be noticed looking at the $\xi_{eq}$-$\mu$ plots.

### 5.3.5 Lightweight aerated concrete masonry (LAC01-LAC04)

Finally, for lightweight aerated concrete masonry, the results of the calculated equivalent viscous damping $\xi_{eq}$ are plotted in the following figure as a function of the displacement ductility ($\delta/\delta_e$) and of the drift ($\delta/H$) of each cycle and considering the first, the second and the third cycle at each target displacement.

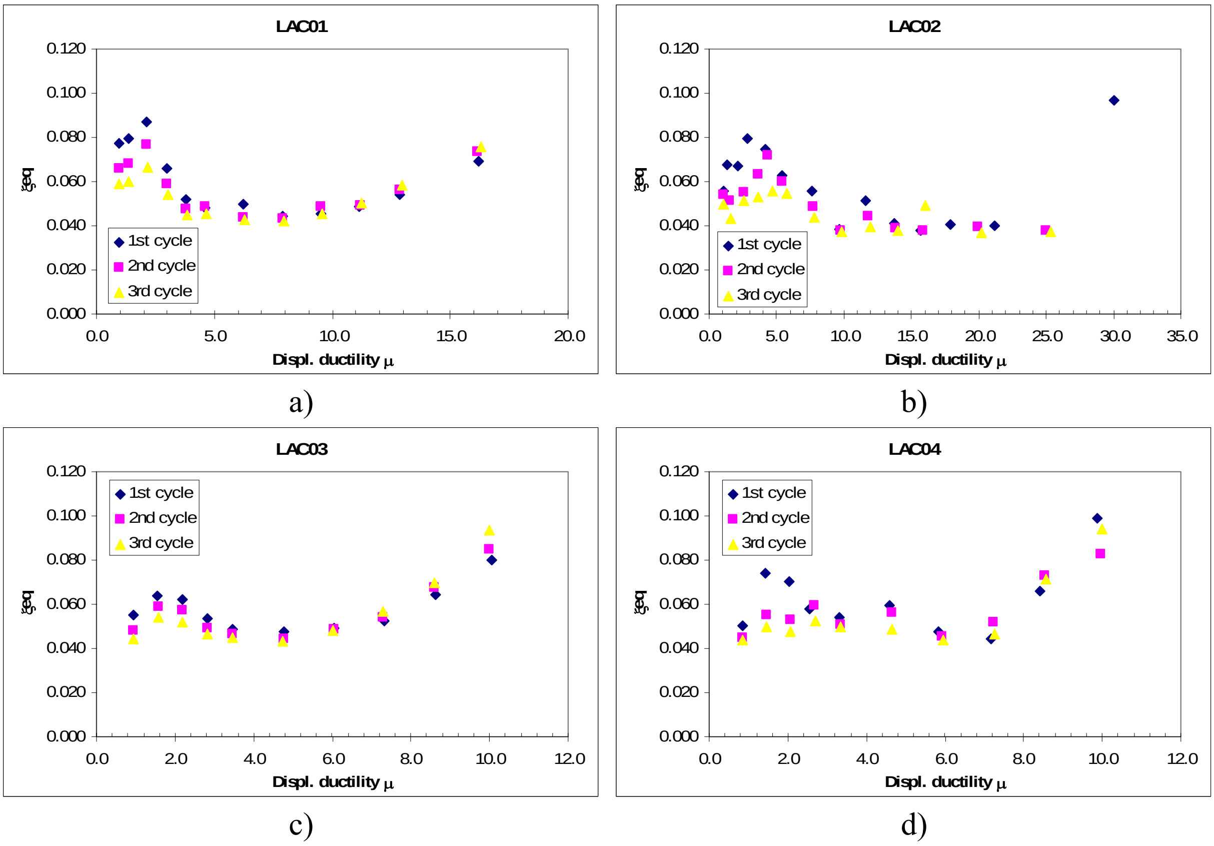


Figure 50. Equivalent viscous damping ratio calculated from the hysteresis loop as a function of ductility. Walls LAC01-LAC04

For the failure mechanism classified conventionally as “hybrid” (coexistence of a force-displacement response typical of rocking systems with the presence of stepped inclined cracks interesting bed- and headjoints) the dissipation of the cycles was rather low. The equivalent viscous damping $\xi_{eq}$ was found to be less than 8% for almost all cycles, most often around 5%.

# 6.CONCLUSIONS

The results of the experimental campaign on in-plane cyclic behaviour of unreinforced and confined masonry walls have been presented. Tests were carried out on walls made of calcium silicate, lightweight hollow clay and aerated concrete units with thin layer mortar and general purpose mortar and the results were here discussed in terms of deformation and energy dissipation capacity. The results represent a useful reference for seismic design purposes.

A wide variation in ductility and drift capacity has been reported depending on the failure mode which is in turn influenced by geometry, level of axial load and boundary conditions. When diagonal cracking in units is avoided, high drift capacities can be attained, sometimes exceeding 1.0% or more, whereas very brittle behaviour is reported when diagonal cracks develop through the units. In particular, very low drift capacity was reported in presence of high mean vertical compression ratios. It appears therefore as an important seismic design criterion to limit compression stresses in walls to avoid bad performance, since the increase in shear strength due to axial compression may not compensate the reduction in deformation capacity.

No evident differences in terms of elastic stiffness, ductility, displacement capacity and shear strength were found for the Italian clay masonry walls with T+G units between different types of mortar bedjoints. The walls with general purpose mortar bedjoints and the same walls with thin layer mortar bedjoints showed very similar values of ultimate ductility and of ultimate drift.

As for the clay masonry with tongue and groove units, also for lightweight aerated concrete masonry walls no main differences in terms of the elastic stiffness were evident between the walls with the two different types of mortar bedjoints.

Further work will be dedicated to the interpretation of the results in terms of measured strengths, especially important for the walls that displayed diagonal cracking failure and hybrid failure mechanisms.

# REFERENCES

[1] Kalksandstein – Bundesverband Kalksanstein Industrie eV. : www.kalksandsteind.de

[2] Magenes, G. and Calvi, G.M., (1997) In-plane seismic response of brick masonry walls, *Earthquake Engineering and Structural Dynamics*, Vol. 26, 1091-1112.

[3] Tomaževič, M. Lutman, M, Petković, (1993) Seismic behaviour of masonry walls: experimental simulation, *J.Struct. Enrg., ASCE,* 122 (9), 1040-1047.

[4] Grabowski, S. (2005), D 5.5 Material properties for the tests in WP 7 and 8 and the verification of the design model of WP 4. *Report of WP 5; Project ESECMaSE*.

[5] Magenes, G., Morandi, P., Penna, A. (2008), In plane cyclic tests of calcium silicate masonry walls, *12th International Brick/Block Masonry Conference, Sydney 18-20 February 2008*.

# ANNEX A: tests on materials

## A1 Tests on mortar used for the “Italian” clay masonry

The tests for the evaluation of flexural and compression strength of the hardened mortar are here presented.

In the following table the results of the tests on the general purpose mortar used for construction of the walls CL04, CL05 and CL06 (M5 pre-mixed mortar according to EN 998-2) are reported.

**FLEXURE-COMPRESSION**

**DATE: 04/06/2007 time 14:00**

**L [mm]** 100

| Mortar speciment | Length [mm] | Width [mm] | Height [mm] | Flexural ultimate load [N] | Compression ultimate load [N] | Mass [kg] | Sp. weight [kg/m$^3$] | $f_{fl}$ [N/mm$^2$] | $f_m$ [N/mm$^2$] | Mean values $f_{fl}$ [N/mm$^2$] | Mean values $f_m$ [N/mm$^2$] | |
|---|---|---|---|---|---|---|---|---|---|---|---|---|
| 29-03-2007 | 160 | 40 | 40 | 1118 | 14519 | | | 2.62 | 9.07 | | | |
| Gen. p. mortar | | | | | 8927 | | | | 5.58 | | | |
| M5 MORTAR (EN 998-2) | 160 | 40 | 40 | 1138 | 9172 | | | 2.67 | 5.73 | | | |
| | | | | | 9074 | | | | 5.67 | | | |
| | 160 | 40 | 40 | 1138 | 12998 | | | 2.67 | 8.12 | | | |
| | | | | | 14077 | | | | 8.80 | **2.65** | **7.16** | |
| 30-03-2007 | 160 | 40 | 40 | 1138 | 10399 | | | 2.67 | 6.50 | | | |
| Gen. p. mortar | | | | | 13783 | | | | 8.61 | | | |
| M5 MORTAR (EN 998-2) | 160 | 40 | 40 | 1059 | 13685 | | | 2.48 | 8.55 | | | |
| | | | | | 13832 | | | | 8.65 | | | |
| | 160 | 40 | 40 | 961 | 9957 | | | 2.25 | 6.22 | | | |
| | | | | | 13047 | | | | 8.15 | **2.47** | **7.78** | |
| 02-04-2007 a) | 160 | 40 | 40 | 1138 | 16039 | | | 2.67 | 10.02 | | | |
| Gen. p. mortar | | | | | 14568 | | | | 9.10 | | | |
| M5 MORTAR (EN 998-2) | 160 | 40 | 40 | 1236 | 12704 | | | 2.90 | 7.94 | | | |
| | | | | | 11919 | | | | 7.45 | | | |
| | 160 | 40 | 40 | 1069 | 14421 | | | 2.51 | 9.01 | | | |
| | | | | | 12361 | | | | 7.73 | **2.69** | **8.54** | |
| 02-04-2007 b) | 160 | 40 | 40 | 952 | 11183 | | | 2.23 | 6.99 | | | |
| Gen. p. mortar | | | | | 10791 | | | | 6.74 | | | |
| M5 MORTAR (EN 998-2) | 160 | 40 | 40 | 942 | 11870 | | | 2.21 | 7.42 | | | |
| | | | | | 12557 | | | | 7.85 | | | |
| | 160 | 40 | 40 | 1010 | 11772 | | | 2.37 | 7.36 | | | |
| | | | | | 9418 | | | | 5.89 | **2.27** | **7.04** | |
| 03-04-2007 | 160 | 40 | 40 | 942 | 11968 | 0.514 | 2009 | 2.21 | 7.48 | | | |
| Gen. p. mortar | | | | | 9025 | | | | 5.64 | | | |
| M5 MORTAR (EN 998-2) | 160 | 40 | 40 | 991 | 13145 | 0.522 | 2039 | 2.32 | 8.22 | | | |
| | | | | | 9516 | | | | 5.95 | | | |
| | 160 | 40 | 40 | 834 | 7750 | 0.519 | 2028 | 1.95 | 4.84 | | | |
| | | | | | 9614 | | | | 6.01 | **2.16** | **6.36** | |
| | | | | | | | | | | **2.45** | **7.38** | **MEAN** |

In the following table the results of the tests on the general purpose mortar used for construction of the walls CL07 and CL08 (M5 pre-mixed mortar according to EN 998-2) are reported.

**FLEXURE-COMPRESSION**
**DATE: 07/11/2007 time 14:00**
**L [mm]** 100

| Mortar speciment | Length [mm] | Width [mm] | Height [mm] | Flexural ultimate load [N] | Compression ultimate load [N] | Mass [kg] | Sp. weight [kg/m³] | $f_{fl}$ [N/mm²] | $f_m$ [N/mm²] | Mean values $f_{fl}$ [N/mm²] | Mean values $f_m$ [N/mm²] |
|---|---|---|---|---|---|---|---|---|---|---|---|
| 27-09-2007 | 160 | 40 | 40 | 1030 | 17805 | | | 2.41 | 11.13 | | |
| Gen. p. mortar | | | | | 17020 | | | | 10.64 | | |
| M5 MORTAR (EN 998-2) | 160 | 40 | 40 | 1069 | 17069 | | | 2.51 | 10.67 | | |
| | | | | | 15892 | | | | 9.93 | | |
| | 160 | 40 | 40 | 1050 | 16236 | | | 2.46 | 10.15 | | |
| | | | | | 14960 | | | | 9.35 | **2.46** | **10.31** |
| 27-09-2007 | 160 | 40 | 40 | 1050 | 17805 | | | 2.46 | 11.13 | | |
| Gen. p. mortar | | | | | 18541 | | | | 11.59 | | |
| M5 MORTAR (EN 998-2) | 160 | 40 | 40 | 1167 | 15696 | | | 2.74 | 9.81 | | |
| | | | | | 16628 | | | | 10.39 | | |
| | 160 | 40 | 40 | 1177 | 16922 | | | 2.76 | 10.58 | | |
| | | | | | 15892 | | | | 9.93 | **2.65** | **10.57** |
| 28-09-2007 | 160 | 40 | 40 | 1207 | 20944 | | | 2.83 | 13.09 | | |
| Gen. p. mortar | | | | | 22073 | | | | 13.80 | | |
| M5 MORTAR (EN 998-2) | 160 | 40 | 40 | 1187 | 20601 | | | 2.78 | 12.88 | | |
| | | | | | 20111 | | | | 12.57 | | |
| | 160 | 40 | 40 | 1197 | 19767 | | | 2.81 | 12.35 | | |
| | | | | | 21239 | | | | 13.27 | **2.81** | **12.99** |
| 29-09-2007 | 160 | 40 | 40 | 1010 | 17903 | | | 2.37 | 11.19 | | |
| Gen. p. mortar | | | | | 18001 | | | | 11.25 | | |
| M5 MORTAR (EN 998-2) | 160 | 40 | 40 | 1059 | 15941 | | | 2.48 | 9.96 | | |
| | | | | | 17069 | | | | 10.67 | | |
| | 160 | 40 | 40 | 1099 | 18688 | | | 2.58 | 11.68 | | |
| | | | | | 18590 | | | | 11.62 | **2.48** | **11.06** |
| 01-10-2007 | 160 | 40 | 40 | 991 | 14421 | | | 2.32 | 9.01 | | |
| Gen. p. mortar | | | | | 13636 | | | | 8.52 | | |
| M5 MORTAR (EN 998-2) | 160 | 40 | 40 | 961 | 12998 | | | 2.25 | 8.12 | | |
| | | | | | 11919 | | | | 7.45 | | |
| | 160 | 40 | 40 | 932 | 12998 | | | 2.18 | 8.12 | | |
| | | | | | 13538 | | | | 8.46 | **2.25** | **8.28** |
| | | | | | | | | | | **2.53** | **10.64** MEAN |

Finally, the results of the tests on the thin layer mortar used for construction of the walls CL09 and CL10 (M10 pre-mixed mortar according to EN 998-2) are shown.

| Mortar speciment | Length [mm] | Width [mm] | Height [mm] | Flexural ultimate load [N] | Compression ultimate load [N] | Mass [kg] | Sp. weight [kg/m³] | $f_{fl}$ [N/mm²] | $f_m$ [N/mm²] | $f_{fl}$ [N/mm²] | $f_m$ [N/mm²] |
|---|---|---|---|---|---|---|---|---|---|---|---|
| 08-10-2007 | 160 | 40 | 40 | 746 | 14568 | | | 1.75 | 9.10 | | |
| Thin. layer. mortar | | | | | 15794 | | | | 9.87 | | |
| M10 mortar (EN 998-2) | 160 | 40 | 40 | 520 | 16481 | | | 1.22 | 10.30 | | |
| | | | | | 16677 | | | | 10.42 | | |
| | 160 | 40 | 40 | 598 | 17069 | | | 1.40 | 10.67 | | |
| | | | | | 16579 | | | | 10.36 | **1.46** | **10.12** |
| 08-10-2007 | 160 | 40 | 40 | 569 | 16334 | | | 1.33 | 10.21 | | |
| Thin. layer. mortar | | | | | 17020 | | | | 10.64 | | |
| M10 mortar (EN 998-2) | 160 | 40 | 40 | 706 | 15892 | | | 1.66 | 9.93 | | |
| | | | | | 16481 | | | | 10.30 | | |
| | 160 | 40 | 40 | 687 | 16971 | | | 1.61 | 10.61 | | |
| | | | | | 16481 | | | | 10.30 | **1.53** | **10.33** |
| | | | | | | | | | | **1.49** | **10.23** MEAN |

# A2 Tests on the calcium-silicate masonry with "optimised" unit

## A3.2 Diagonal compression strength on masonry specimens

The results of three diagonal compression tests are reported in the tables below. The tests have been carried out on approximately square panels ($t$ x $l_1$ x $l_2$=175 x 998 x 992 mm) made up by calcium-silicate "optimesed" units with thin layer bedjoints.

The mean value of the tensile stress computed as $f_t$=$P_{max}$/($t$*($l_1$+$l_2$) is 0.27 MPa where $P_{max}$ is the maximum compression force applied to the panel corresponding to the failure for diagonal cracking.

| P max [KN] | 72.7 |
|---|---|
| l1 [mm] | 998 |
| l2 [mm] | 992 |
| t [mm] | 175 |
| ft [MPa] | 0.209 |

| P max [KN] | 91.6 |
|---|---|
| l1 [mm] | 998 |
| l2 [mm] | 992 |
| t [mm] | 175 |
| ft [MPa] | 0.263 |

| P max [KN] | 112.7 |
|---|---|
| l1 [mm] | 998 |
| l2 [mm] | 992 |
| t [mm] | 175 |
| ft [MPa] | 0.324 |

# A3 Tests on the "Italian" clay masonry

## A3.1 Compression strength of masonry

In the following tables the results of the compression tests on six masonry specimens (300 x 990 x 510 mm = $t$ x $h$ x $l$) built with lightweight hollow clay units with general purpose mortar bedjoints and headjoints, six masonry specimens (300 x 1010 x 470 mm = $t$ x $h$ x $l$) built with lightweight hollow clay units with general purpose mortar bedjoints with unfilled headjoints (T+G units) and six masonry specimens (300 x 1010 x 470 mm = $t$ x $h$ x $l$) built with lightweight hollow clay units with thin layer mortar bedjoints with unfilled headjoints (T+G units) are presented. The compression strength and the elastic modulus have been computed according to EN 1052-1.

Table 12. Lightweight hollow clay units with
general purpose mortar bedjoints and headjoints

| Wallet | $f_i$ [MPa] | $E_i$ [MPa] |
|---|---|---|
| 1 | 11.3 | 6675 |
| 2 | 10.3 | 6764 |
| 3 | 8.7 | 4731 |
| 4 | 9.1 | 5807 |
| 5 | 8.9 | 5514 |
| 6 | 8.9 | 5940 |
| **Mean** | **9.5** | **5905** |
| **fk (a)** | 8.0 | |
| **fk (b)** | 7.8 | |
| **fk** | **8.0** | |

Table 13. Lightweight hollow clay units with
general purpose mortar bedjoints with unfilled headjoints (T+G units)

| Wallet | $f_i$ [MPa] | $E_i$ [MPa] |
|---|---|---|
| 1 | 6.1 | 2657 |
| 2 | 6.4 | 3075 |
| 3 | 7.0 | 3541 |
| 4 | 7.4 | 3998 |
| 5 | 6.4 | 3084 |
| 6 | 6.1 | 2922 |
| **Mean** | **6.6** | **3213** |
| **fk (a)** | 5.5 | |
| **fk (b)** | 5.7 | |
| **fk** | **5.7** | |

Table 14. Lightweight hollow clay units with
thin layer mortar bedjoints with unfilled headjoints (T+G units)

| Wallet | $f_i$ [MPa] | $E_i$ [MPa] |
|---|---|---|
| 1 | 5.0 | 2571 |
| 2 | 5.5 | 6634 |
| 3 | 5.4 | 3218 |
| 4 | 5.9 | 3403 |
| 5 | 5.5 | 3754 |
| 6 | 4.7 | 3664 |
| **Mean** | **5.3** | **3874** |
| **fk (a)** | 4.5 | |
| **fk (b)** | 4.7 | |
| **fk** | **4.7** | |

### A3.2 Diagonal compression strength on masonry specimens

The results of three diagonal compression tests are reported in the 3 tables below. The tests have been carried out on approximately square panels ($t$ x $l_1$ x $l_2$=300 x 1000 x 980 mm) made up by clay units with general purpose mortar bedjoints and headjoints and "traditional" plain clay units (without tongue and groove).

The mean value of the tensile stress computed as $f_t=P_{max}/(t*(l_1+l_2)$ is 0.278 MPa where $P_{max}$ is the maximum compression force applied to the panel corresponding to the failure for diagonal cracking.

| P max [KN] | 143.9 |
|---|---|
| l1 [mm] | 1000 |
| l2 [mm] | 980 |
| t [mm] | 295 |
| ft [MPa] | 0.246 |

| P max [KN] | 148.2 |
|---|---|
| l1 [mm] | 1000 |
| l2 [mm] | 980 |
| t [mm] | 295 |
| ft [MPa] | 0.254 |

| P max [KN] | 194.9 |
|---|---|
| l1 [mm] | 1000 |
| l2 [mm] | 980 |
| t [mm] | 295 |
| ft [MPa] | 0.334 |

# ANNEX B: F-d envelopes, bilinear curves and transducer displacements for all the cyclic tests

In this annex the envelopes of the force-displacement cyclic hysteretic curves and the corresponding bilinear curves of the three positive and negative cycles for all the tested walls are reported.

Moreover, the force of the horizontal actuator and the displacements of the 25 transducers applied to the specimens as a function of the time of the test are also shown.

The typical wall instrumentation is proposed again in Figure 51 (it is the same figure of paragraph 2).

The plots of the displacements of the transducers are grouped in the following way:

1) Instruments 15, 16 and 24 that measured the horizontal displacement at the top of the wall (in the case of r.c. beam is placed at the top of tested walls, the potentiometer n. 16 measured the relative sliding displacements between the r.c. beam and the steel beam on which the horizontal actuator is fixed. In these cases, the measures of the potentiometer n.16 are included in the plot of the instruments 13, 14 and 17).
2) Instruments 2-5 that measured the wall flexural deformations at the 4 corners of the wall thickness
3) Instruments 6-11 that measured the wall flexural deformations at the center of the wall thickness
4) Instruments 0 and 1 that measured shear deformations and Instrument 12 that measured the horizontal displacement at the center of the panel
5) Instruments 13, 14 and 17 that measured relative sliding displacements between the wall and the footing, between the top beam and the wall and between the strong floor and the footing respectively.
6) Instruments 18 and 19 that measured the out-of-plane displacements, instruments 20-21 that measured the flexural deformations of the steel frame placed at the top of the vertical actuators and, finally instruments 22-23 that measured the sliding between the steel plates welded at the steel frame at the top of the vertical actuators and the reaction wall.

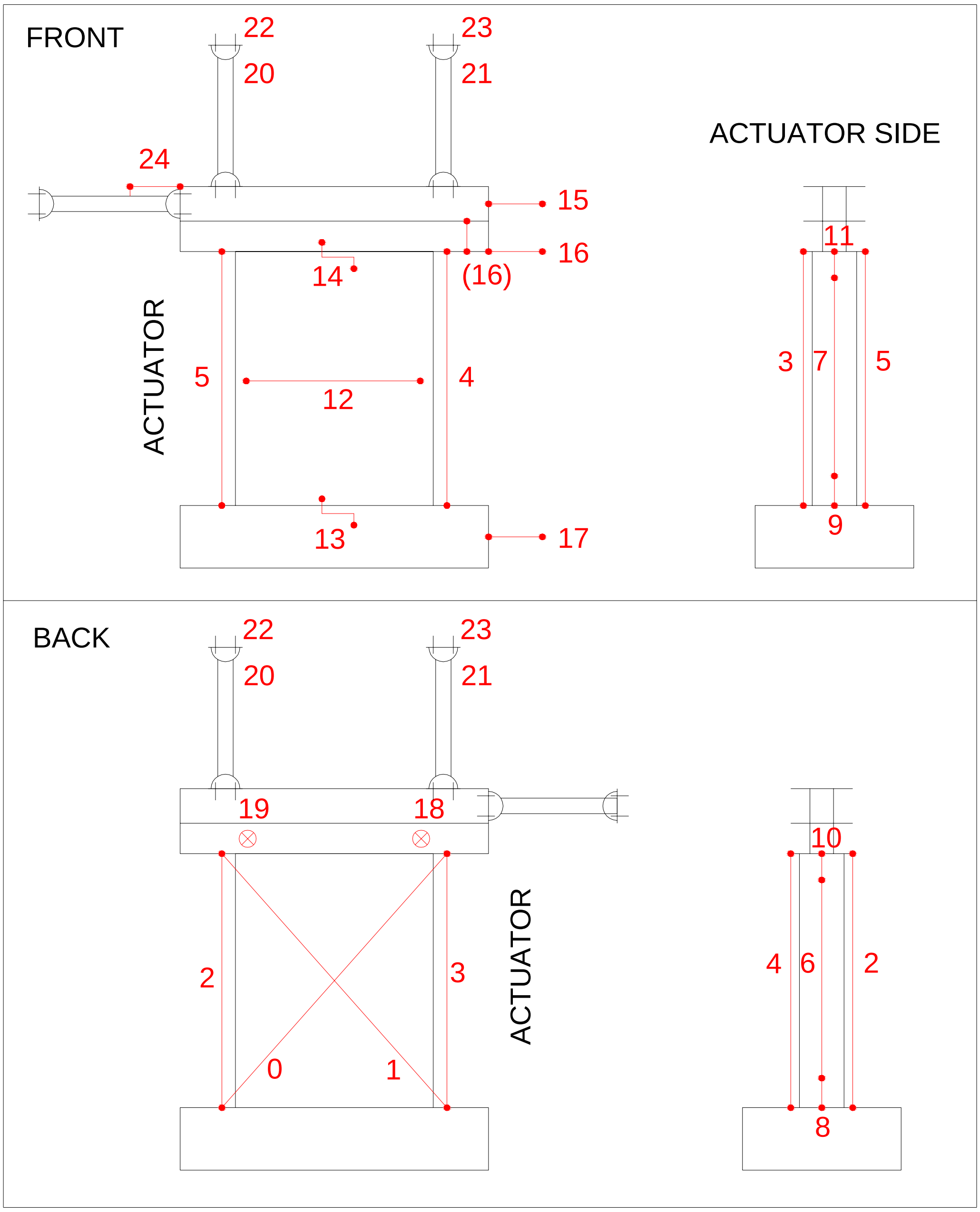


Figure 51. Instrumentation

# WALL CS01

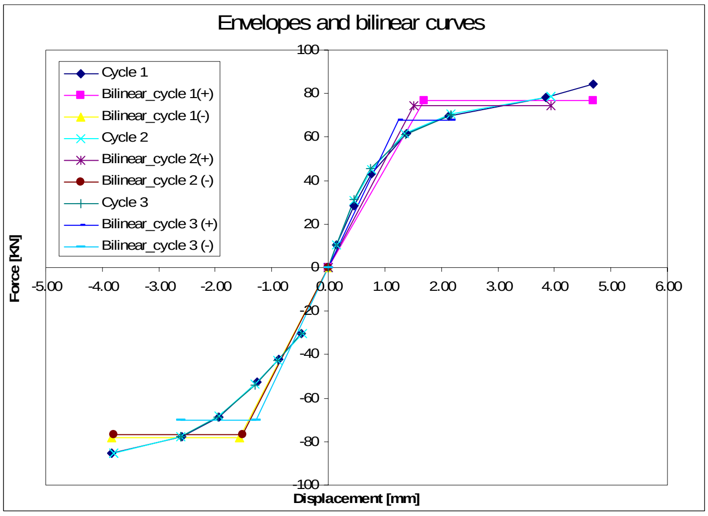
Envelopes and bilinear curves
Cycle 1
Bilinear_cycle 1(+)
Bilinear_cycle 1(-)
Cycle 2
Bilinear_cycle 2(+)
Bilinear_cycle 2 (-)
Cycle 3
Bilinear_cycle 3 (+)
Bilinear_cycle 3 (-)
Force [kN]
Displacement [mm]
-5.00
-4.00
-3.00
-2.00
-1.00
0.00
1.00
2.00
3.00
4.00
5.00
6.00
100
80
60
40
20
0
-20
-40
-60
-80
-100

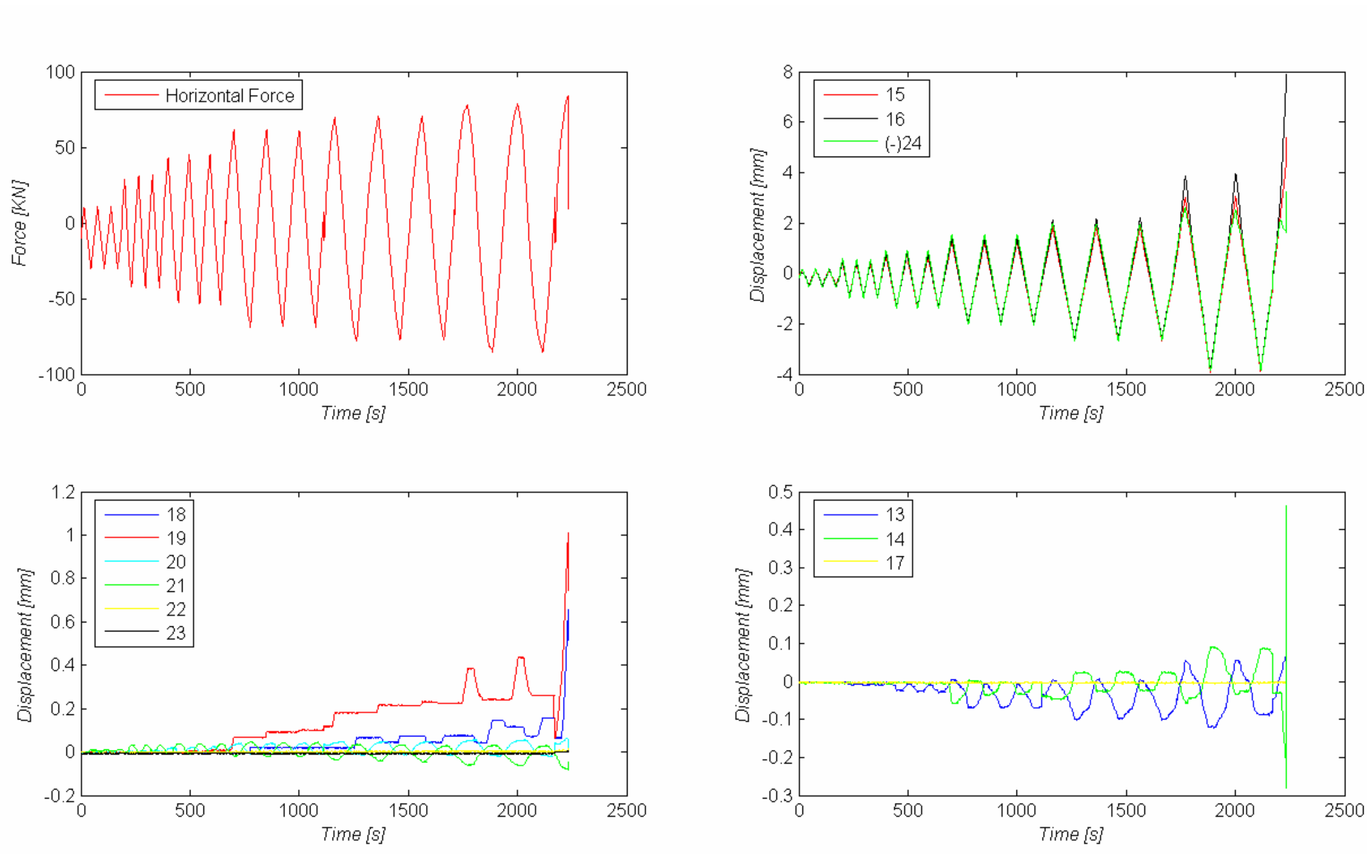
Horizontal Force
Force [kN]
Time [s]
15
16
(-)24
Displacement [mm]
Time [s]
18
19
20
21
22
23
Displacement [mm]
Time [s]
13
14
17
Displacement [mm]
Time [s]

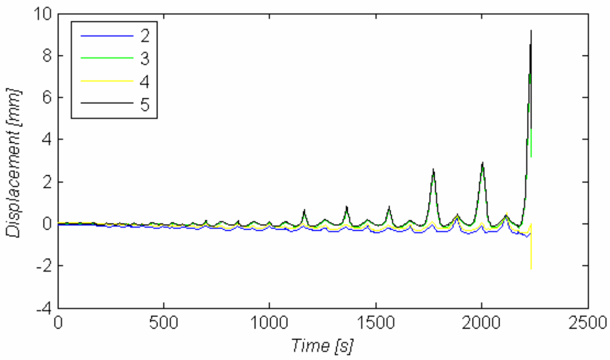
Displacement [mm]
Time [s]
2
3
4
5

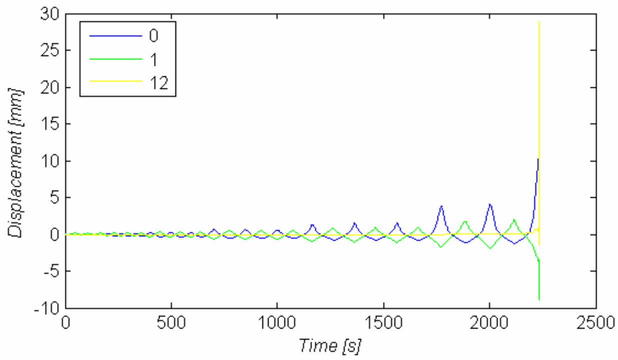
Displacement [mm]
Time [s]
0
1
12

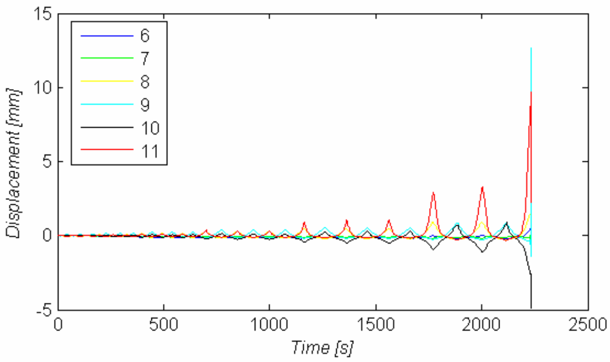
Displacement [mm]
Time [s]
6
7
8
9
10
11

# WALL CS02

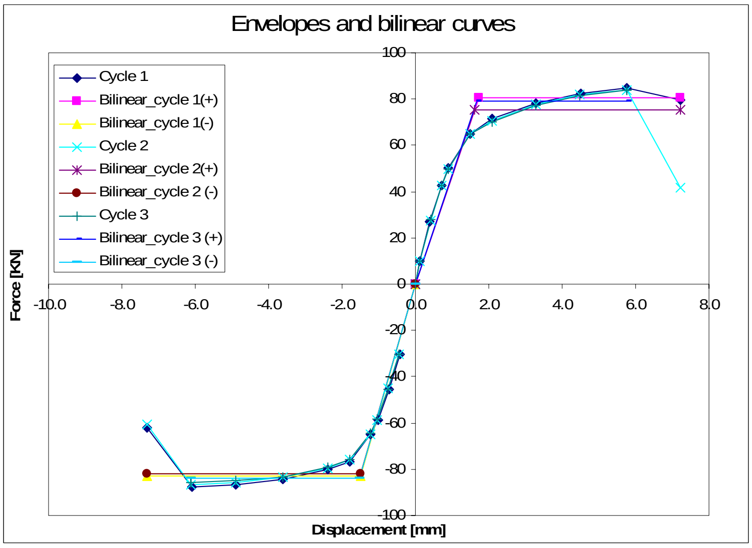
Envelopes and bilinear curves
Cycle 1
Bilinear_cycle 1(+)
Bilinear_cycle 1(-)
Cycle 2
Bilinear_cycle 2(+)
Bilinear_cycle 2 (-)
Cycle 3
Bilinear_cycle 3 (+)
Bilinear_cycle 3 (-)
Force [KN]
Displacement [mm]

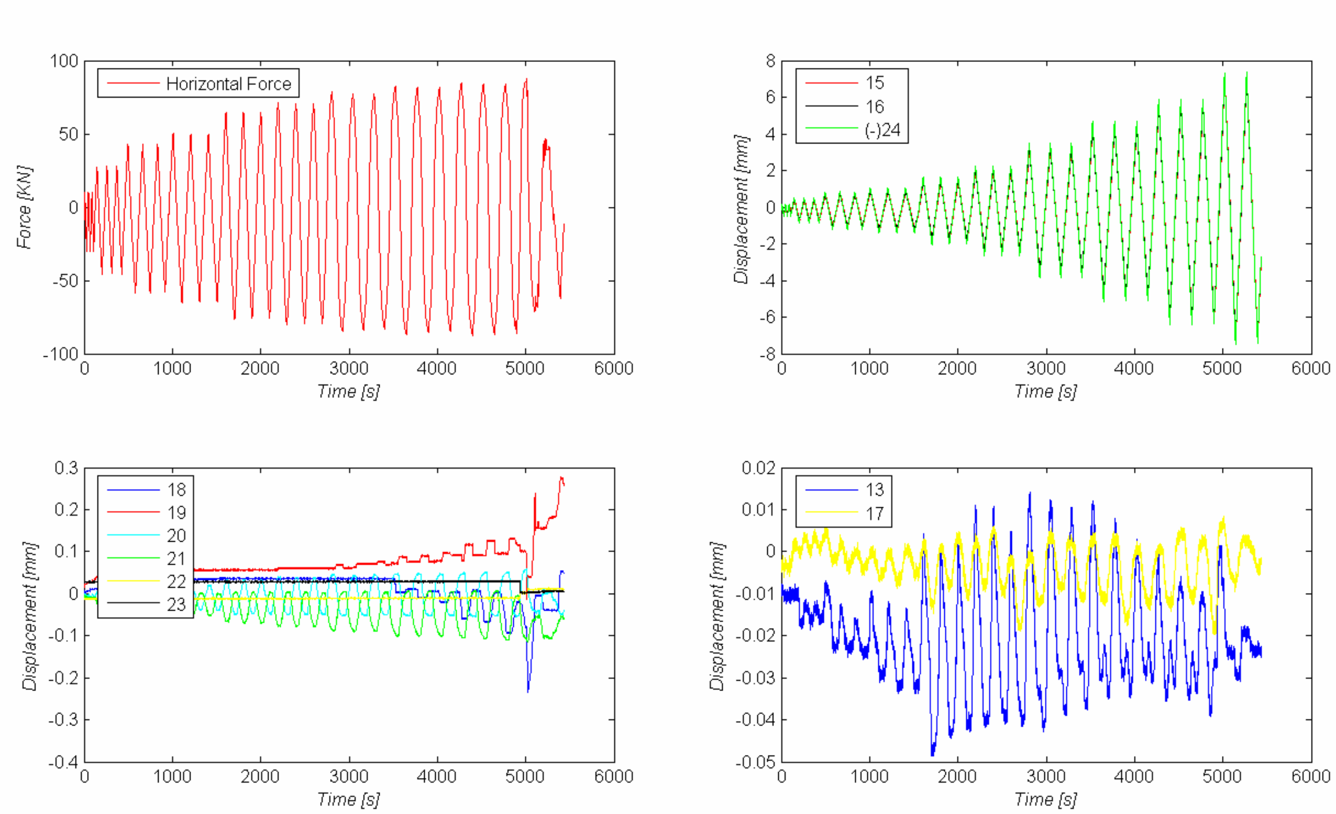
Horizontal Force
Force [KN]
Time [s]
15
16
(-)24
Displacement [mm]
Time [s]
18
19
20
21
22
23
Displacement [mm]
Time [s]
13
17
Displacement [mm]
Time [s]

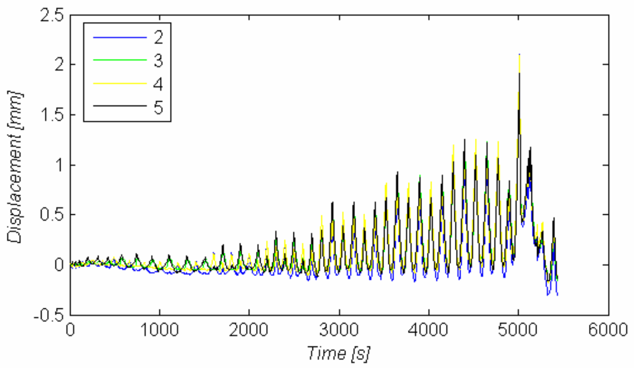
2.5
2
1.5
1
0.5
0
-0.5
Displacement [mm]
2
3
4
5
0
1000
2000
3000
4000
5000
6000
Time [s]

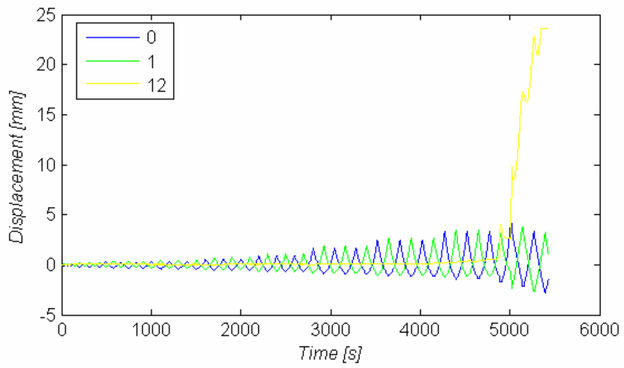
25
20
15
10
5
0
-5
Displacement [mm]
0
1
12
0
1000
2000
3000
4000
5000
6000
Time [s]

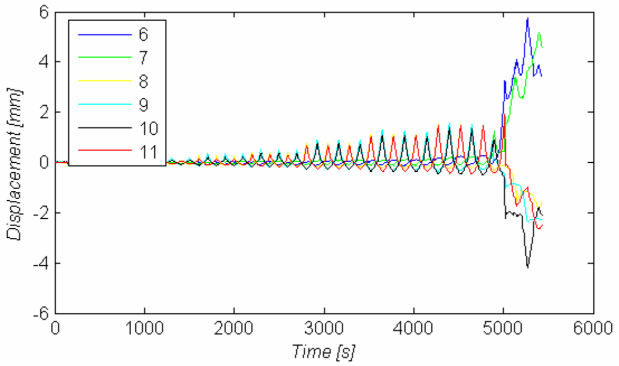
6
4
2
0
-2
-4
-6
Displacement [mm]
6
7
8
9
10
11
0
1000
2000
3000
4000
5000
6000
Time [s]

## WALL CS03

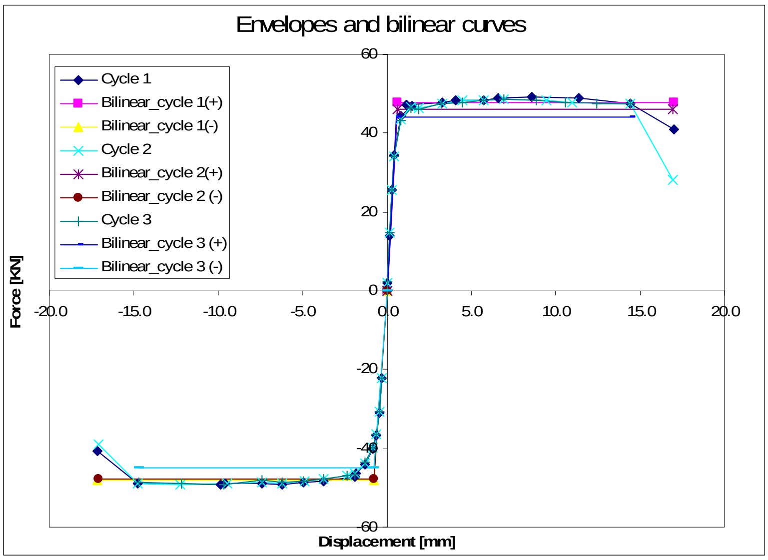
Envelopes and bilinear curves
Cycle 1
Bilinear_cycle 1(+)
Bilinear_cycle 1(-)
Cycle 2
Bilinear_cycle 2(+)
Bilinear_cycle 2 (-)
Cycle 3
Bilinear_cycle 3 (+)
Bilinear_cycle 3 (-)
Force [KN]
Displacement [mm]

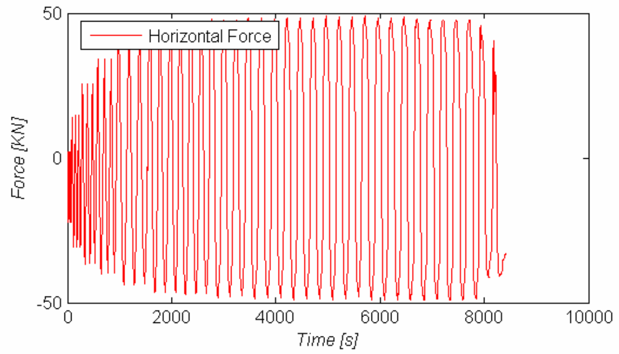
Horizontal Force
Force [KN]
Time [s]

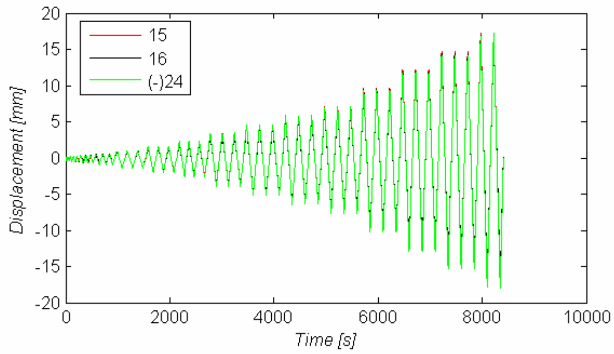
15
16
(-)24
Displacement [mm]
Time [s]

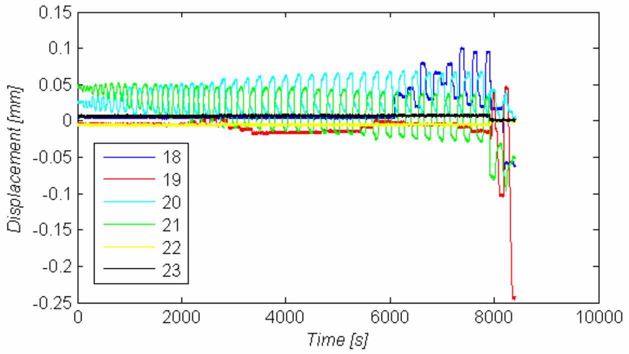
18
19
20
21
22
23
Displacement [mm]
Time [s]

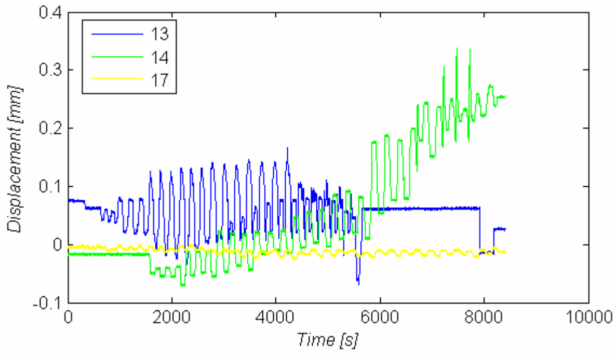
13
14
17
Displacement [mm]
Time [s]

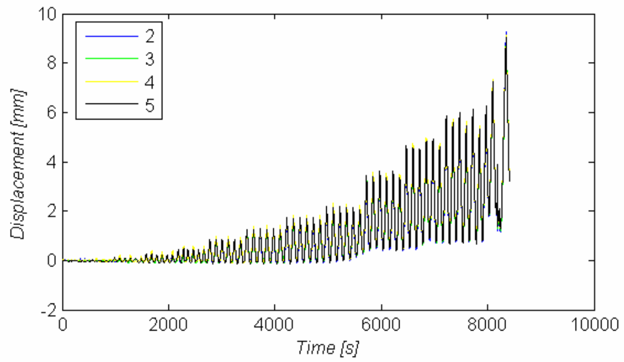
10
8
6
4
2
0
-2
Displacement [mm]
0
2000
4000
6000
8000
10000
Time [s]
2
3
4
5

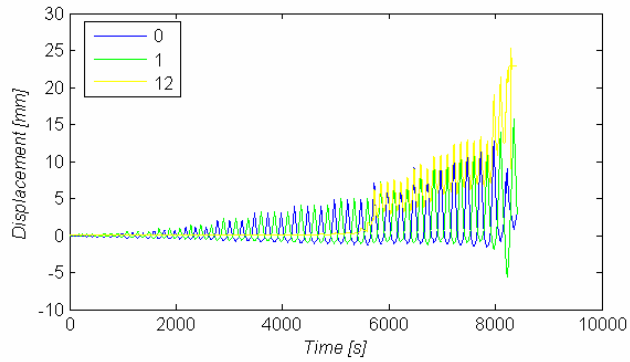
30
25
20
15
10
5
0
-5
-10
Displacement [mm]
0
2000
4000
6000
8000
10000
Time [s]
0
1
12

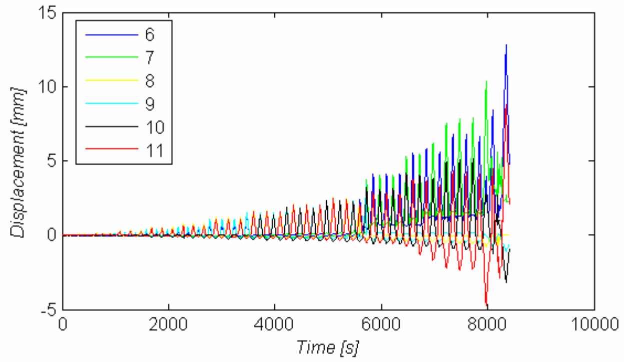
15
10
5
0
-5
Displacement [mm]
0
2000
4000
6000
8000
10000
Time [s]
6
7
8
9
10
11

## WALL CS04

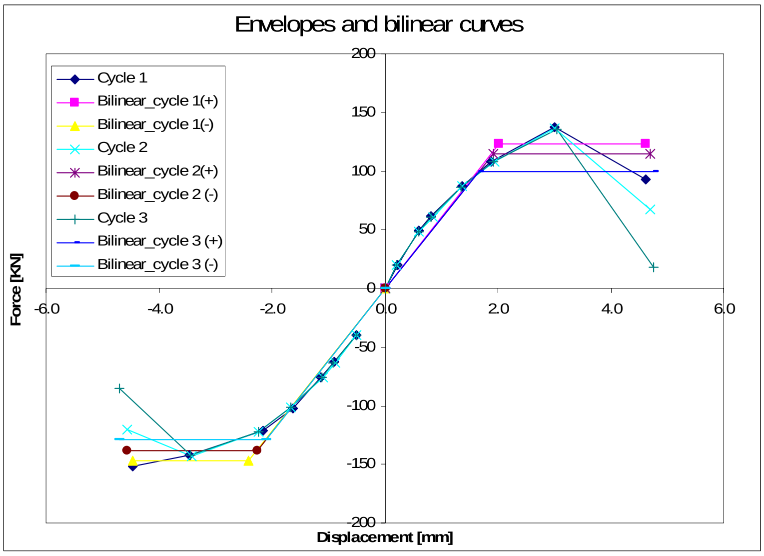
Envelopes and bilinear curves
Cycle 1
Bilinear_cycle 1(+)
Bilinear_cycle 1(-)
Cycle 2
Bilinear_cycle 2(+)
Bilinear_cycle 2 (-)
Cycle 3
Bilinear_cycle 3 (+)
Bilinear_cycle 3 (-)
Force [KN]
Displacement [mm]

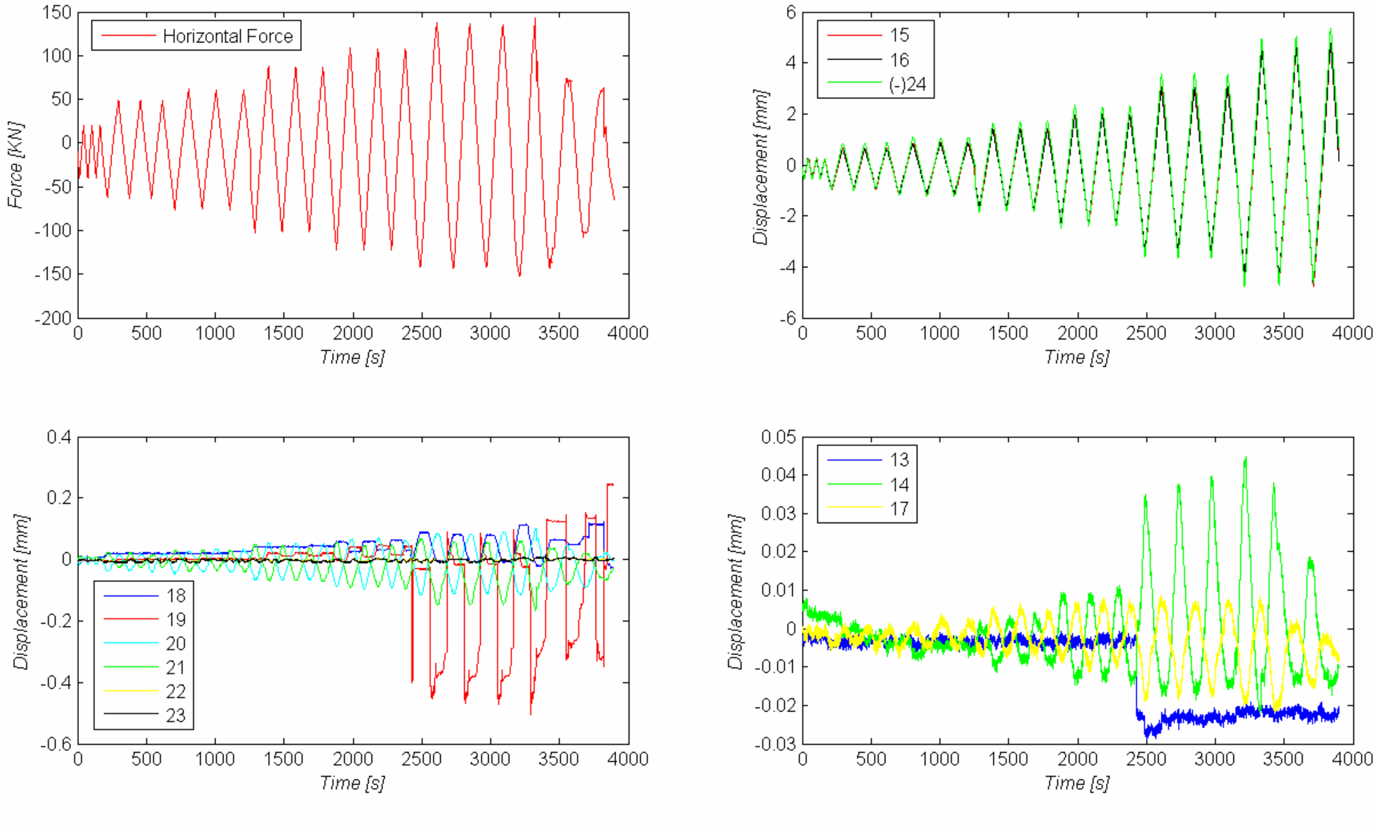
Horizontal Force
Force [KN]
Time [s]
15
16
(-)24
Displacement [mm]
Time [s]
18
19
20
21
22
23
Displacement [mm]
Time [s]
13
14
17
Displacement [mm]
Time [s]

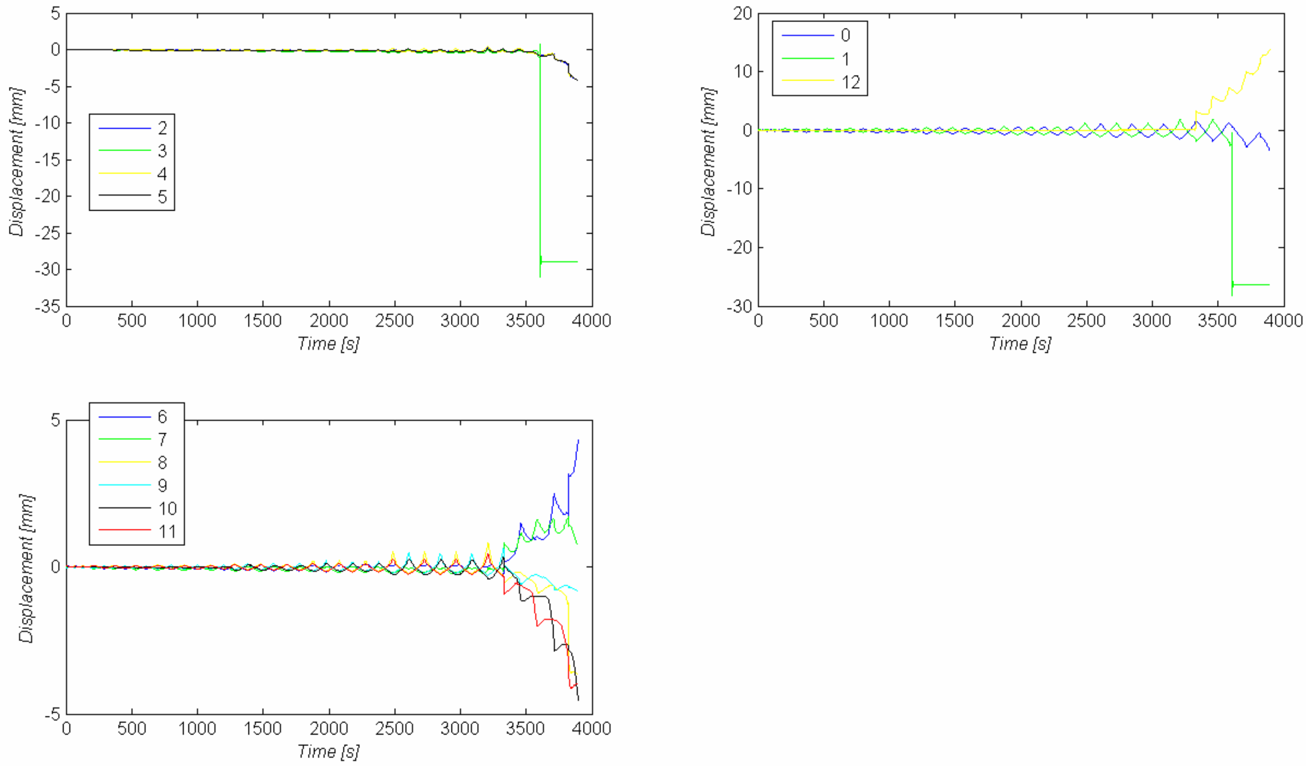
Displacement [mm]
Time [s]
2
3
4
5
Displacement [mm]
Time [s]
0
1
12
Displacement [mm]
Time [s]
6
7
8
9
10
11

## WALL CS05

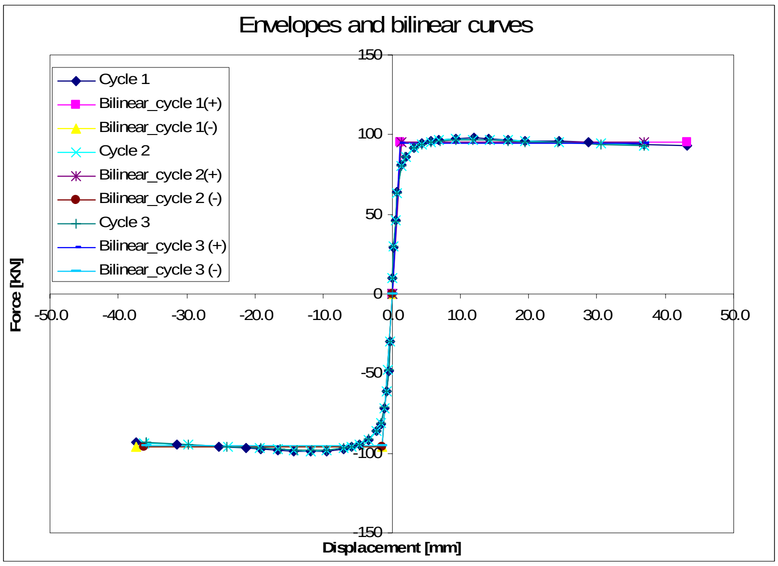
Envelopes and bilinear curves
Cycle 1
Bilinear_cycle 1(+)
Bilinear_cycle 1(-)
Cycle 2
Bilinear_cycle 2(+)
Bilinear_cycle 2 (-)
Cycle 3
Bilinear_cycle 3 (+)
Bilinear_cycle 3 (-)
Force [KN]
Displacement [mm]

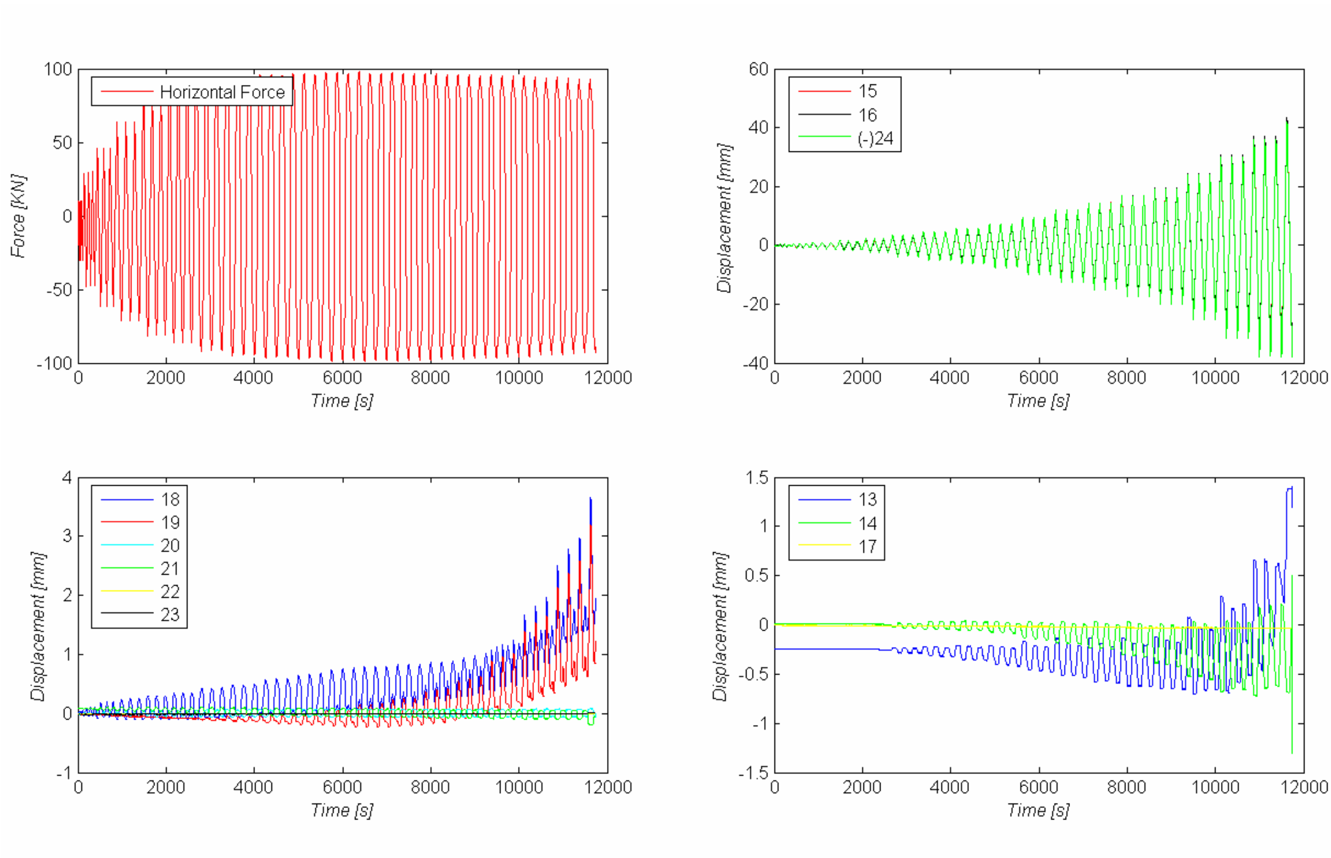
Horizontal Force
Force [KN]
Time [s]
15
16
(-)24
Displacement [mm]
Time [s]
18
19
20
21
22
23
Displacement [mm]
Time [s]
13
14
17
Displacement [mm]
Time [s]

## WALL CS06

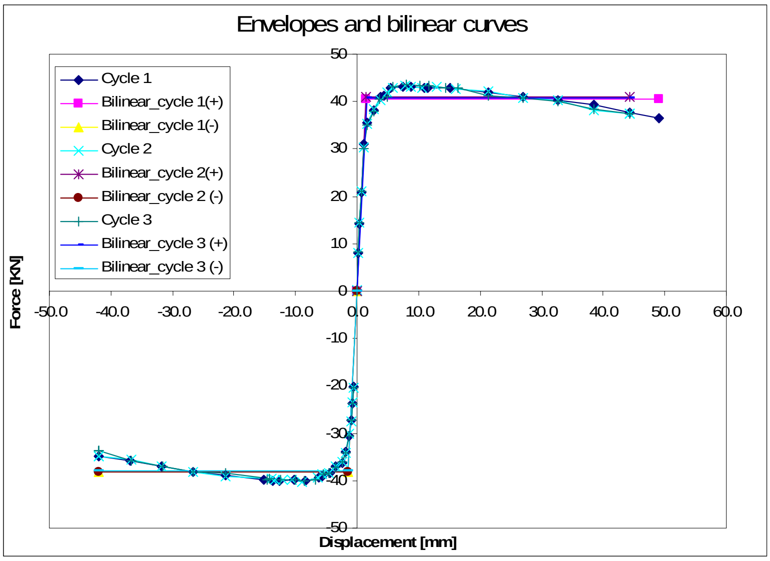
Envelopes and bilinear curves
Cycle 1
Bilinear_cycle 1(+)
Bilinear_cycle 1(-)
Cycle 2
Bilinear_cycle 2(+)
Bilinear_cycle 2 (-)
Cycle 3
Bilinear_cycle 3 (+)
Bilinear_cycle 3 (-)
Force [KN]
Displacement [mm]

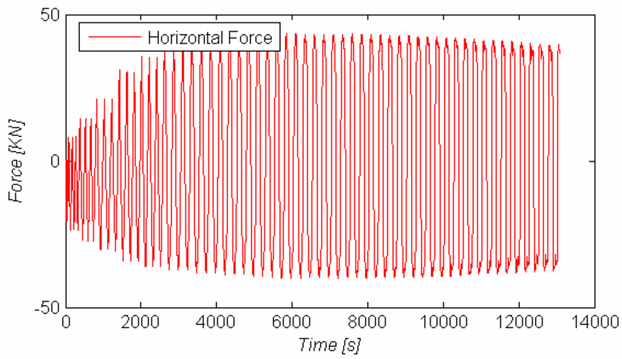
Horizontal Force
Force [KN]
Time [s]

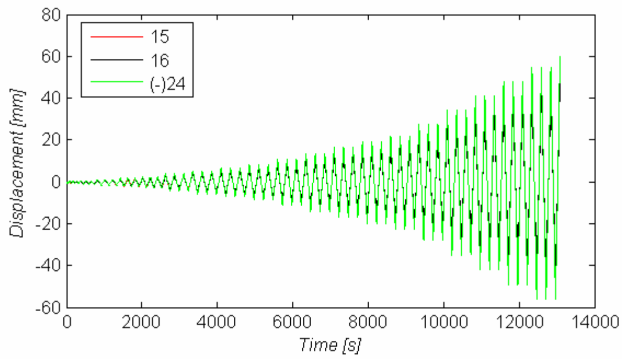
15
16
(-)24
Displacement [mm]
Time [s]

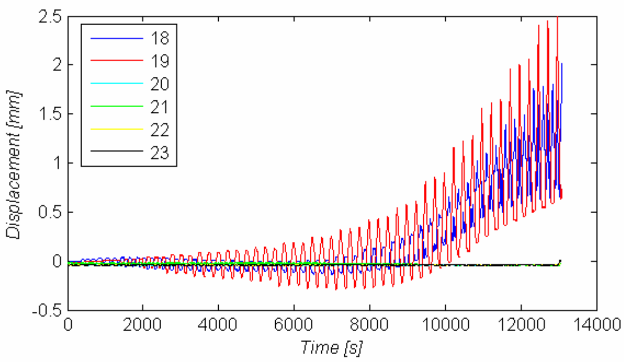
18
19
20
21
22
23
Displacement [mm]
Time [s]

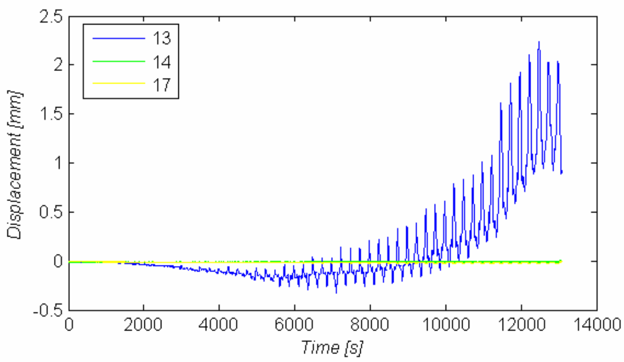
13
14
17
Displacement [mm]
Time [s]

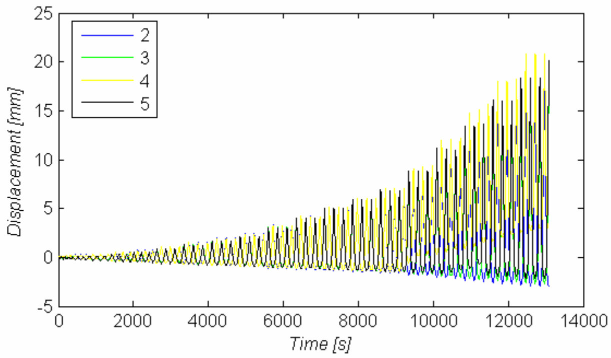
Displacement [mm]
Time [s]
2
3
4
5

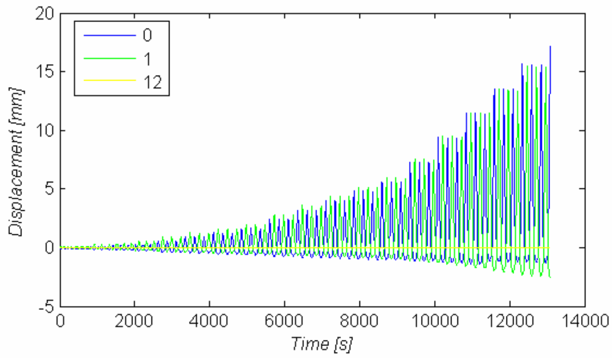
Displacement [mm]
Time [s]
0
1
12

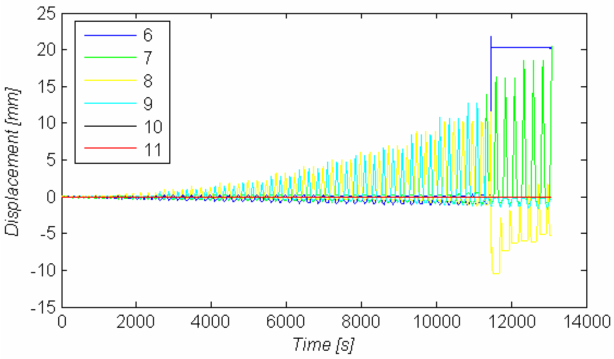
Displacement [mm]
Time [s]
6
7
8
9
10
11

# WALL CS07

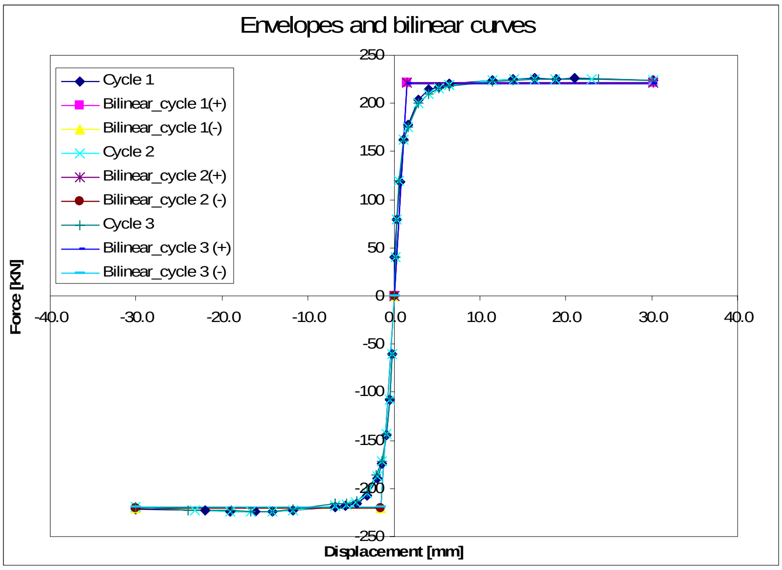
Envelopes and bilinear curves
Cycle 1
Bilinear_cycle 1(+)
Bilinear_cycle 1(-)
Cycle 2
Bilinear_cycle 2(+)
Bilinear_cycle 2 (-)
Cycle 3
Bilinear_cycle 3 (+)
Bilinear_cycle 3 (-)
Force [KN]
Displacement [mm]

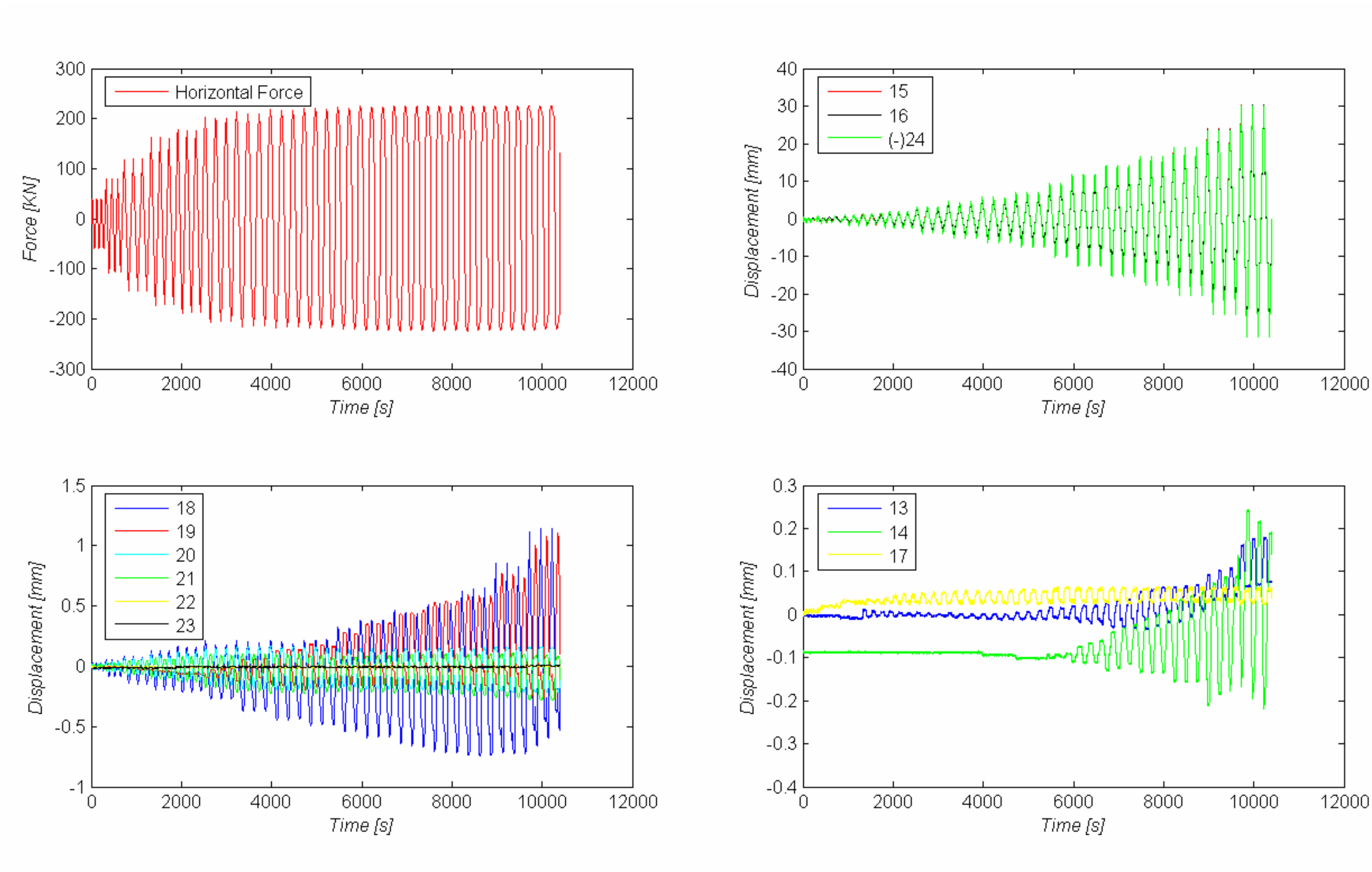
Horizontal Force
Force [KN]
Time [s]
15
16
(-)24
Displacement [mm]
Time [s]
18
19
20
21
22
23
Displacement [mm]
Time [s]
13
14
17
Displacement [mm]
Time [s]

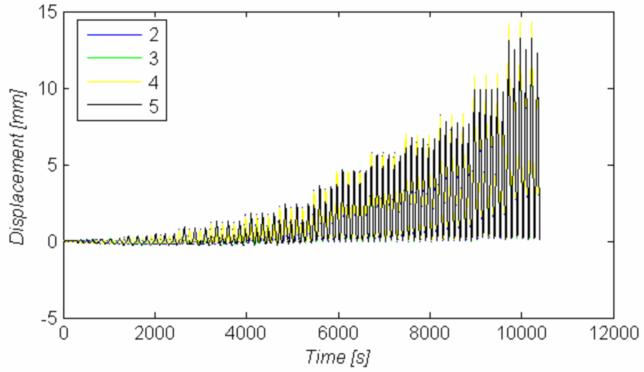
Displacement [mm]
Time [s]
2
3
4
5

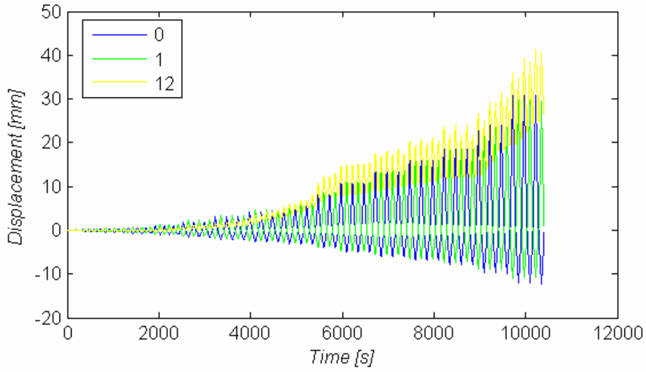
Displacement [mm]
Time [s]
0
1
12

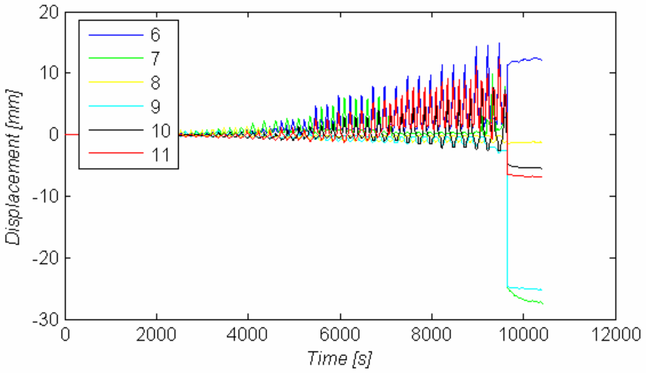
Displacement [mm]
Time [s]
6
7
8
9
10
11

## WALL CS08

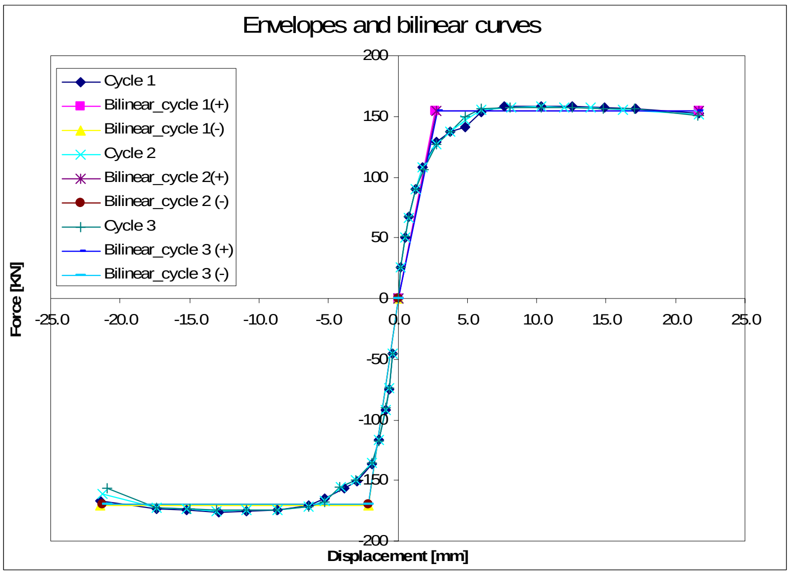
Envelopes and bilinear curves
Cycle 1
Bilinear_cycle 1(+)
Bilinear_cycle 1(-)
Cycle 2
Bilinear_cycle 2(+)
Bilinear_cycle 2 (-)
Cycle 3
Bilinear_cycle 3 (+)
Bilinear_cycle 3 (-)
Force [KN]
Displacement [mm]

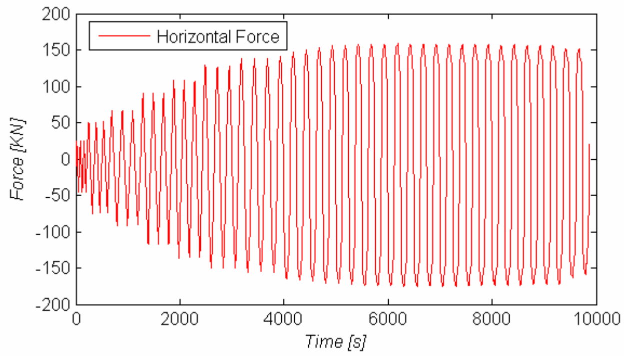
Horizontal Force
Force [KN]
Time [s]

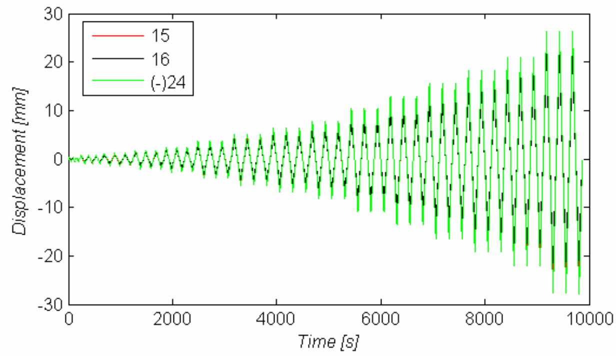
15
16
(-)24
Displacement [mm]
Time [s]

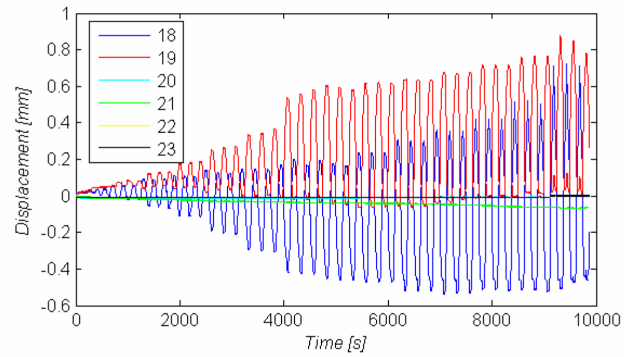
18
19
20
21
22
23
Displacement [mm]
Time [s]

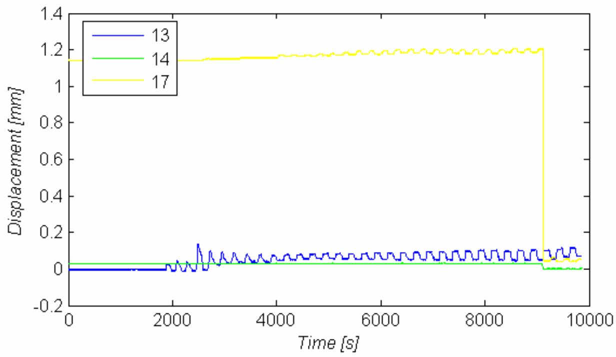
13
14
17
Displacement [mm]
Time [s]

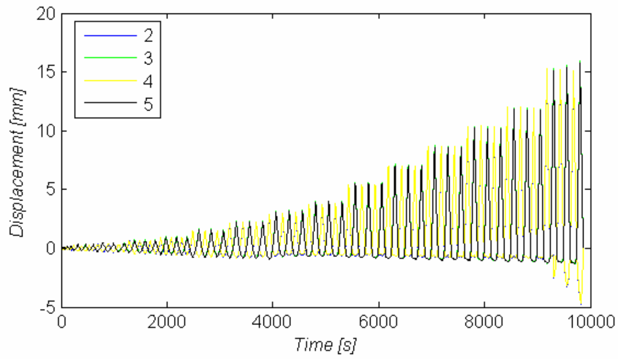
Displacement [mm]
Time [s]
2
3
4
5

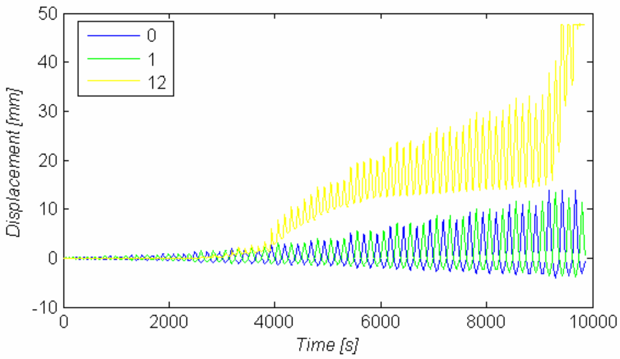
Displacement [mm]
Time [s]
0
1
12

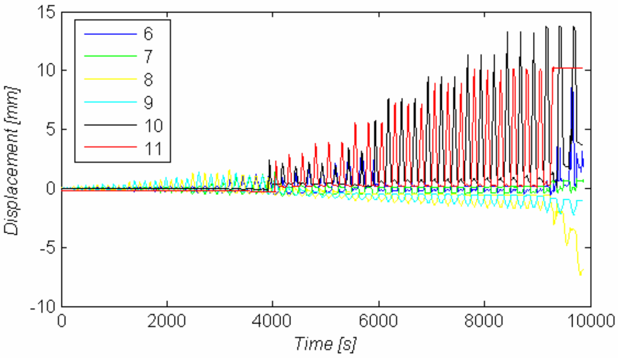
Displacement [mm]
Time [s]
6
7
8
9
10
11

## WALL CS09

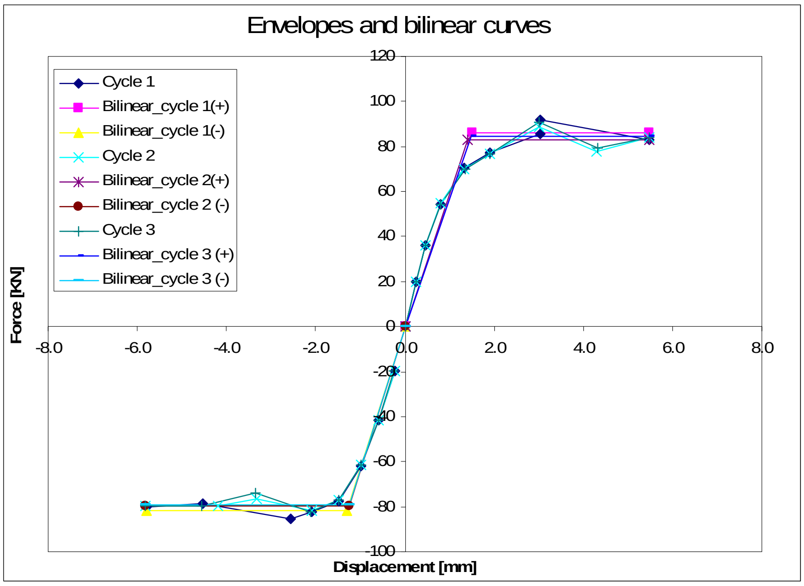
Envelopes and bilinear curves
Cycle 1
Bilinear_cycle 1(+)
Bilinear_cycle 1(-)
Cycle 2
Bilinear_cycle 2(+)
Bilinear_cycle 2 (-)
Cycle 3
Bilinear_cycle 3 (+)
Bilinear_cycle 3 (-)
Force [KN]
Displacement [mm]

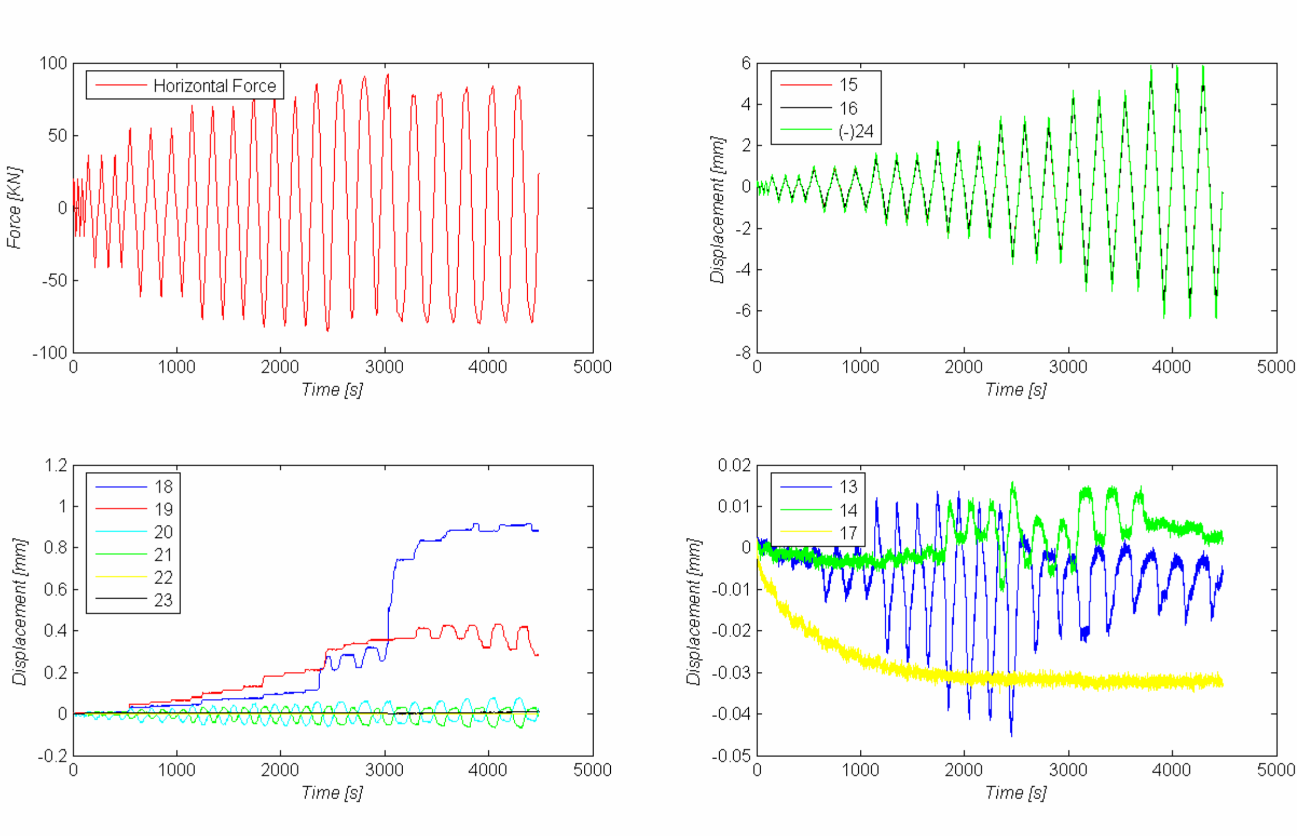
Horizontal Force
Force [KN]
Time [s]
15
16
(-)24
Displacement [mm]
Time [s]
18
19
20
21
22
23
Displacement [mm]
Time [s]
13
14
17
Displacement [mm]
Time [s]

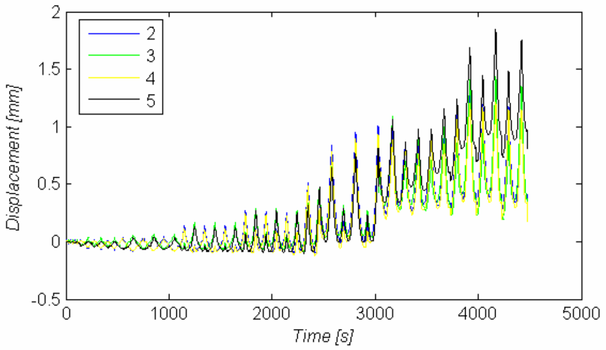
2
3
4
5
Displacement [mm]
Time [s]

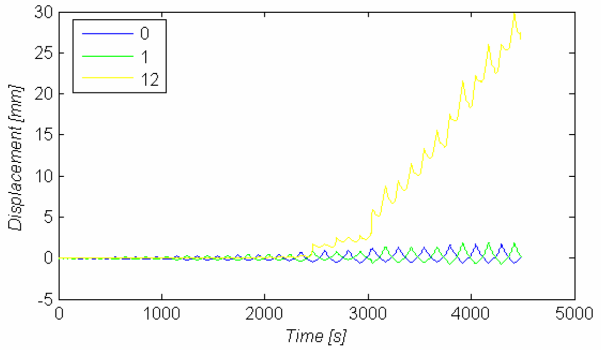
0
1
12
Displacement [mm]
Time [s]

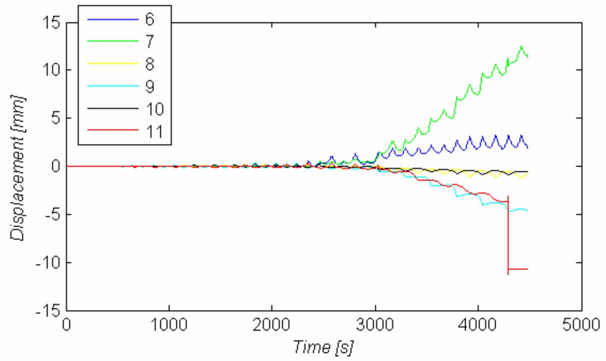
6
7
8
9
10
11
Displacement [mm]
Time [s]

# WALL CS010

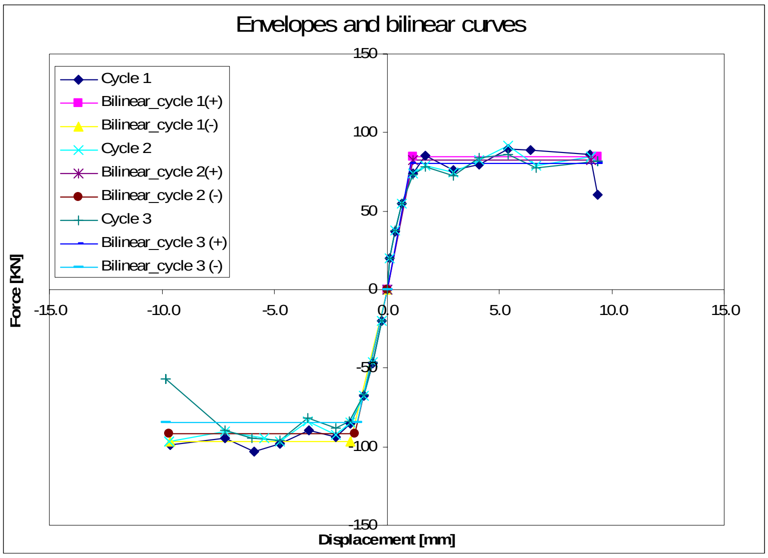
Envelopes and bilinear curves
Cycle 1
Bilinear_cycle 1(+)
Bilinear_cycle 1(-)
Cycle 2
Bilinear_cycle 2(+)
Bilinear_cycle 2 (-)
Cycle 3
Bilinear_cycle 3 (+)
Bilinear_cycle 3 (-)
Force [KN]
Displacement [mm]

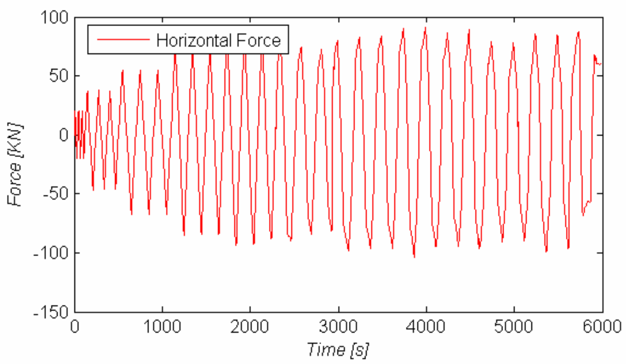
Horizontal Force
Force [KN]
Time [s]

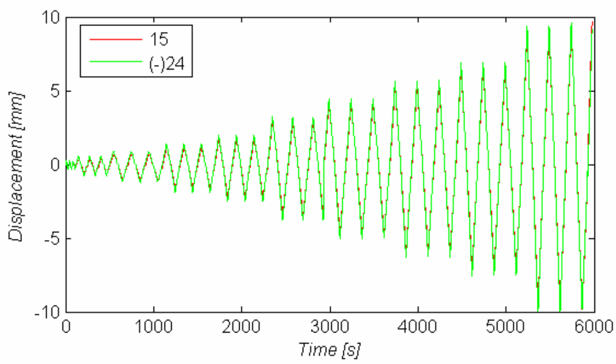
15
(-)24
Displacement [mm]
Time [s]

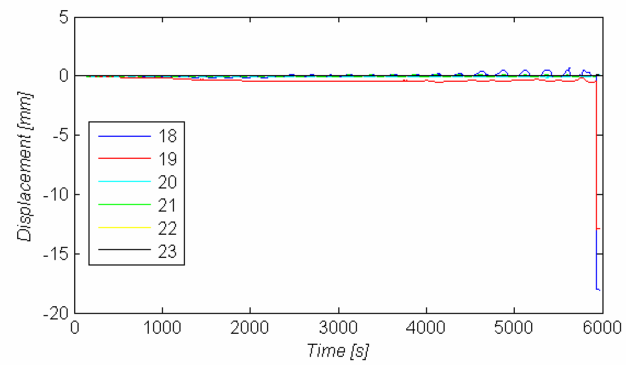
18
19
20
21
22
23
Displacement [mm]
Time [s]

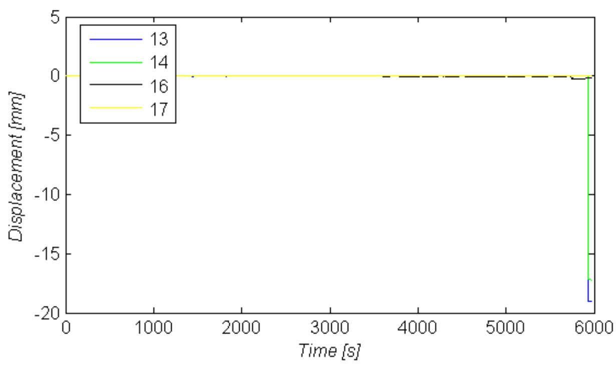
13
14
16
17
Displacement [mm]
Time [s]

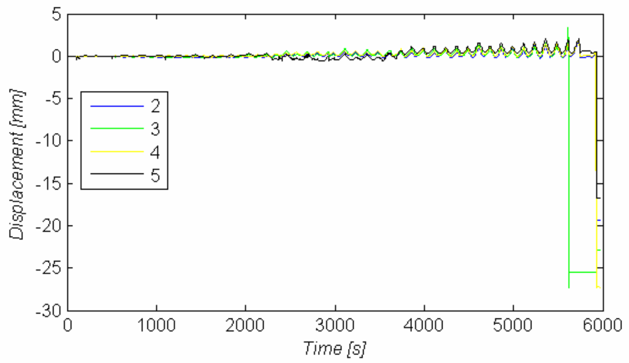
Displacement [mm]
Time [s]
2
3
4
5

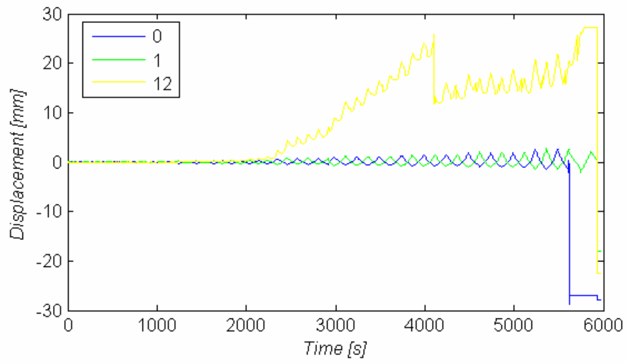
Displacement [mm]
Time [s]
0
1
12

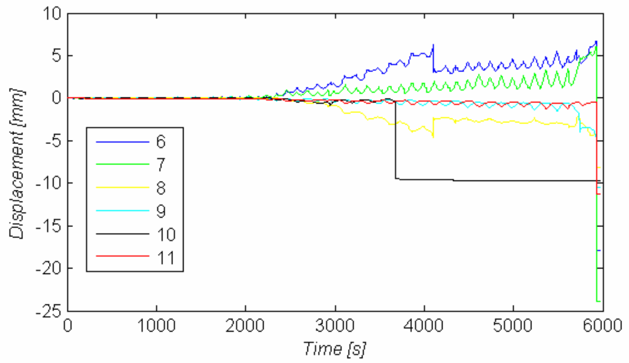
Displacement [mm]
Time [s]
6
7
8
9
10
11

## WALL CS11

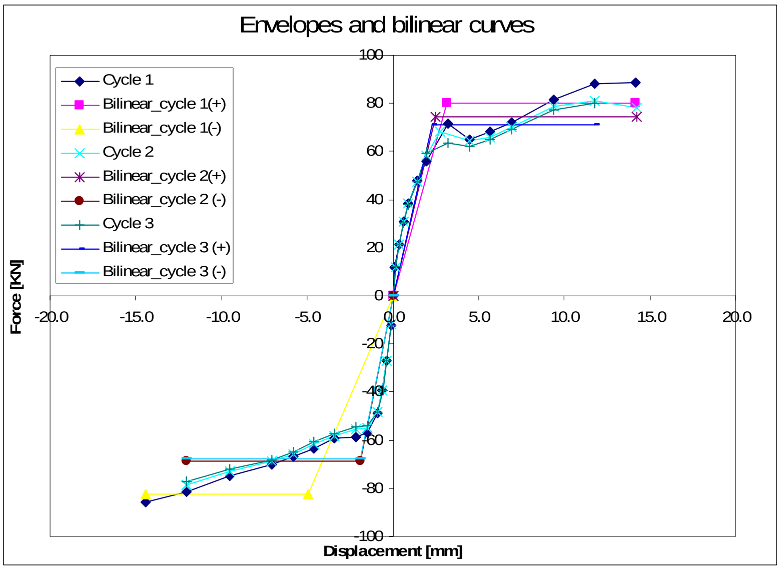
Envelopes and bilinear curves
Cycle 1
Bilinear_cycle 1(+)
Bilinear_cycle 1(-)
Cycle 2
Bilinear_cycle 2(+)
Bilinear_cycle 2 (-)
Cycle 3
Bilinear_cycle 3 (+)
Bilinear_cycle 3 (-)
Force [KN]
Displacement [mm]

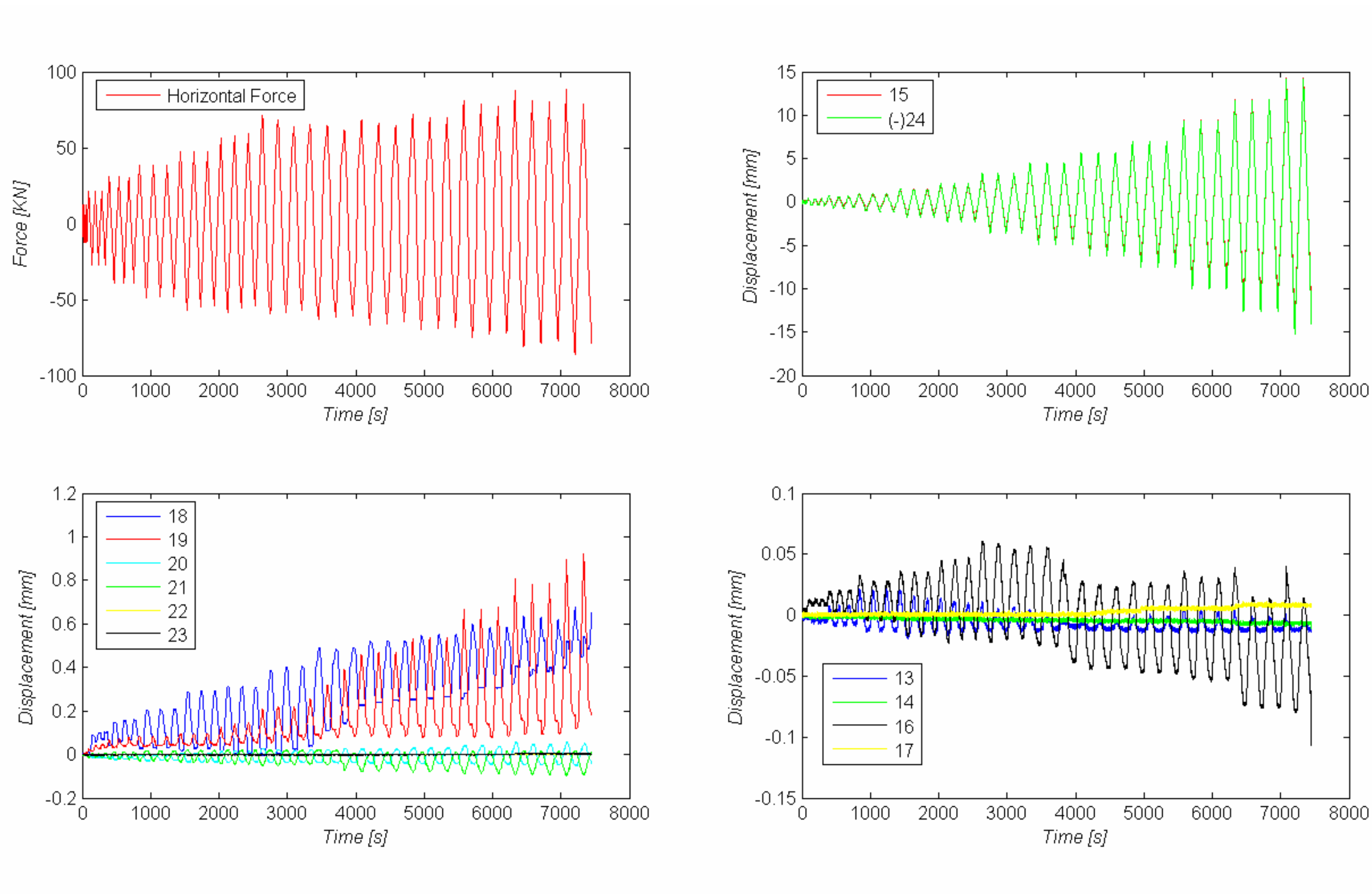
Horizontal Force
Force [KN]
Time [s]
15
(-)24
Displacement [mm]
Time [s]
18
19
20
21
22
23
Displacement [mm]
Time [s]
13
14
16
17
Displacement [mm]
Time [s]

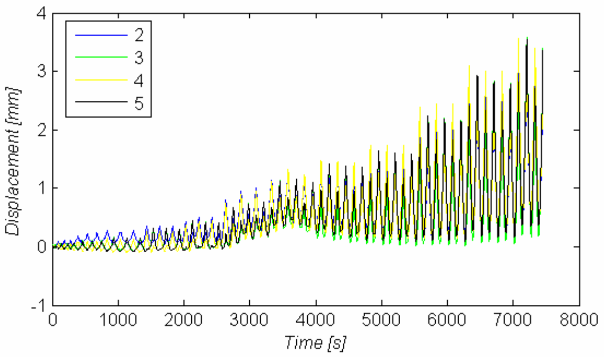
Displacement [mm]
Time [s]
2
3
4
5

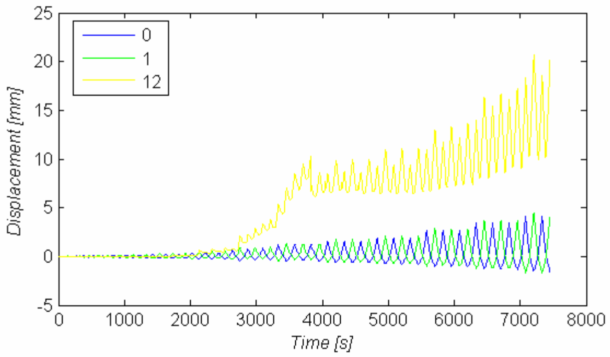
Displacement [mm]
Time [s]
0
1
12

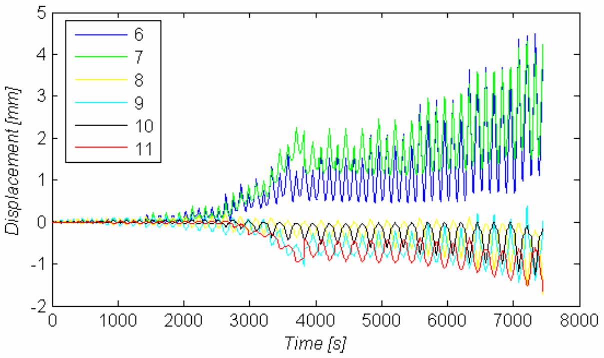
Displacement [mm]
Time [s]
6
7
8
9
10
11

## WALL CS12

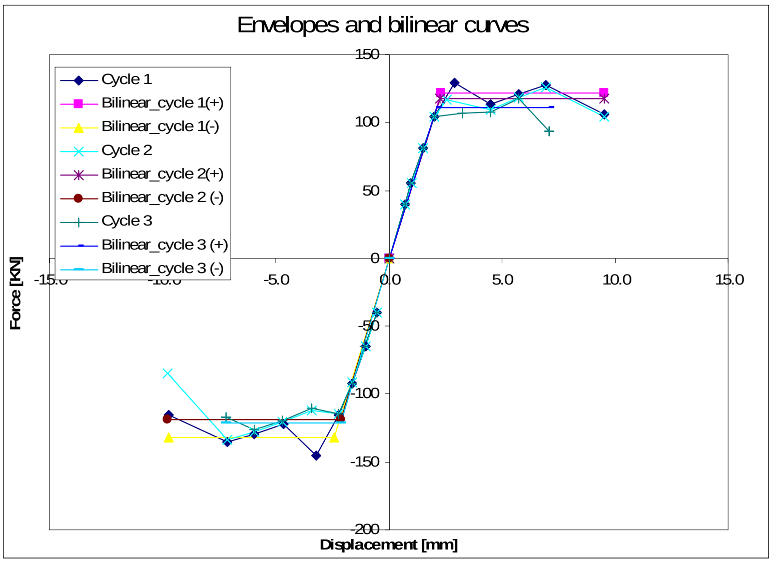
Envelopes and bilinear curves
Cycle 1
Bilinear_cycle 1(+)
Bilinear_cycle 1(-)
Cycle 2
Bilinear_cycle 2(+)
Bilinear_cycle 2 (-)
Cycle 3
Bilinear_cycle 3 (+)
Bilinear_cycle 3 (-)
Force [KN]
Displacement [mm]

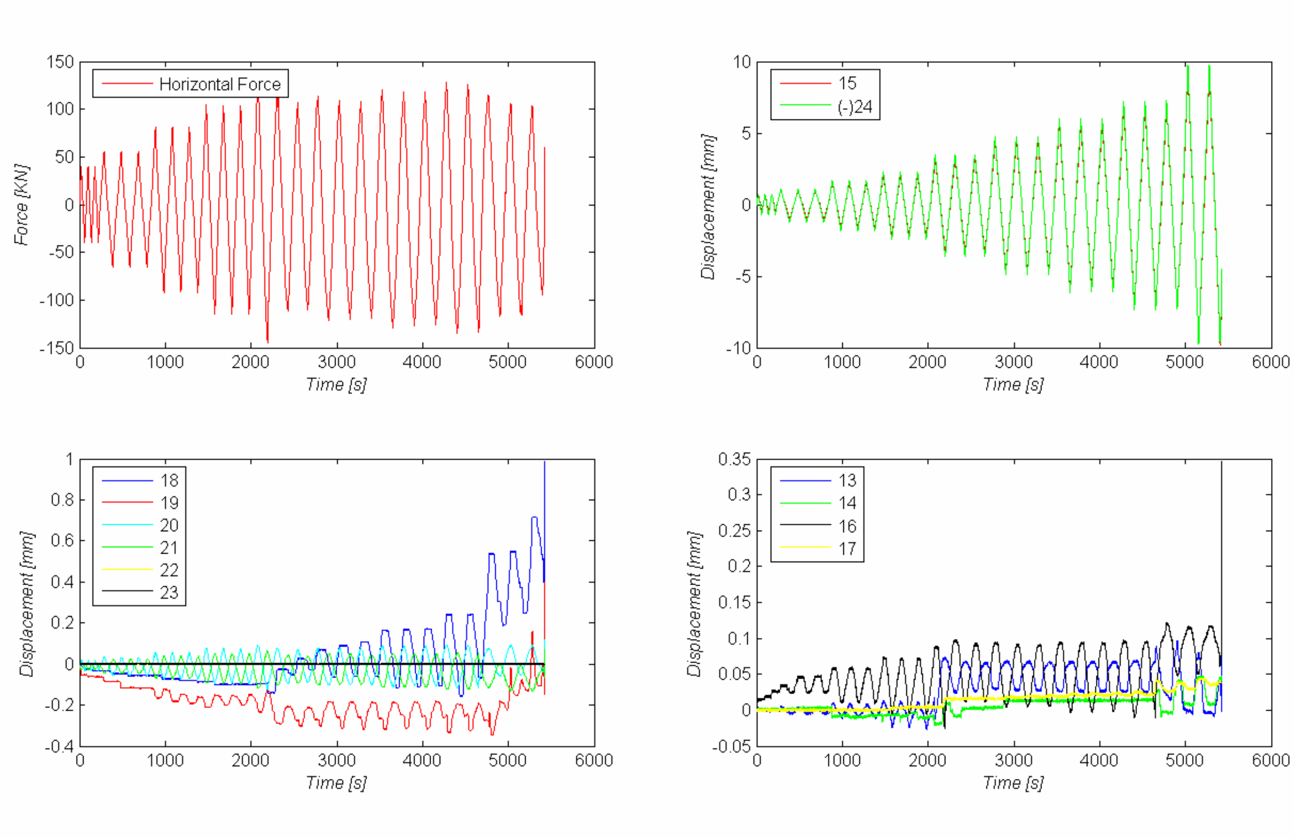
Horizontal Force
Force [KN]
Time [s]
15
(-)24
Displacement [mm]
Time [s]
18
19
20
21
22
23
Displacement [mm]
Time [s]
13
14
16
17
Displacement [mm]
Time [s]

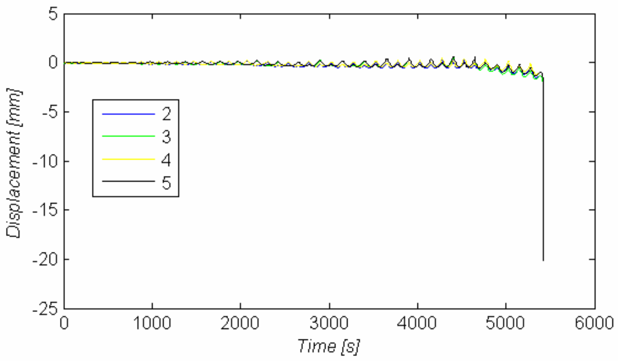
5
0
-5
-10
-15
-20
-25
Displacement [mm]
0
1000
2000
3000
4000
5000
6000
Time [s]
2
3
4
5

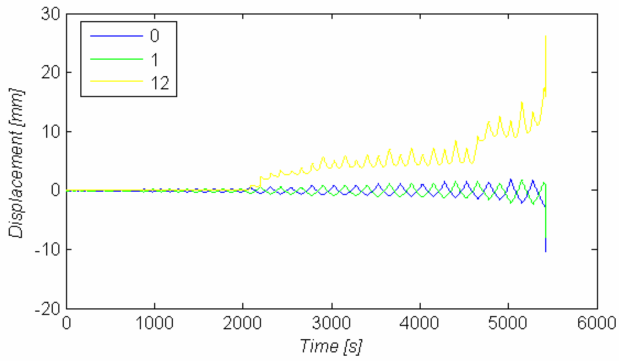
30
20
10
0
-10
-20
Displacement [mm]
0
1000
2000
3000
4000
5000
6000
Time [s]
0
1
12

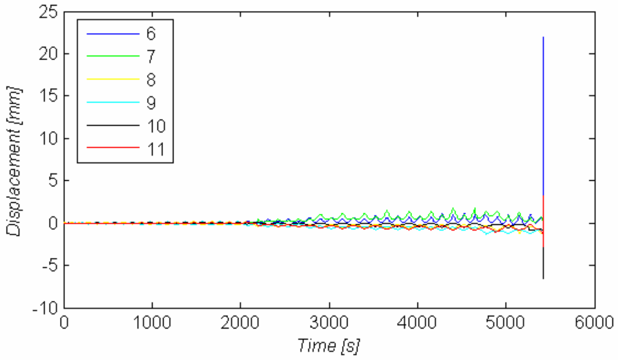
25
20
15
10
5
0
-5
-10
Displacement [mm]
0
1000
2000
3000
4000
5000
6000
Time [s]
6
7
8
9
10
11

# WALL CS13

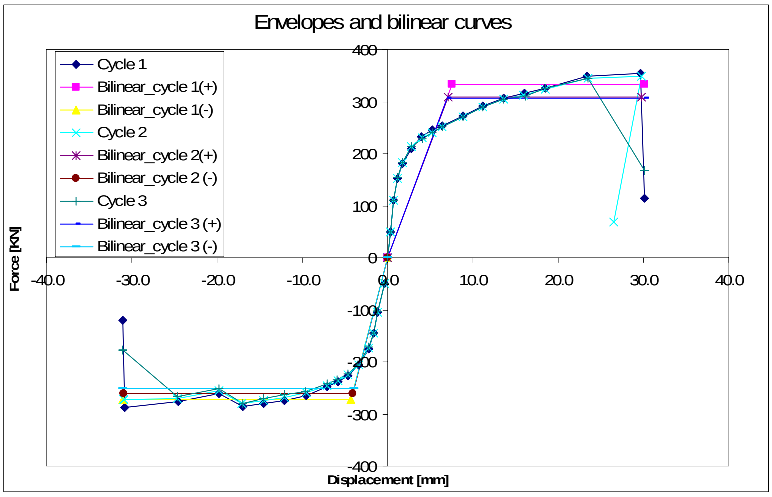
Envelopes and bilinear curves
Cycle 1
Bilinear_cycle 1(+)
Bilinear_cycle 1(-)
Cycle 2
Bilinear_cycle 2(+)
Bilinear_cycle 2 (-)
Cycle 3
Bilinear_cycle 3 (+)
Bilinear_cycle 3 (-)
Force [KN]
Displacement [mm]

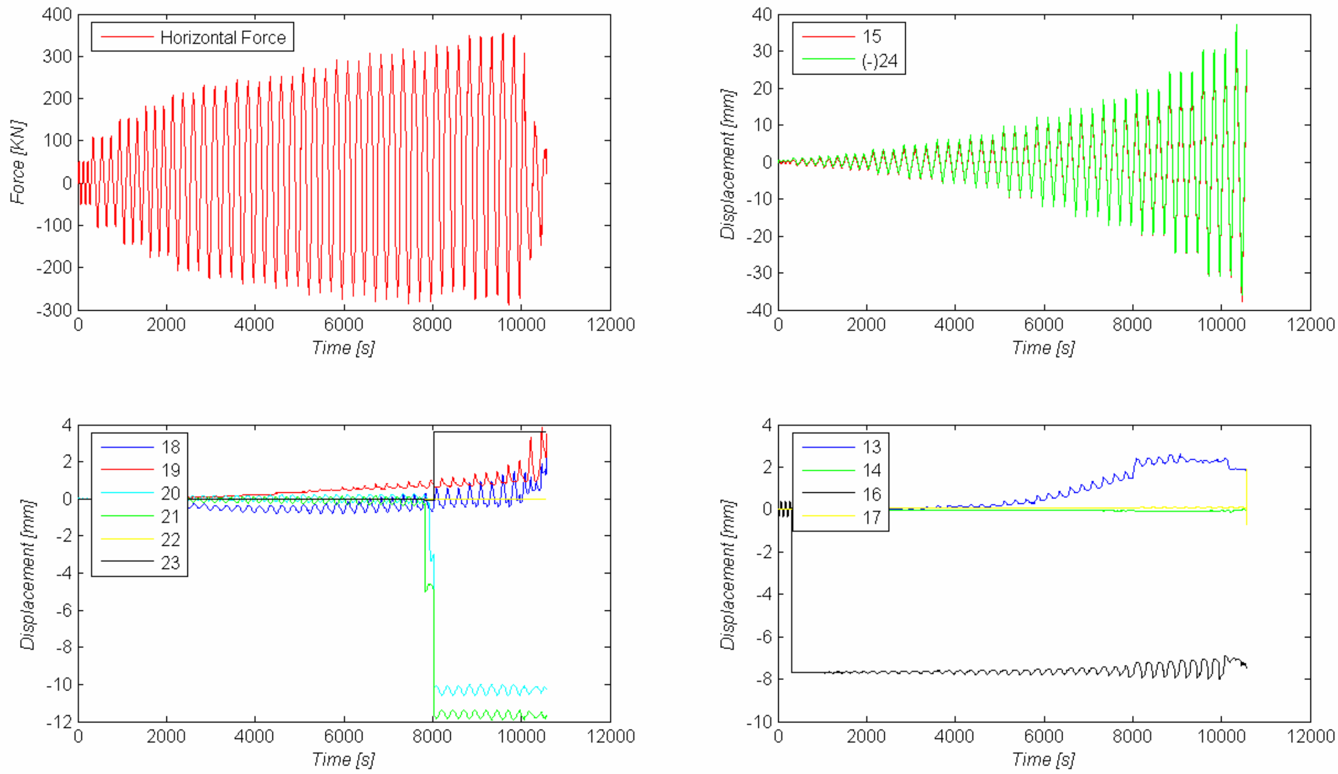
Horizontal Force
Force [KN]
Time [s]
15
(-)24
Displacement [mm]
Time [s]
18
19
20
21
22
23
Displacement [mm]
Time [s]
13
14
16
17
Displacement [mm]
Time [s]

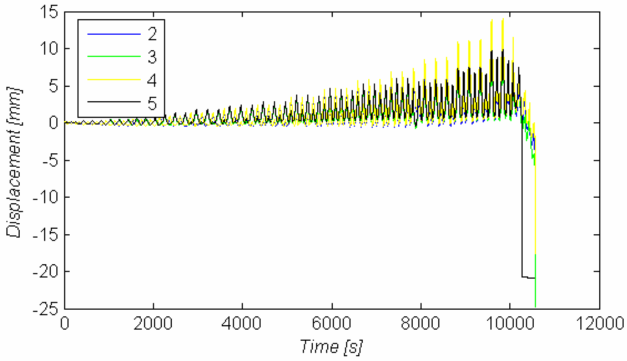
2
3
4
5
Displacement [mm]
Time [s]

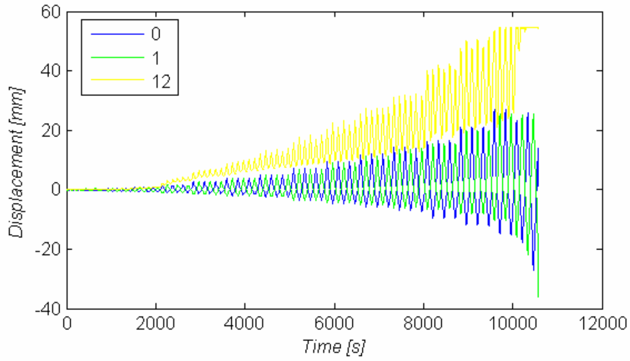
0
1
12
Displacement [mm]
Time [s]

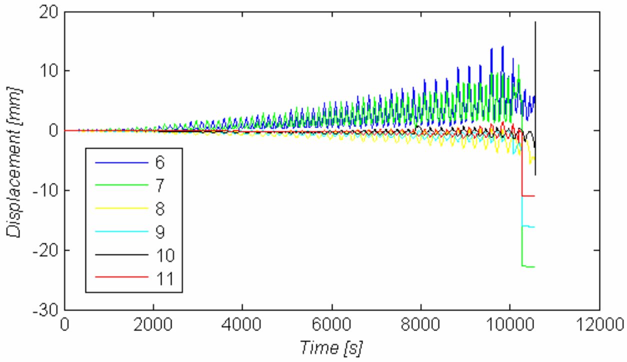
6
7
8
9
10
11
Displacement [mm]
Time [s]

## WALL CS14

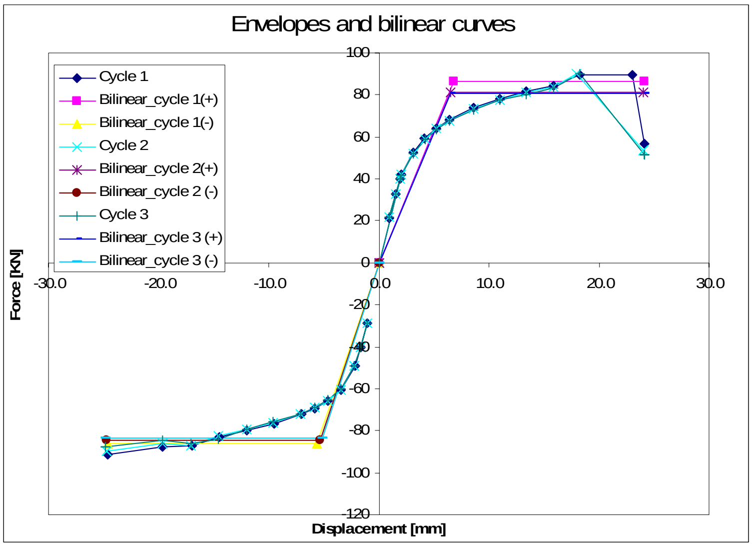
Envelopes and bilinear curves
Cycle 1
Bilinear_cycle 1(+)
Bilinear_cycle 1(-)
Cycle 2
Bilinear_cycle 2(+)
Bilinear_cycle 2 (-)
Cycle 3
Bilinear_cycle 3 (+)
Bilinear_cycle 3 (-)
Force [KN]
Displacement [mm]

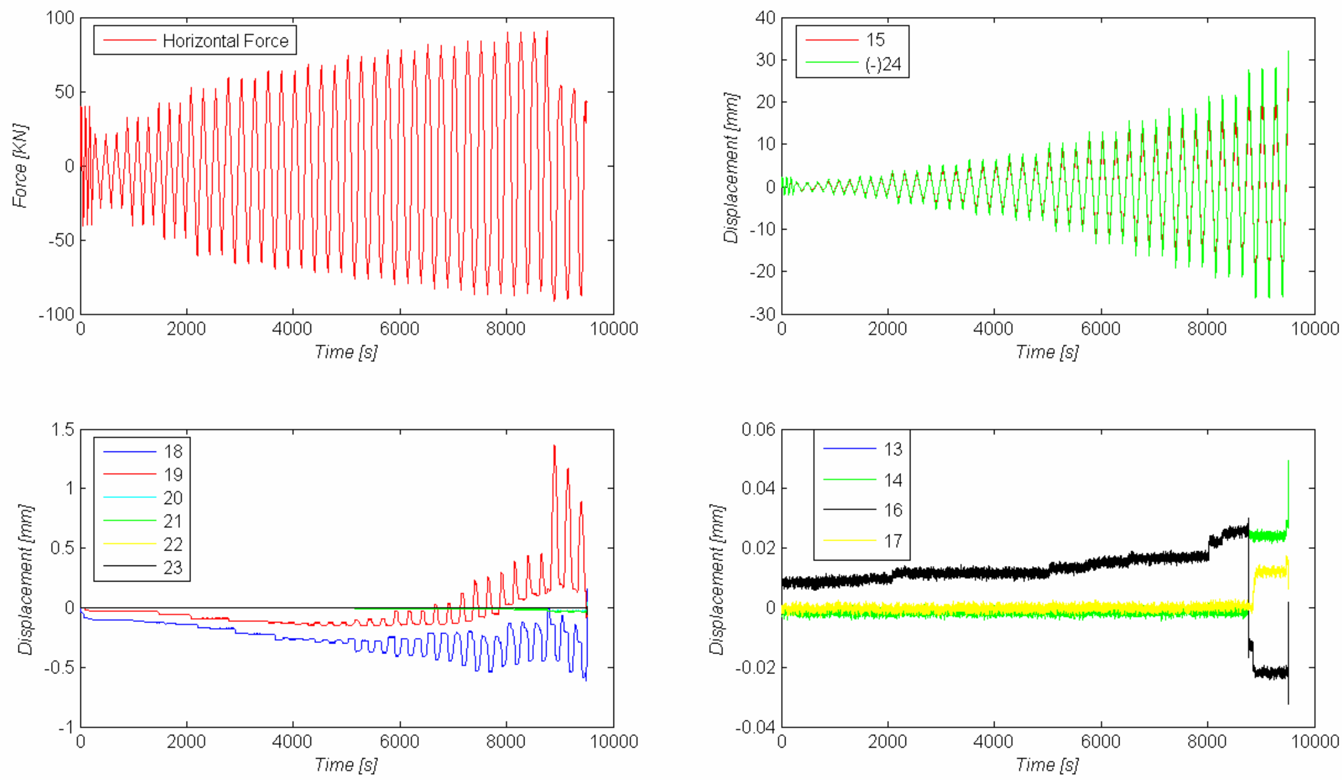
Horizontal Force
Force [KN]
Time [s]
15
(-)24
Displacement [mm]
Time [s]
18
19
20
21
22
23
Displacement [mm]
Time [s]
13
14
16
17
Displacement [mm]
Time [s]

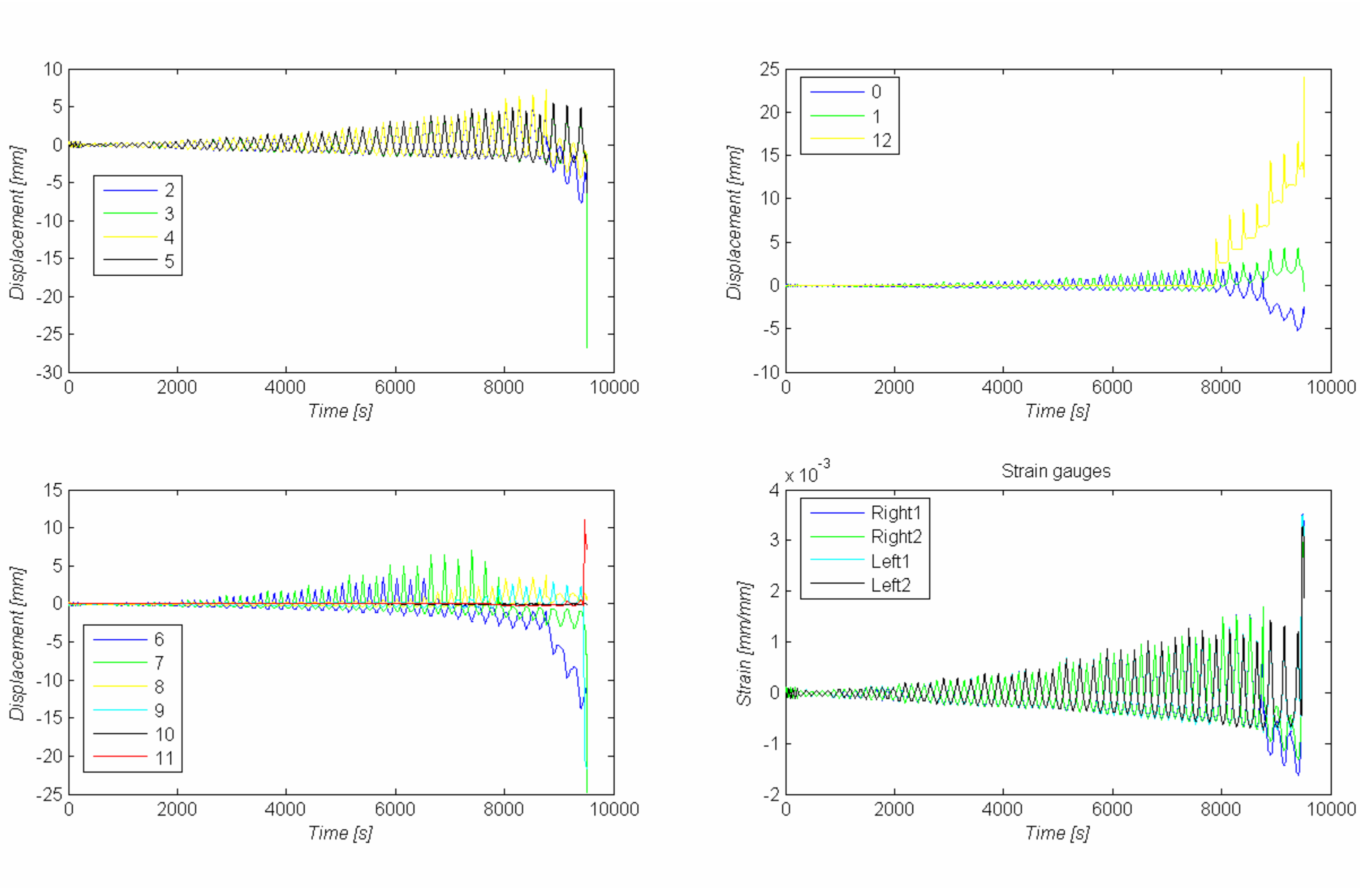
Displacement [mm]
Time [s]
2
3
4
5
0
1
12
6
7
8
9
10
11
Strain gauges
x 10^-3
Strain [mm/mm]
Right1
Right2
Left1
Left2

## WALL CL01

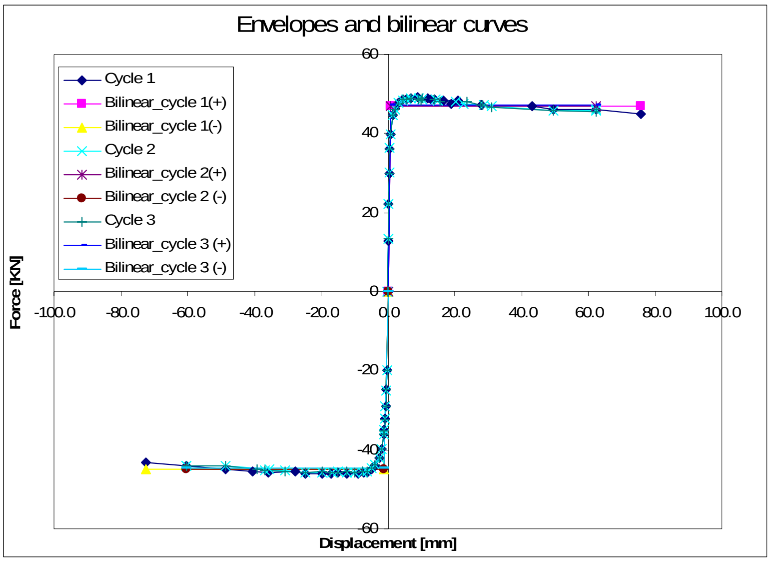
Envelopes and bilinear curves
Cycle 1
Bilinear_cycle 1(+)
Bilinear_cycle 1(-)
Cycle 2
Bilinear_cycle 2(+)
Bilinear_cycle 2 (-)
Cycle 3
Bilinear_cycle 3 (+)
Bilinear_cycle 3 (-)
Force [KN]
Displacement [mm]

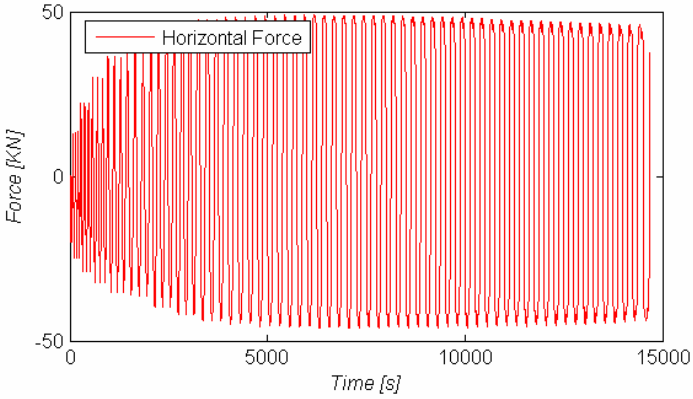
Horizontal Force
Force [KN]
Time [s]

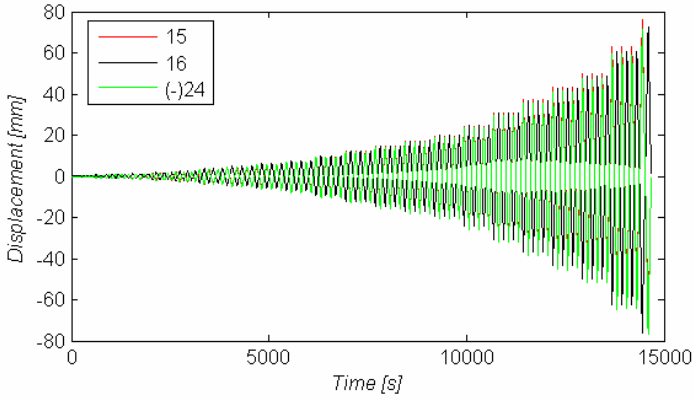
15
16
(-)24
Displacement [mm]
Time [s]

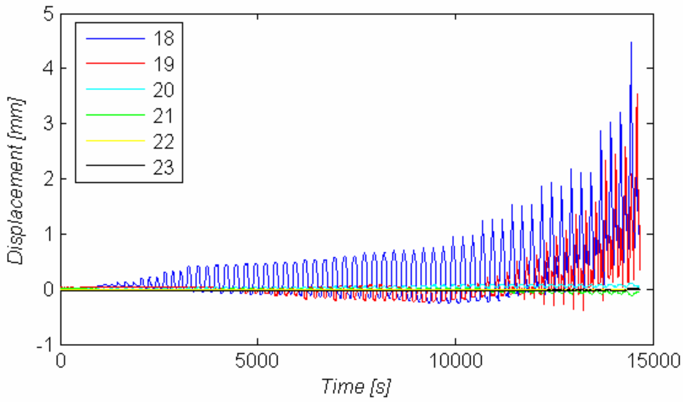
18
19
20
21
22
23
Displacement [mm]
Time [s]

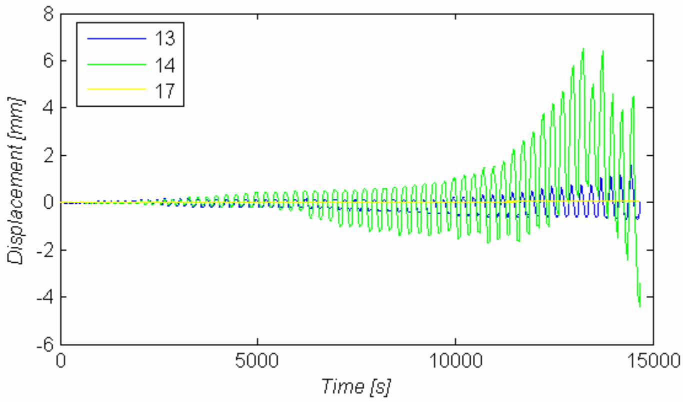
13
14
17
Displacement [mm]
Time [s]

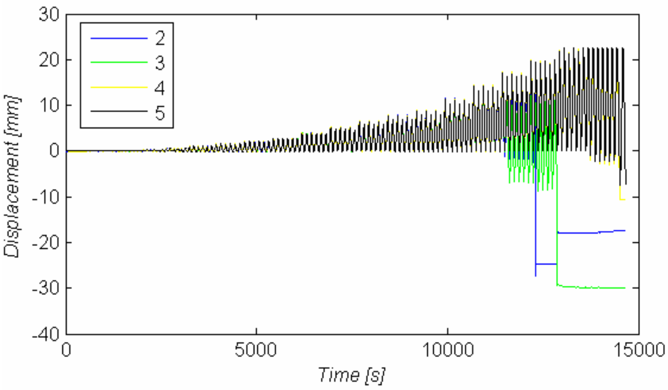
Displacement [mm]
Time [s]
2
3
4
5

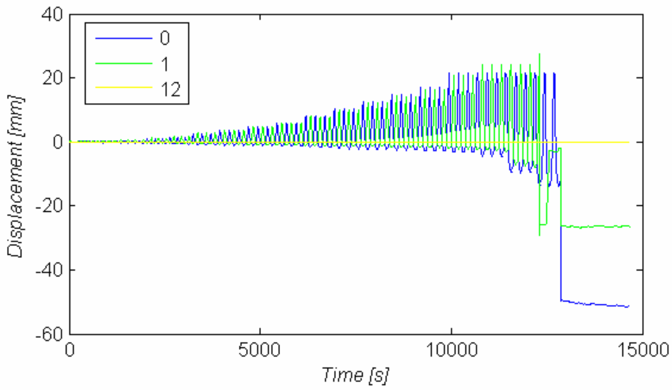
Displacement [mm]
Time [s]
0
1
12

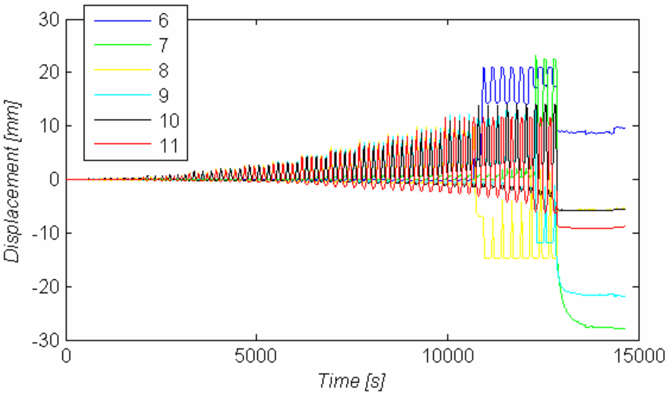
Displacement [mm]
Time [s]
6
7
8
9
10
11

# WALL CL02

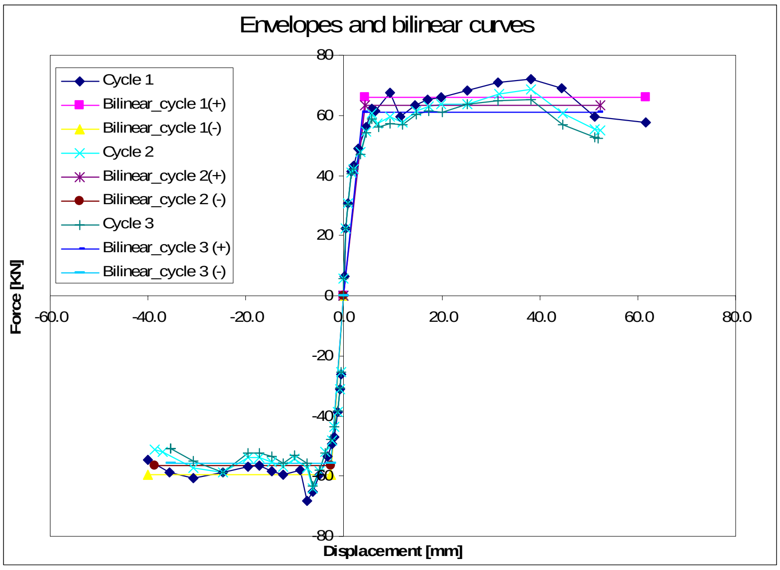
Envelopes and bilinear curves
Cycle 1
Bilinear_cycle 1(+)
Bilinear_cycle 1(-)
Cycle 2
Bilinear_cycle 2(+)
Bilinear_cycle 2 (-)
Cycle 3
Bilinear_cycle 3 (+)
Bilinear_cycle 3 (-)
Force [KN]
Displacement [mm]

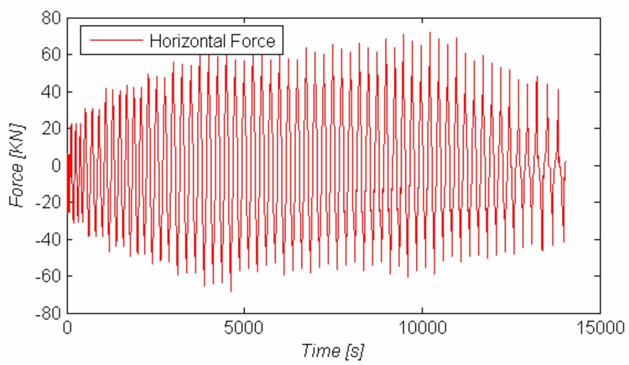
Horizontal Force
Force [KN]
Time [s]

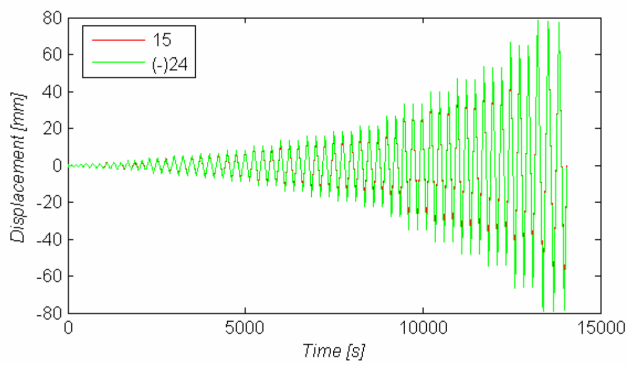
15
(-)24
Displacement [mm]
Time [s]

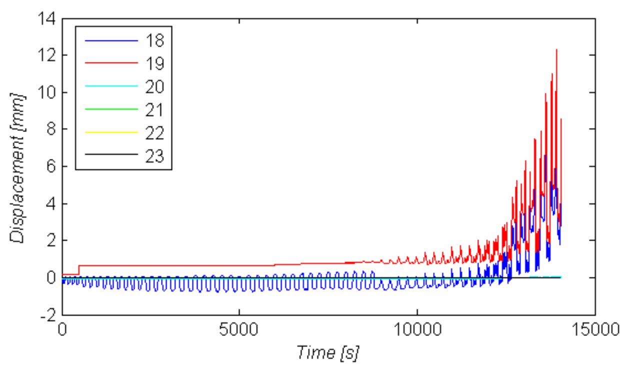
18
19
20
21
22
23
Displacement [mm]
Time [s]

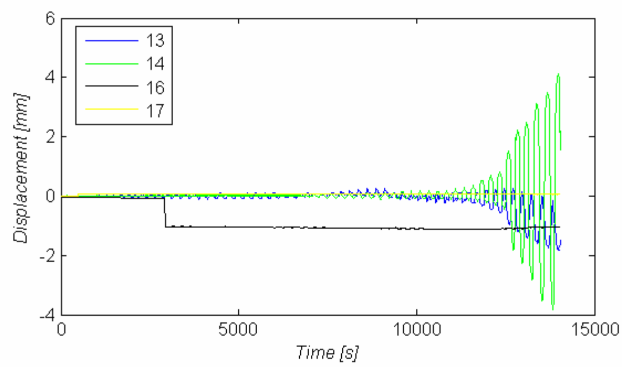
13
14
16
17
Displacement [mm]
Time [s]

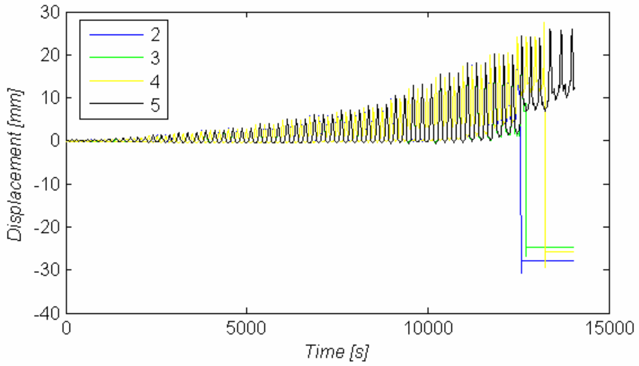
Displacement [mm]
Time [s]
2
3
4
5

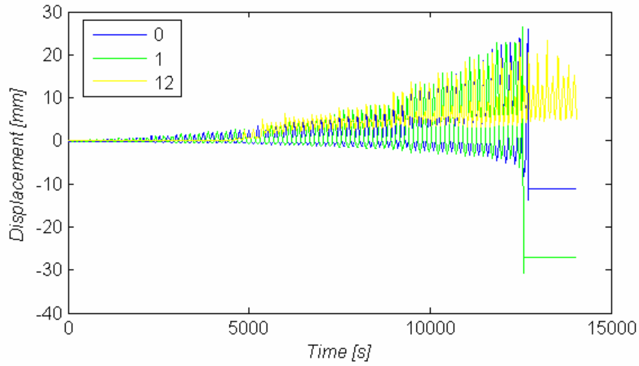
Displacement [mm]
Time [s]
0
1
12

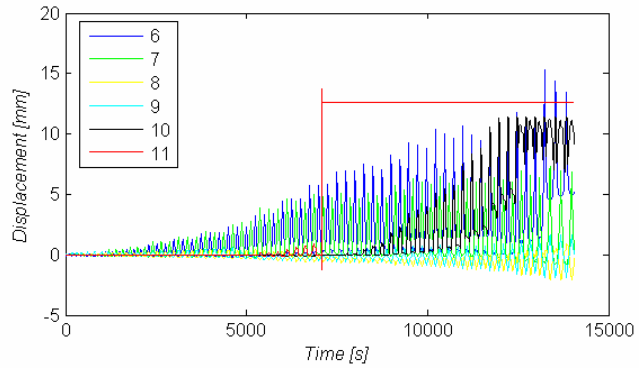
Displacement [mm]
Time [s]
6
7
8
9
10
11

## WALL CL03

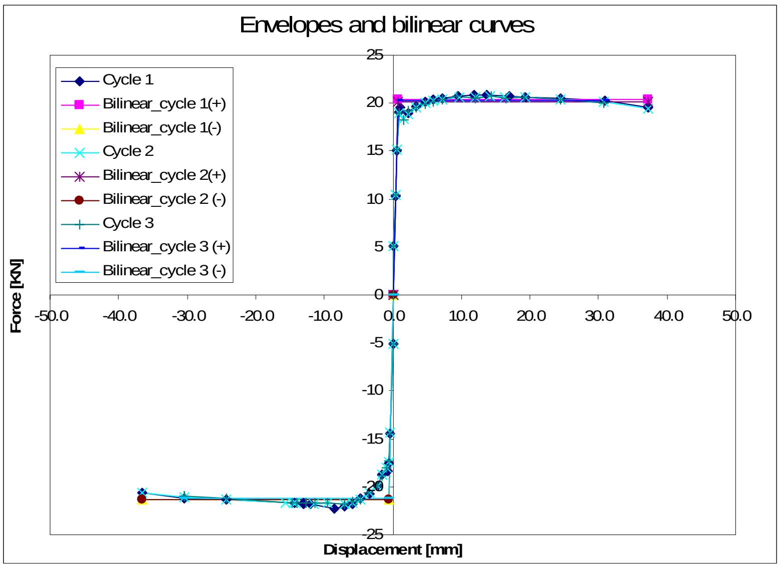
Envelopes and bilinear curves
Cycle 1
Bilinear_cycle 1(+)
Bilinear_cycle 1(-)
Cycle 2
Bilinear_cycle 2(+)
Bilinear_cycle 2 (-)
Cycle 3
Bilinear_cycle 3 (+)
Bilinear_cycle 3 (-)
Force [KN]
Displacement [mm]

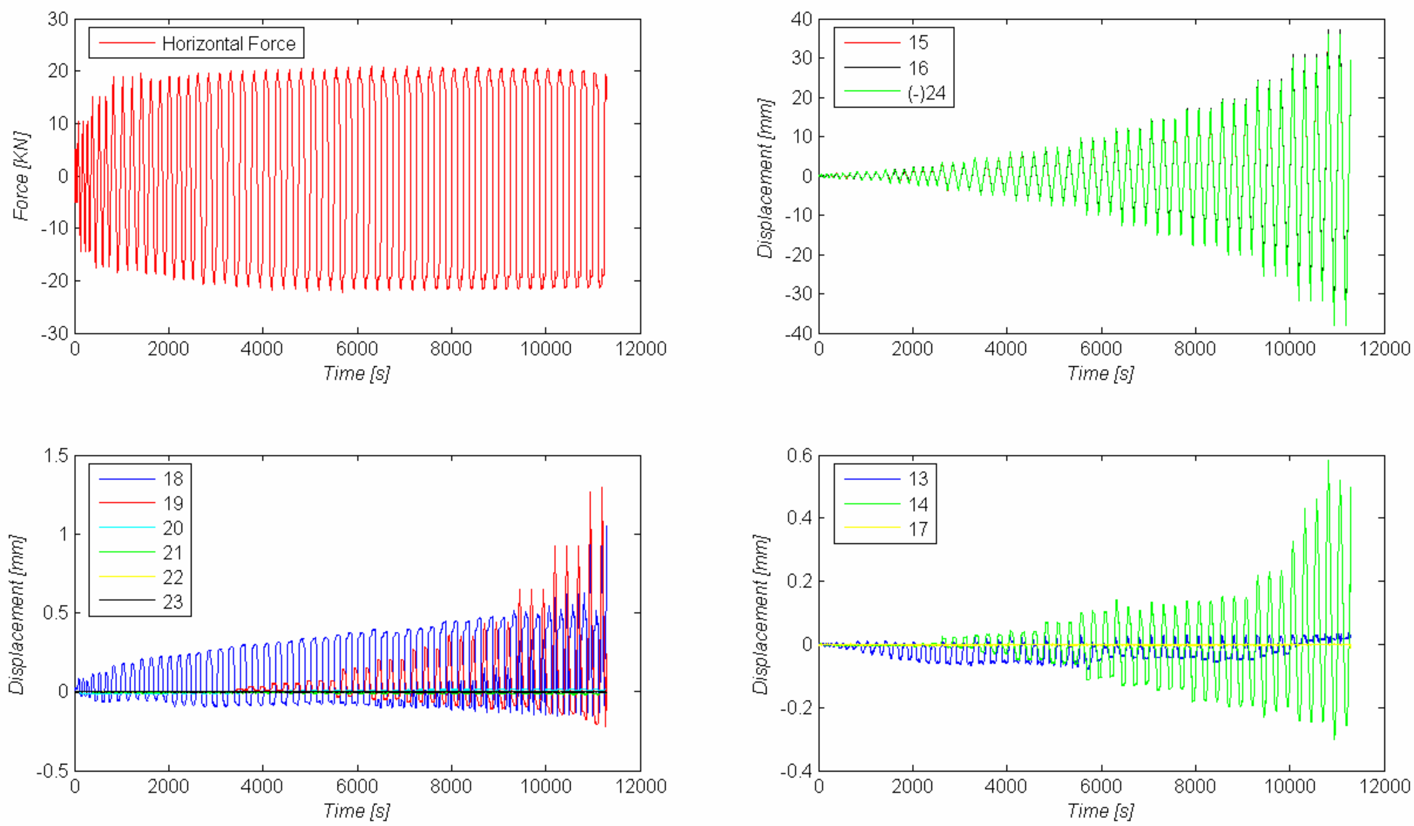
Horizontal Force
Force [KN]
Time [s]
15
16
(-)24
Displacement [mm]
Time [s]
18
19
20
21
22
23
Displacement [mm]
Time [s]
13
14
17
Displacement [mm]
Time [s]

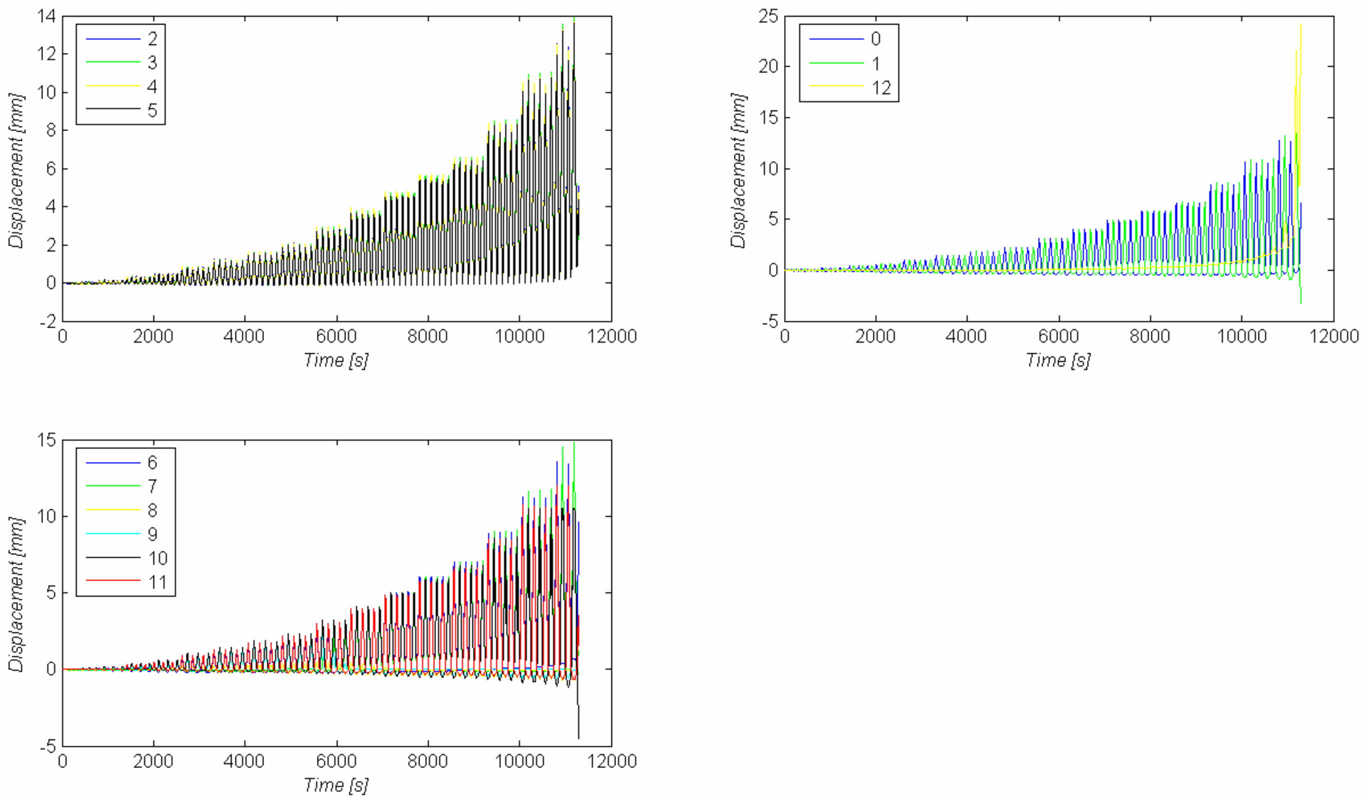
2
3
4
5
Displacement [mm]
Time [s]
0
1
12
Displacement [mm]
Time [s]
6
7
8
9
10
11
Displacement [mm]
Time [s]

# WALL CL05

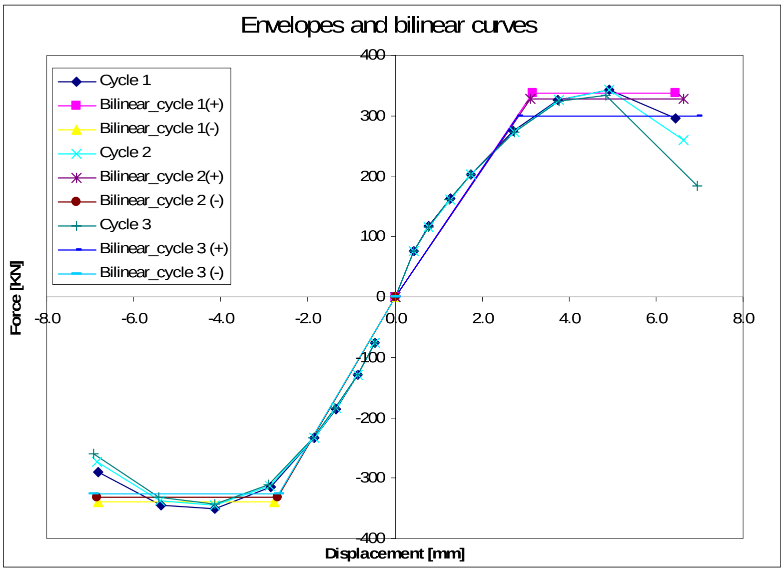
Envelopes and bilinear curves
Cycle 1
Bilinear_cycle 1(+)
Bilinear_cycle 1(-)
Cycle 2
Bilinear_cycle 2(+)
Bilinear_cycle 2 (-)
Cycle 3
Bilinear_cycle 3 (+)
Bilinear_cycle 3 (-)
Force [KN]
Displacement [mm]

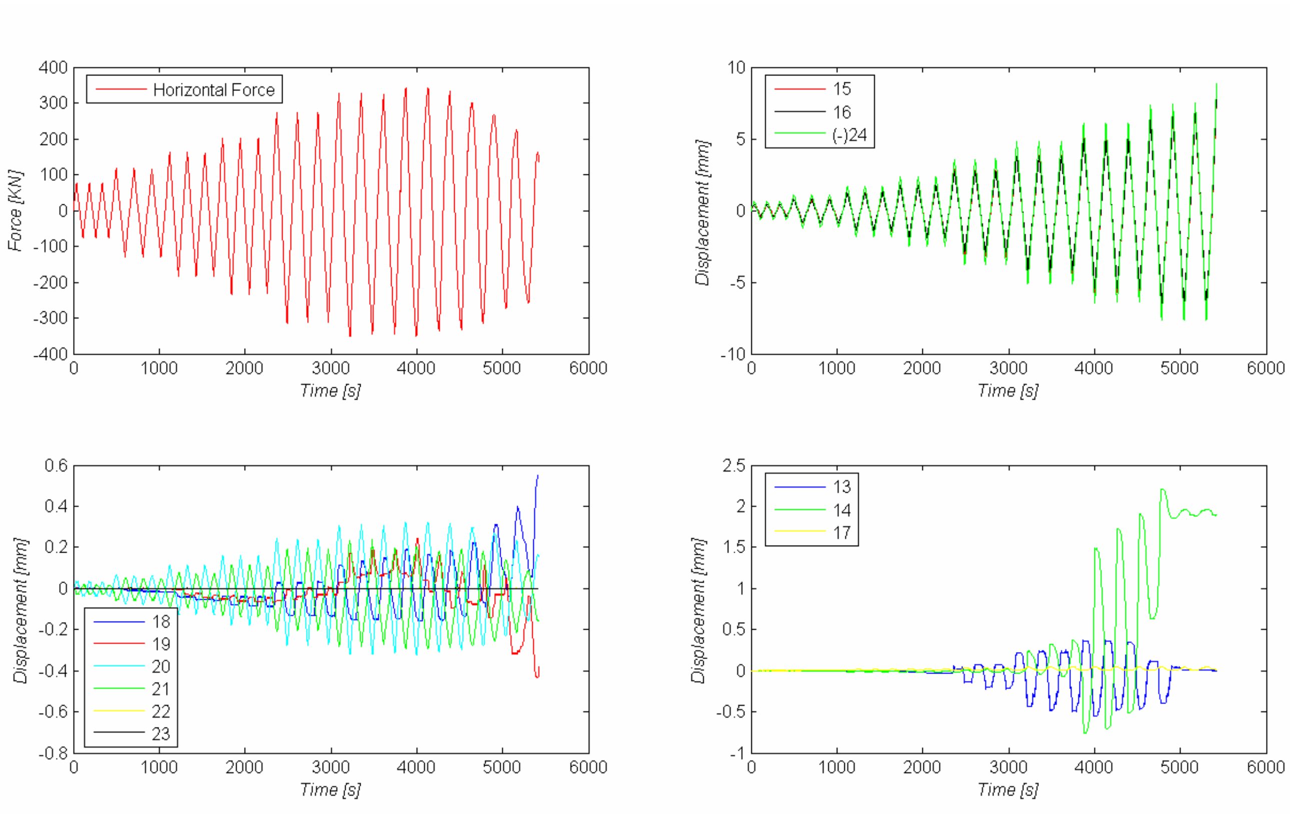
Horizontal Force
Force [KN]
Time [s]
15
16
(-)24
Displacement [mm]
Time [s]
18
19
20
21
22
23
Displacement [mm]
Time [s]
13
14
17
Displacement [mm]
Time [s]

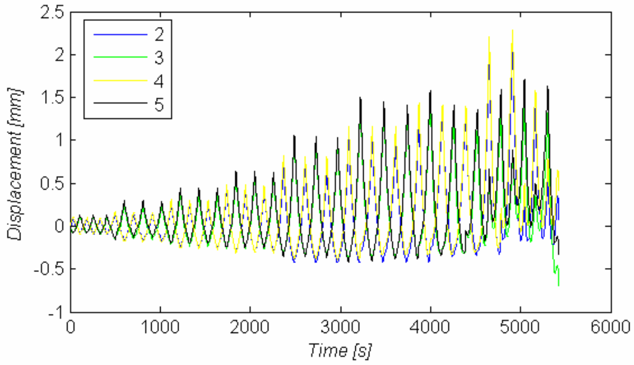
2
3
4
5
Displacement [mm]
Time [s]

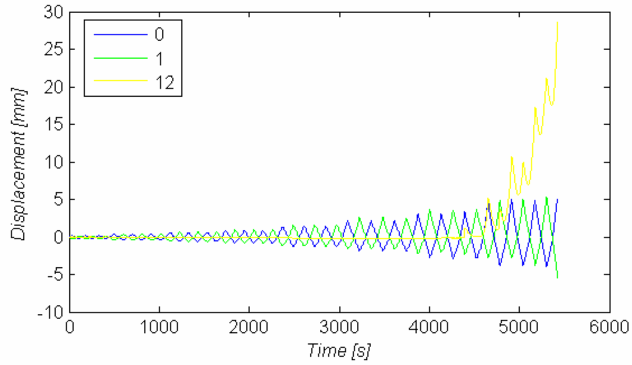
0
1
12
Displacement [mm]
Time [s]

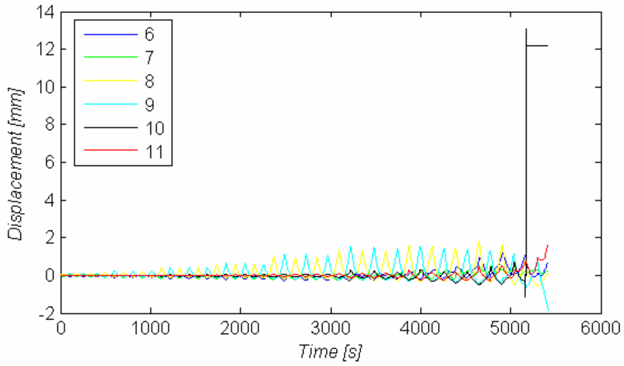
6
7
8
9
10
11
Displacement [mm]
Time [s]

# WALL CL06

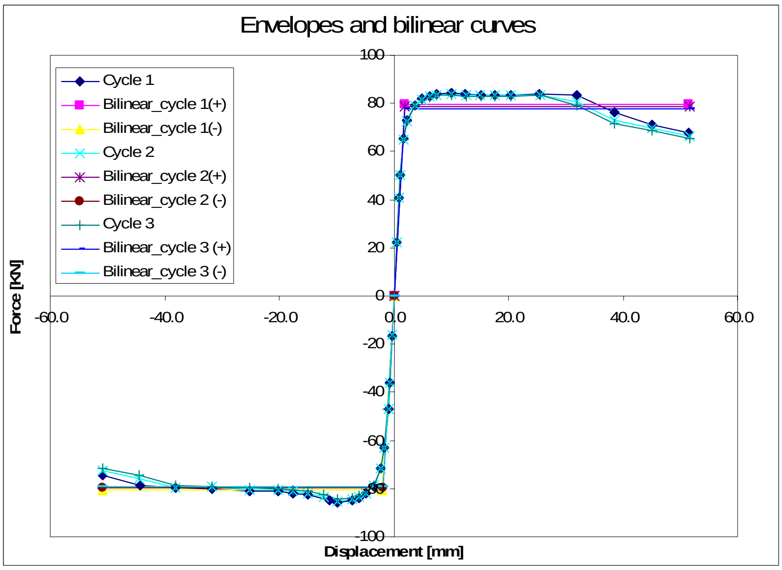
Envelopes and bilinear curves
Cycle 1
Bilinear_cycle 1(+)
Bilinear_cycle 1(-)
Cycle 2
Bilinear_cycle 2(+)
Bilinear_cycle 2 (-)
Cycle 3
Bilinear_cycle 3 (+)
Bilinear_cycle 3 (-)
Force [KN]
Displacement [mm]

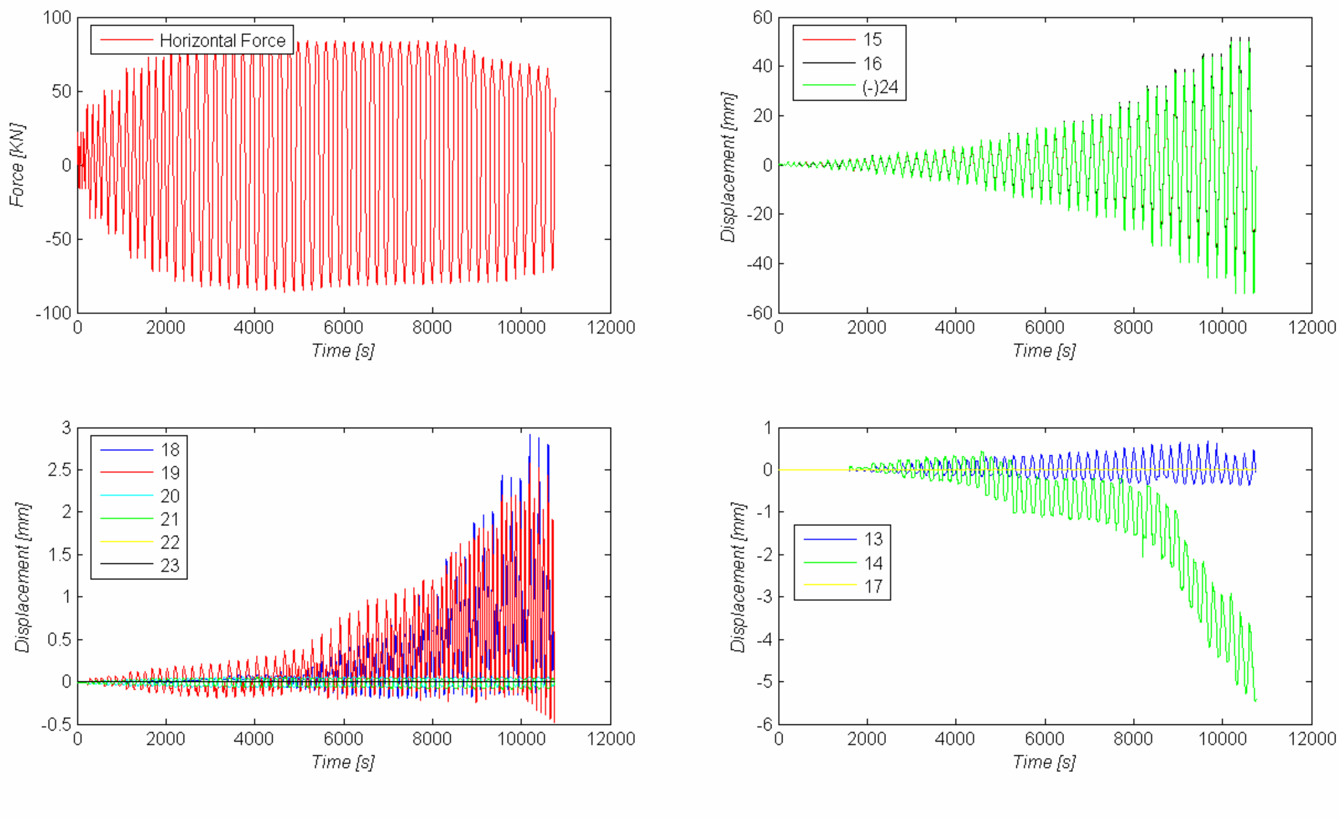
Horizontal Force
Force [KN]
Time [s]
15
16
(-)24
Displacement [mm]
Time [s]
18
19
20
21
22
23
Displacement [mm]
Time [s]
13
14
17
Displacement [mm]
Time [s]

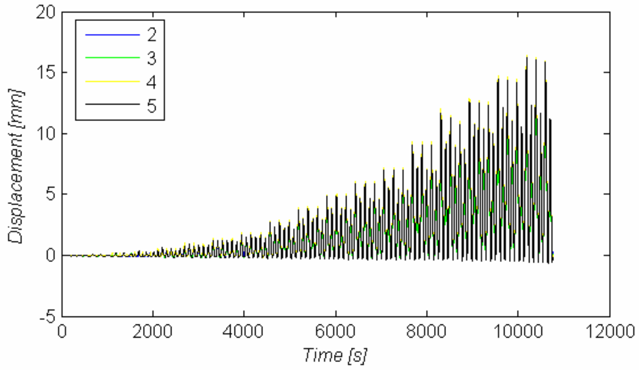
2
3
4
5
Displacement [mm]
Time [s]

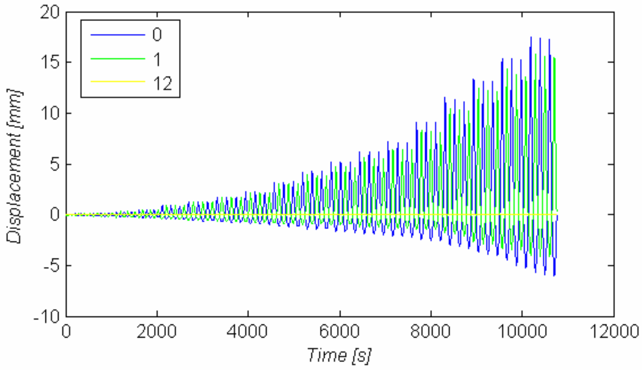
0
1
12
Displacement [mm]
Time [s]

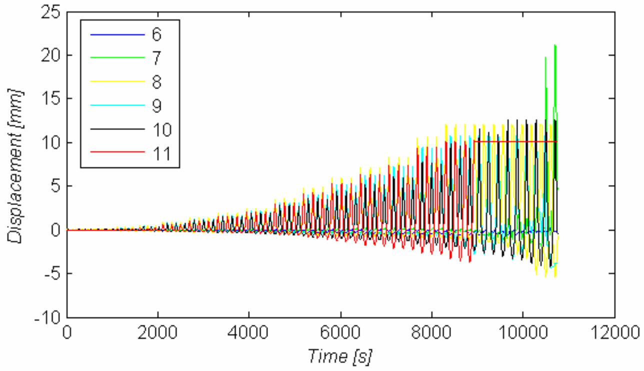
6
7
8
9
10
11
Displacement [mm]
Time [s]

# WALL CL07

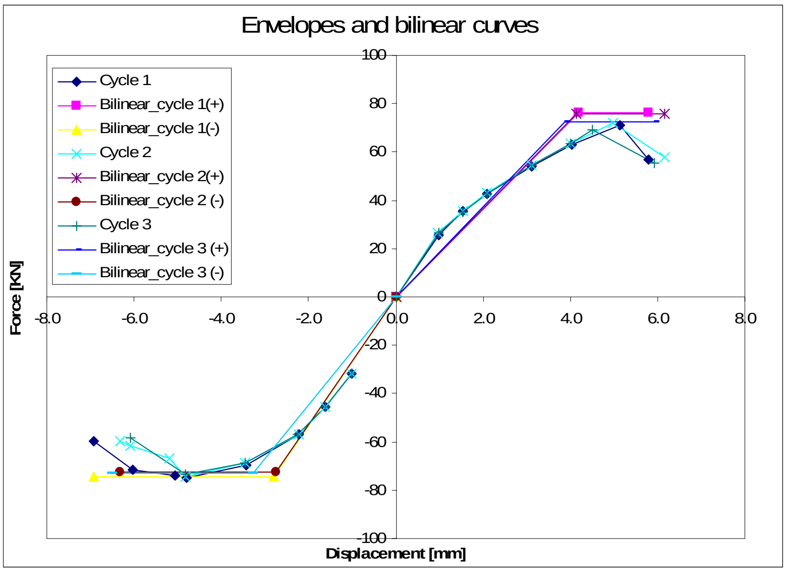
Envelopes and bilinear curves
Cycle 1
Bilinear_cycle 1(+)
Bilinear_cycle 1(-)
Cycle 2
Bilinear_cycle 2(+)
Bilinear_cycle 2 (-)
Cycle 3
Bilinear_cycle 3 (+)
Bilinear_cycle 3 (-)
Force [KN]
Displacement [mm]

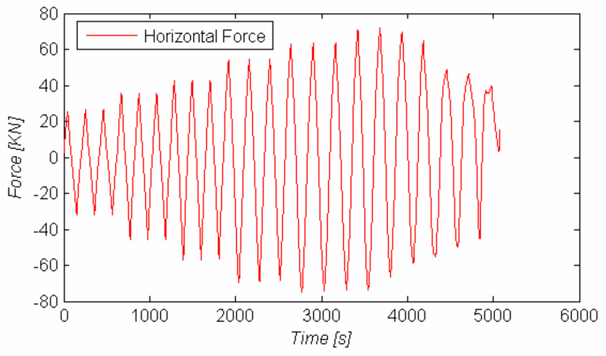
Horizontal Force
Force [KN]
Time [s]

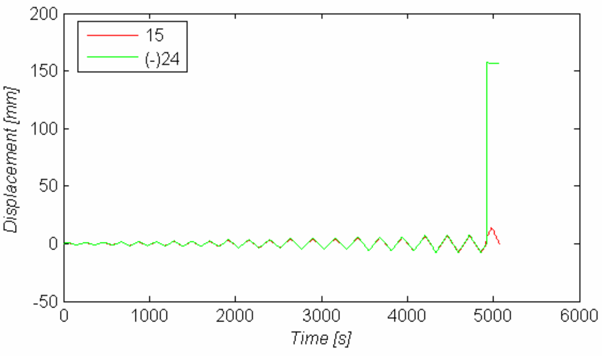
15
(-)24
Displacement [mm]
Time [s]

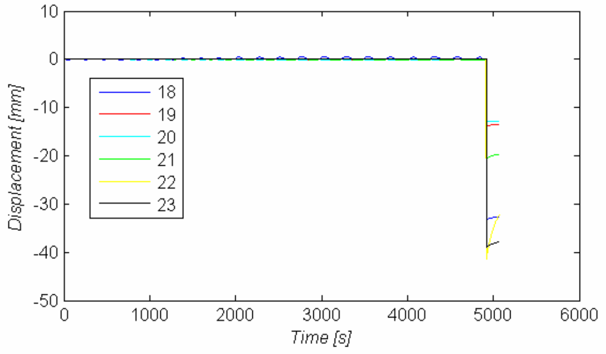
18
19
20
21
22
23
Displacement [mm]
Time [s]

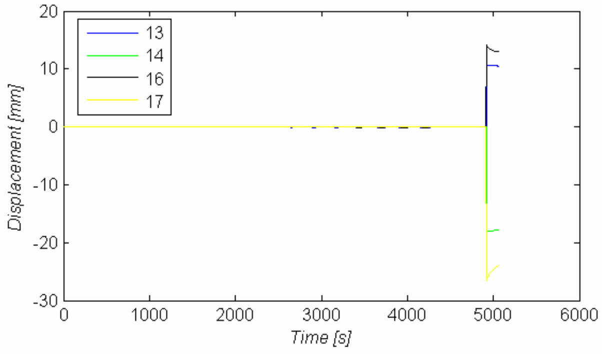
13
14
16
17
Displacement [mm]
Time [s]

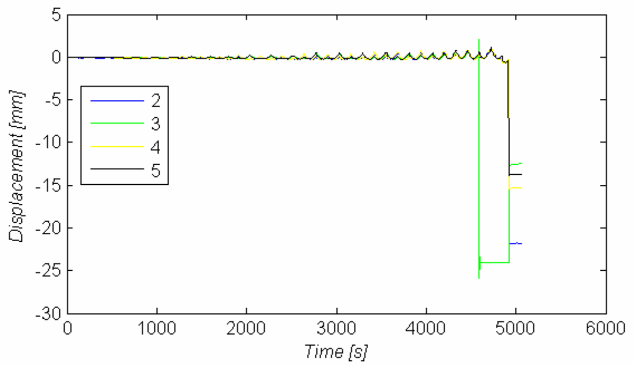
Displacement [mm]
Time [s]
2
3
4
5

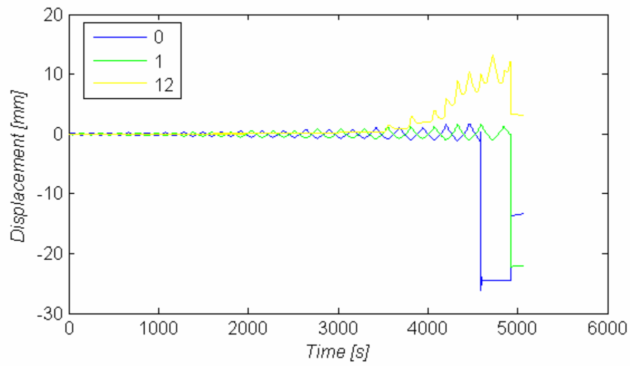
Displacement [mm]
Time [s]
0
1
12

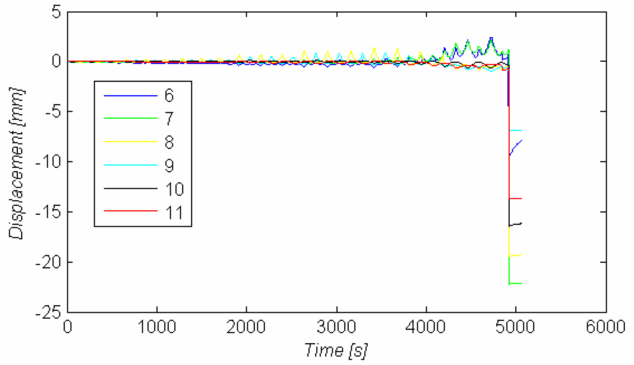
Displacement [mm]
Time [s]
6
7
8
9
10
11

# WALL CL08

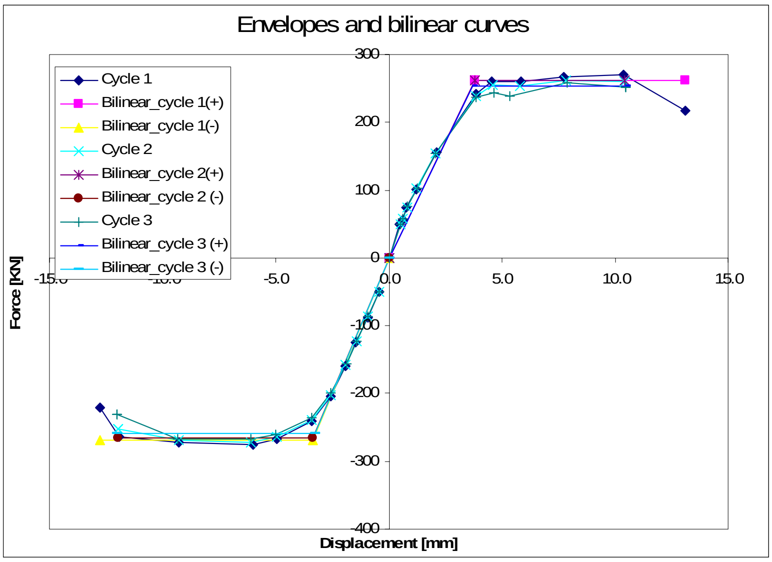
Envelopes and bilinear curves
Cycle 1
Bilinear_cycle 1(+)
Bilinear_cycle 1(-)
Cycle 2
Bilinear_cycle 2(+)
Bilinear_cycle 2 (-)
Cycle 3
Bilinear_cycle 3 (+)
Bilinear_cycle 3 (-)
Force [KN]
Displacement [mm]

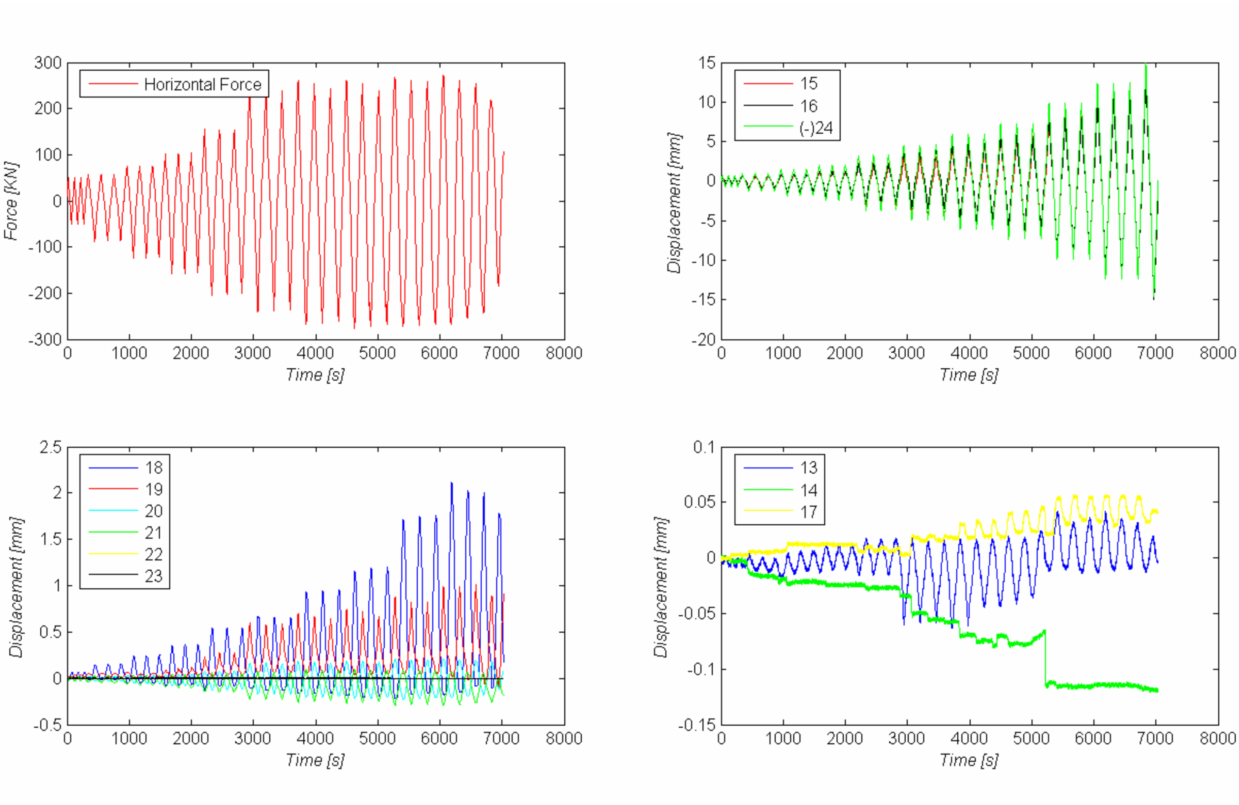
Horizontal Force
Force [KN]
Time [s]
15
16
(-)24
Displacement [mm]
Time [s]
18
19
20
21
22
23
Displacement [mm]
Time [s]
13
14
17
Displacement [mm]
Time [s]

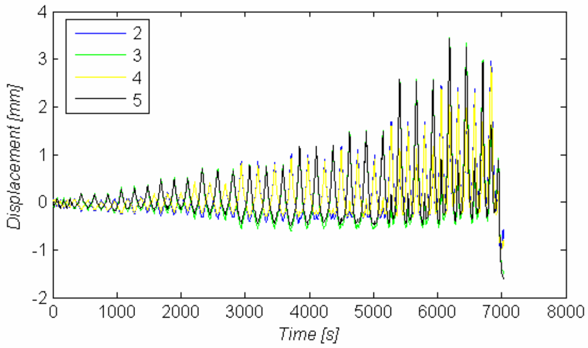
Displacement [mm]
Time [s]
2
3
4
5

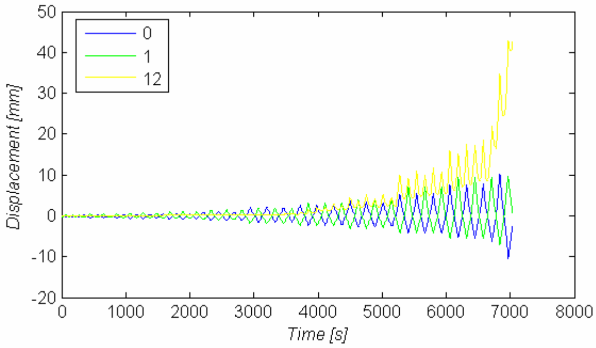
Displacement [mm]
Time [s]
0
1
12

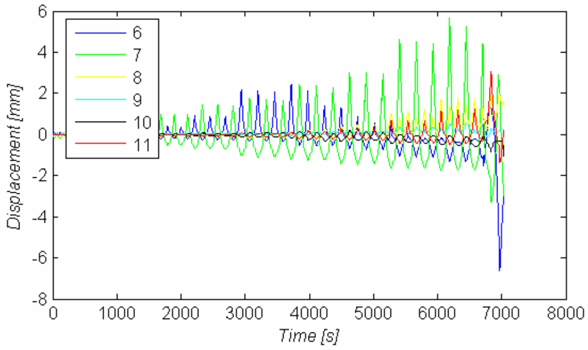
Displacement [mm]
Time [s]
6
7
8
9
10
11

# WALL CL09

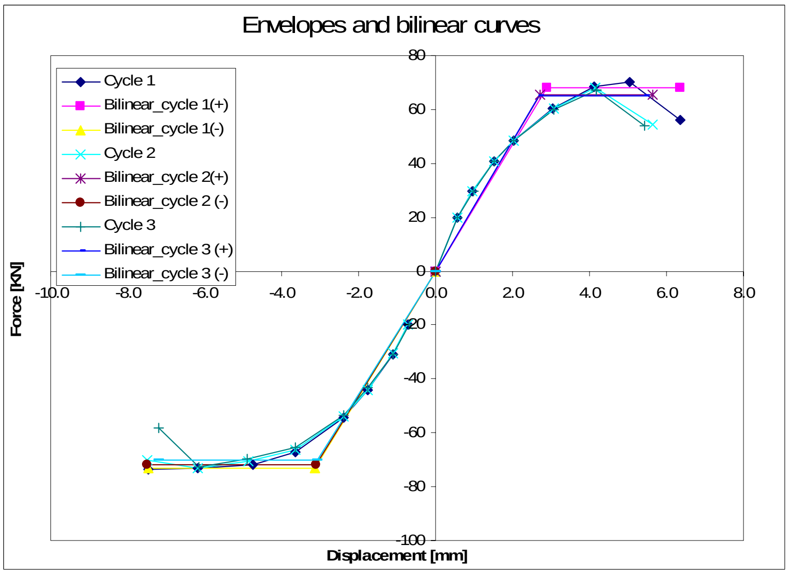
Envelopes and bilinear curves
Cycle 1
Bilinear_cycle 1(+)
Bilinear_cycle 1(-)
Cycle 2
Bilinear_cycle 2(+)
Bilinear_cycle 2 (-)
Cycle 3
Bilinear_cycle 3 (+)
Bilinear_cycle 3 (-)
Force [KN]
Displacement [mm]

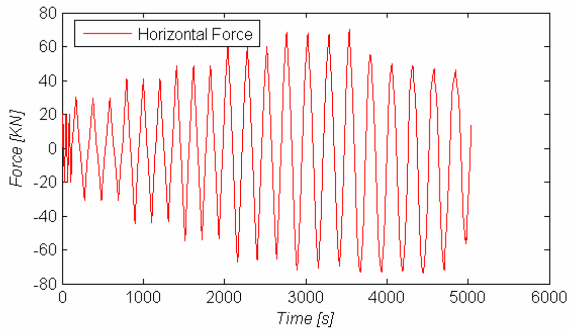
Horizontal Force
Force [KN]
Time [s]

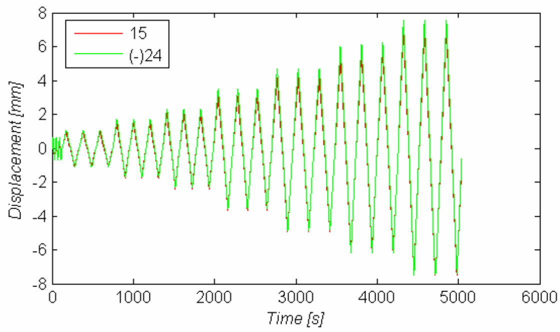
15
(-)24
Displacement [mm]
Time [s]

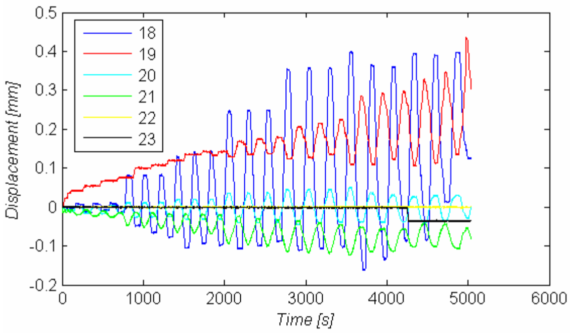
18
19
20
21
22
23
Displacement [mm]
Time [s]

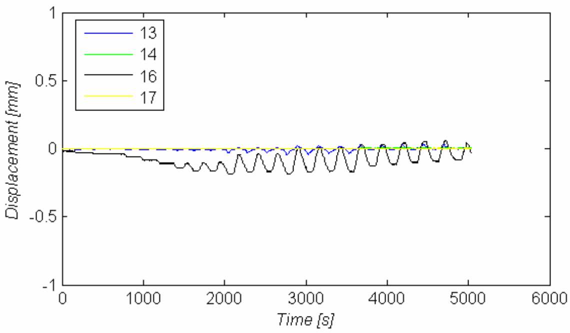
13
14
16
17
Displacement [mm]
Time [s]

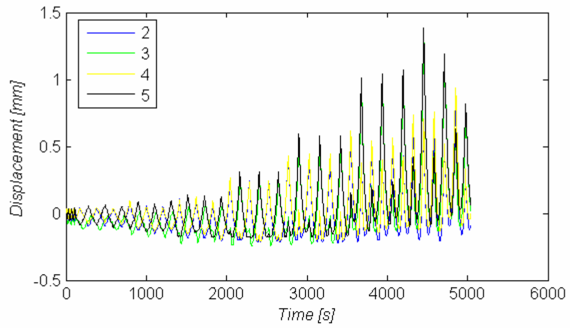
2
3
4
5
Displacement [mm]
Time [s]

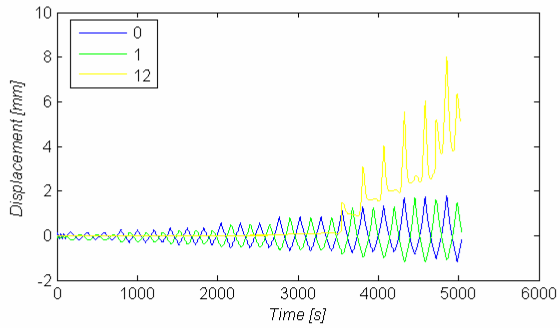
0
1
12
Displacement [mm]
Time [s]

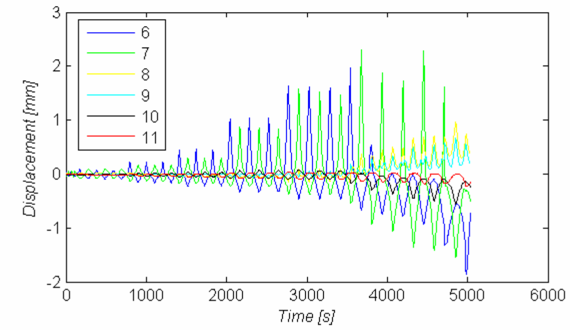
6
7
8
9
10
11
Displacement [mm]
Time [s]

## WALL CL10

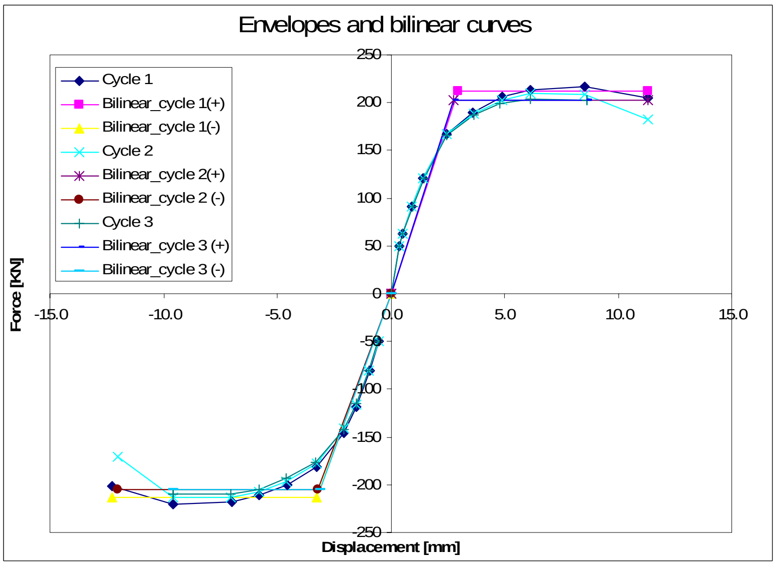
Envelopes and bilinear curves
Cycle 1
Bilinear_cycle 1(+)
Bilinear_cycle 1(-)
Cycle 2
Bilinear_cycle 2(+)
Bilinear_cycle 2 (-)
Cycle 3
Bilinear_cycle 3 (+)
Bilinear_cycle 3 (-)
Force [KN]
Displacement [mm]

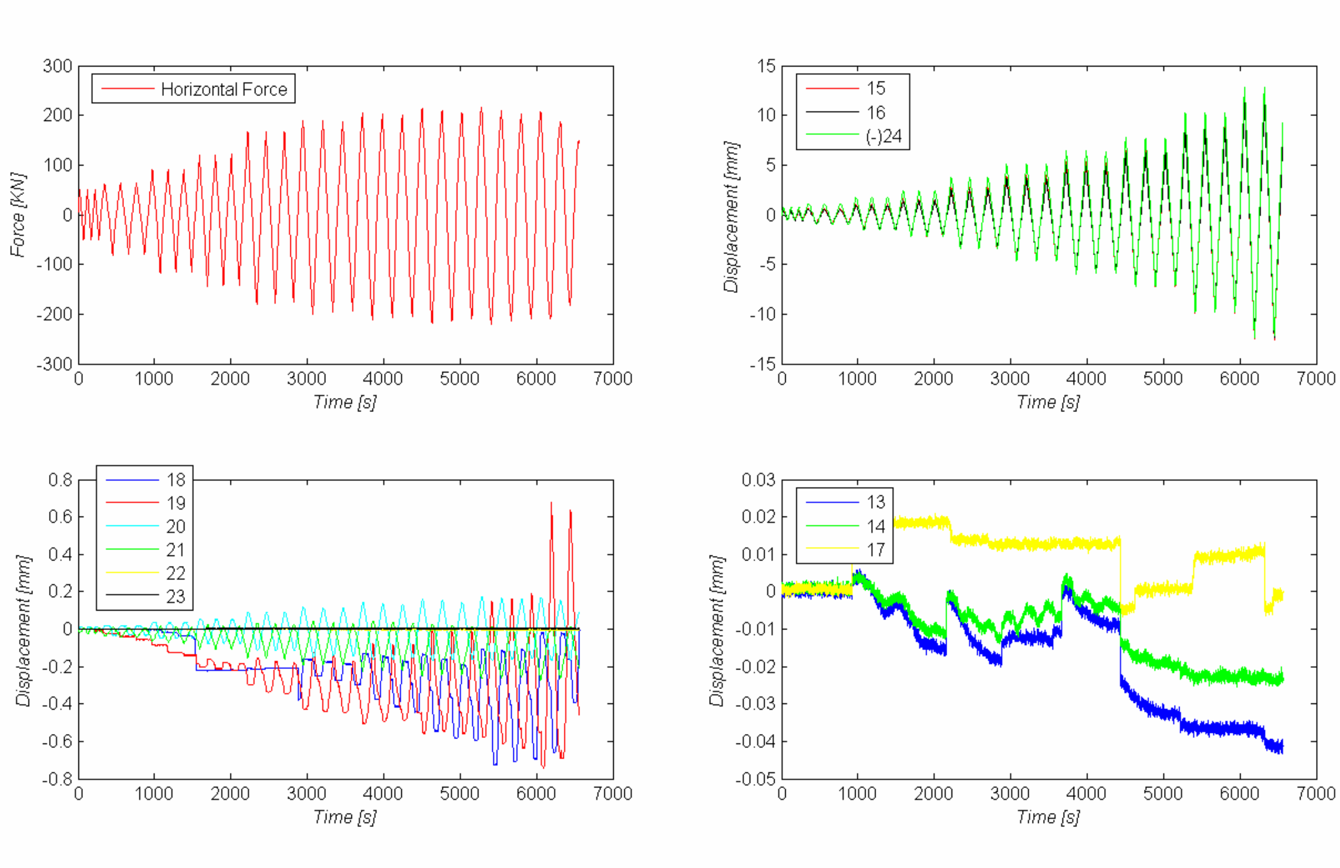
Horizontal Force
Force [KN]
Time [s]
15
16
(-)24
Displacement [mm]
Time [s]
18
19
20
21
22
23
Displacement [mm]
Time [s]
13
14
17
Displacement [mm]
Time [s]

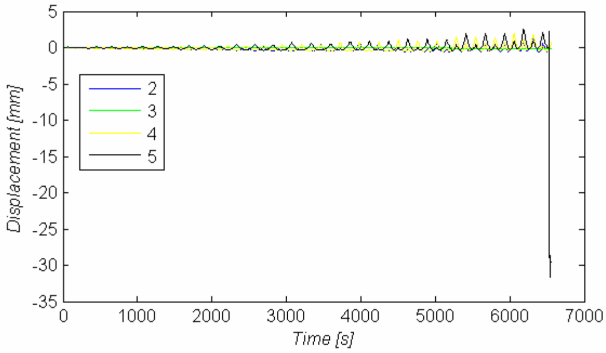
Displacement [mm]
Time [s]
2
3
4
5

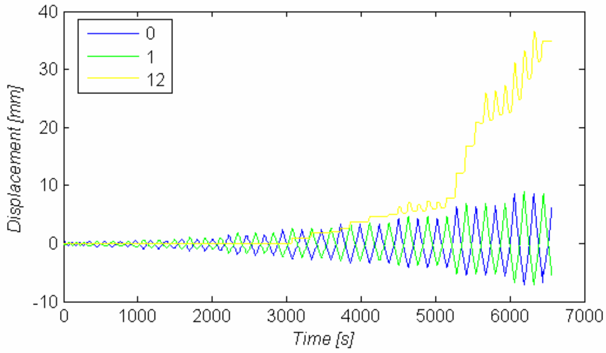
Displacement [mm]
Time [s]
0
1
12

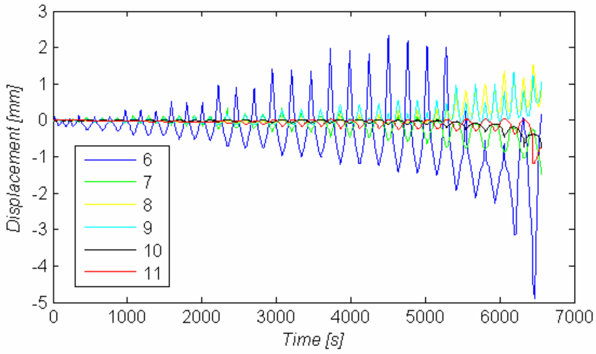
Displacement [mm]
Time [s]
6
7
8
9
10
11

# WALL LAC01

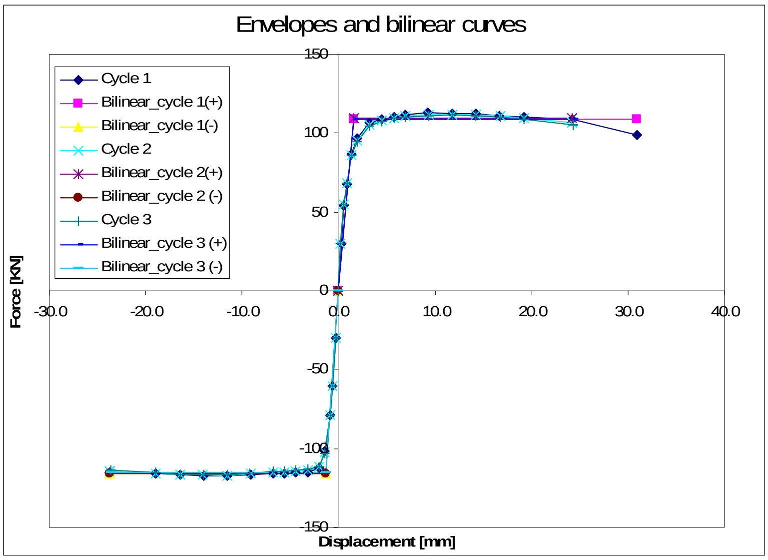
Envelopes and bilinear curves
Cycle 1
Bilinear_cycle 1(+)
Bilinear_cycle 1(-)
Cycle 2
Bilinear_cycle 2(+)
Bilinear_cycle 2 (-)
Cycle 3
Bilinear_cycle 3 (+)
Bilinear_cycle 3 (-)
Force [KN]
Displacement [mm]

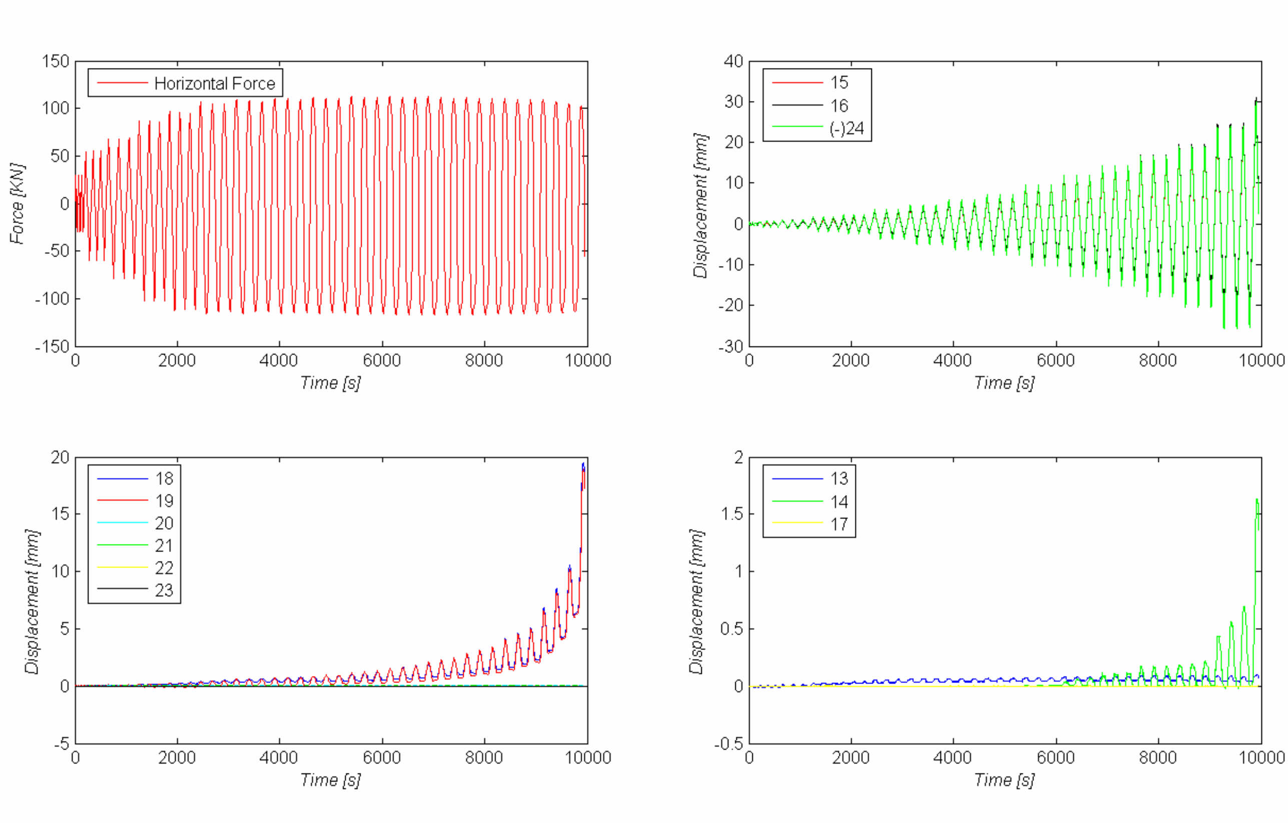
Horizontal Force
Force [KN]
Time [s]
15
16
(-)24
Displacement [mm]
18
19
20
21
22
23
13
14
17

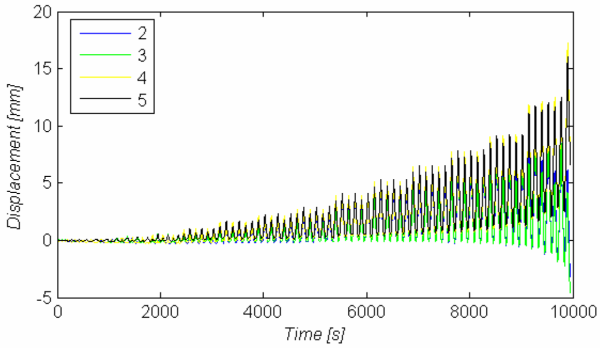
20
15
10
5
0
-5
Displacement [mm]
0
2000
4000
6000
8000
10000
Time [s]
2
3
4
5

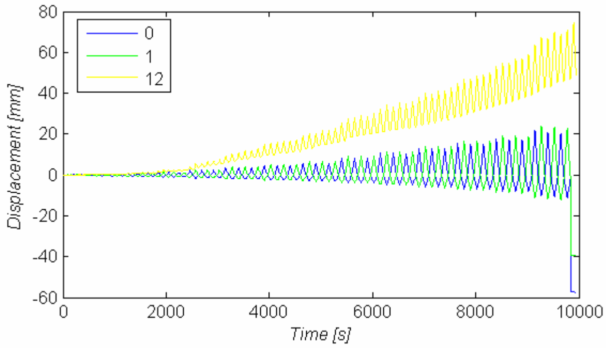
80
60
40
20
0
-20
-40
-60
Displacement [mm]
0
2000
4000
6000
8000
10000
Time [s]
0
1
12

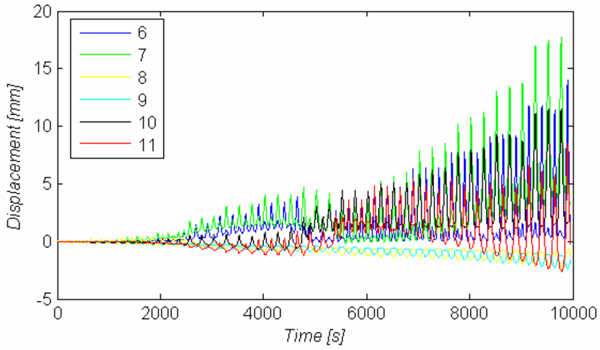
20
15
10
5
0
-5
Displacement [mm]
0
2000
4000
6000
8000
10000
Time [s]
6
7
8
9
10
11

# WALL LAC02

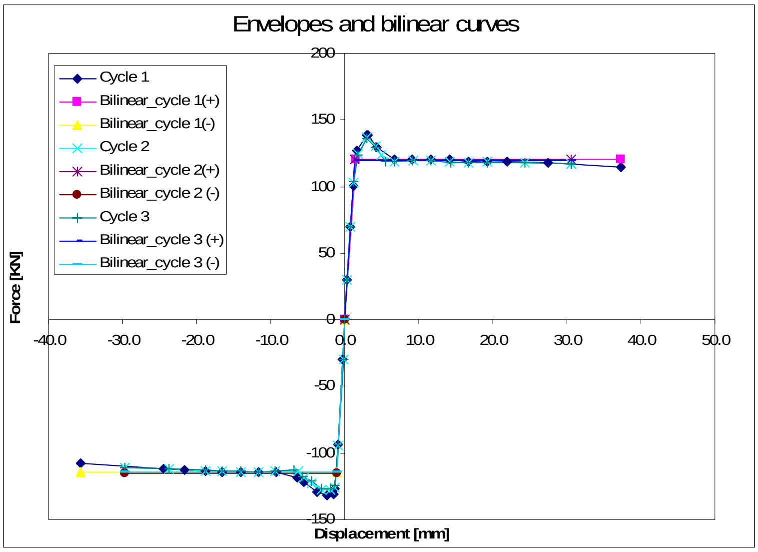
Envelopes and bilinear curves
Cycle 1
Bilinear_cycle 1(+)
Bilinear_cycle 1(-)
Cycle 2
Bilinear_cycle 2(+)
Bilinear_cycle 2 (-)
Cycle 3
Bilinear_cycle 3 (+)
Bilinear_cycle 3 (-)
Force [KN]
Displacement [mm]

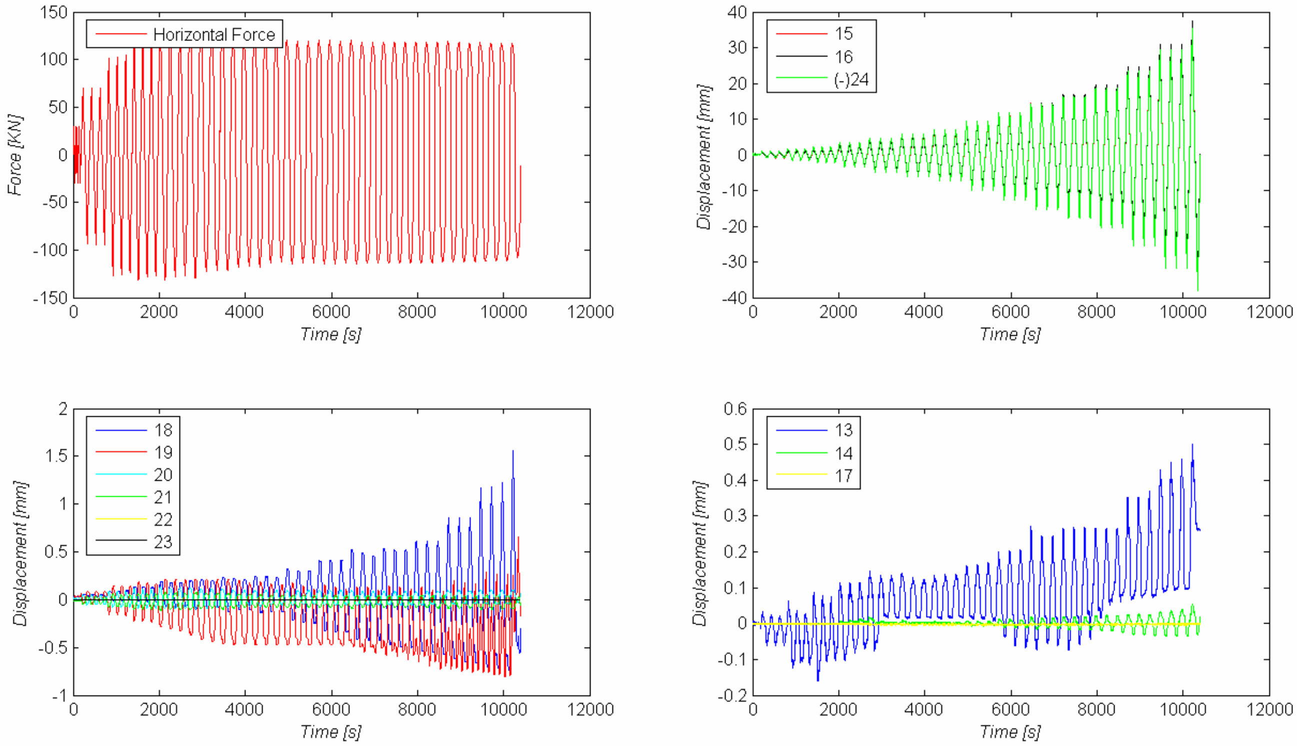
Horizontal Force
Force [KN]
Time [s]
15
16
(-)24
Displacement [mm]
Time [s]
18
19
20
21
22
23
Displacement [mm]
Time [s]
13
14
17
Displacement [mm]
Time [s]

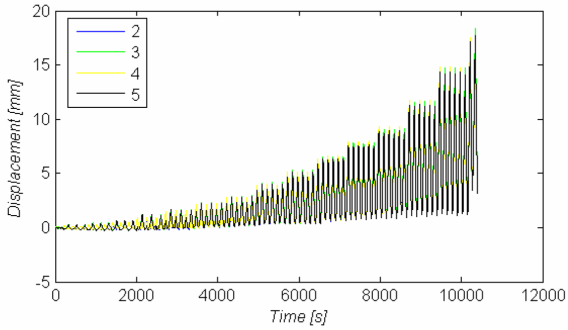
Displacement [mm]
Time [s]
2
3
4
5

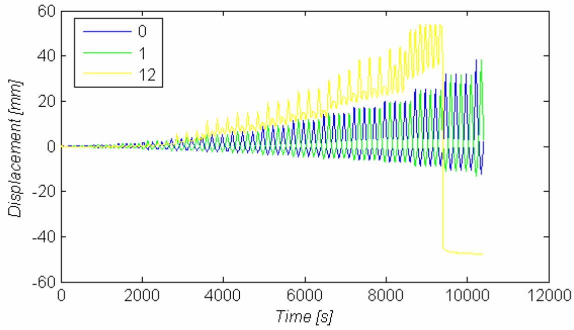
Displacement [mm]
Time [s]
0
1
12

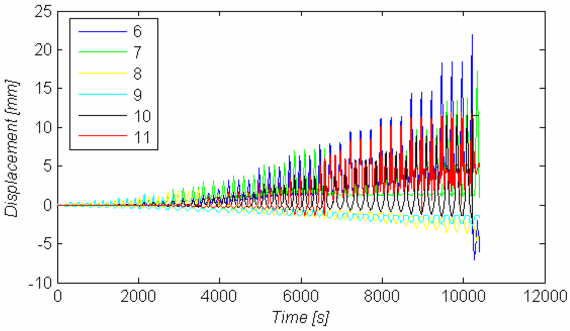
Displacement [mm]
Time [s]
6
7
8
9
10
11

# WALL LAC03

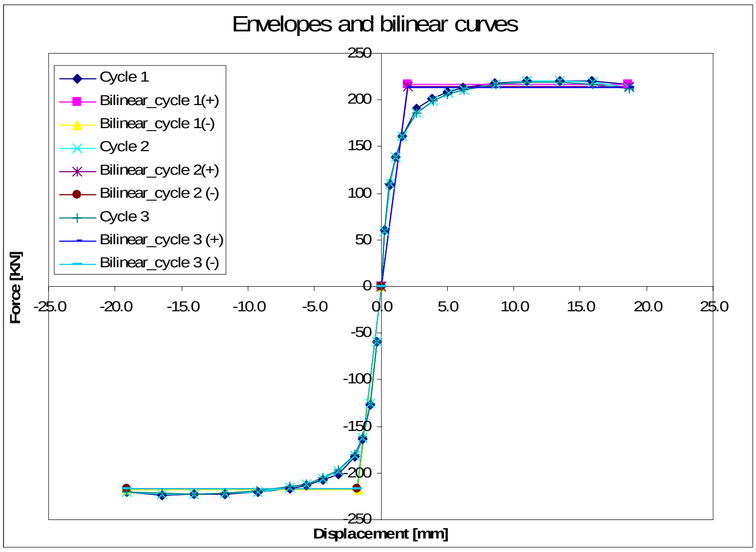
Envelopes and bilinear curves
Cycle 1
Bilinear_cycle 1(+)
Bilinear_cycle 1(-)
Cycle 2
Bilinear_cycle 2(+)
Bilinear_cycle 2 (-)
Cycle 3
Bilinear_cycle 3 (+)
Bilinear_cycle 3 (-)
Force [KN]
Displacement [mm]

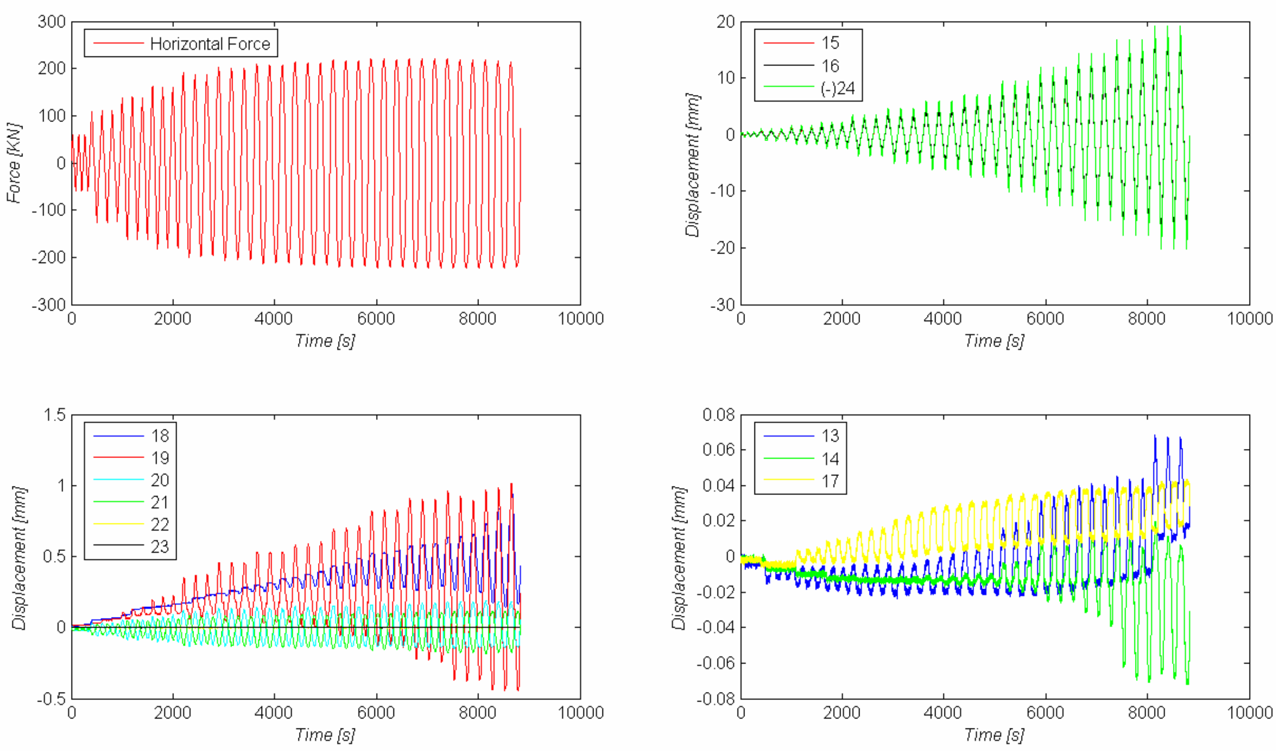
Horizontal Force
Force [KN]
Time [s]
15
16
(-)24
Displacement [mm]
Time [s]
18
19
20
21
22
23
Displacement [mm]
Time [s]
13
14
17
Displacement [mm]
Time [s]

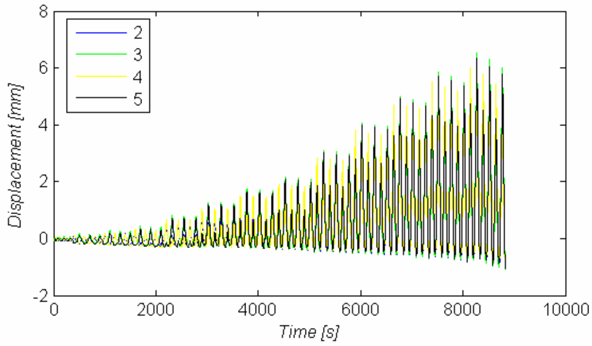
Displacement [mm]
Time [s]
2
3
4
5

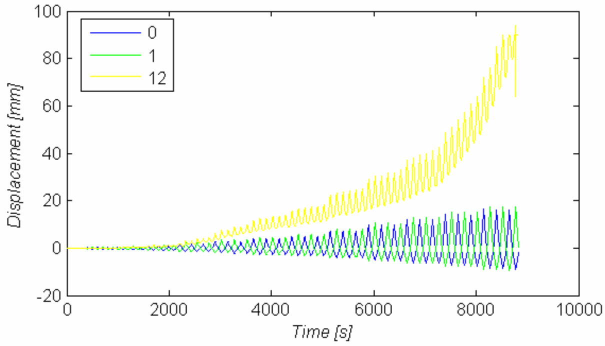
Displacement [mm]
Time [s]
0
1
12

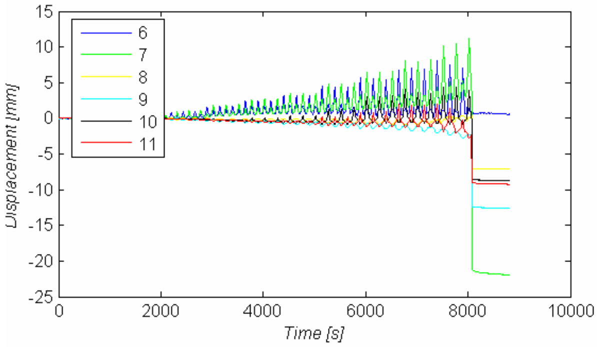
Displacement [mm]
Time [s]
6
7
8
9
10
11

## WALL LAC04

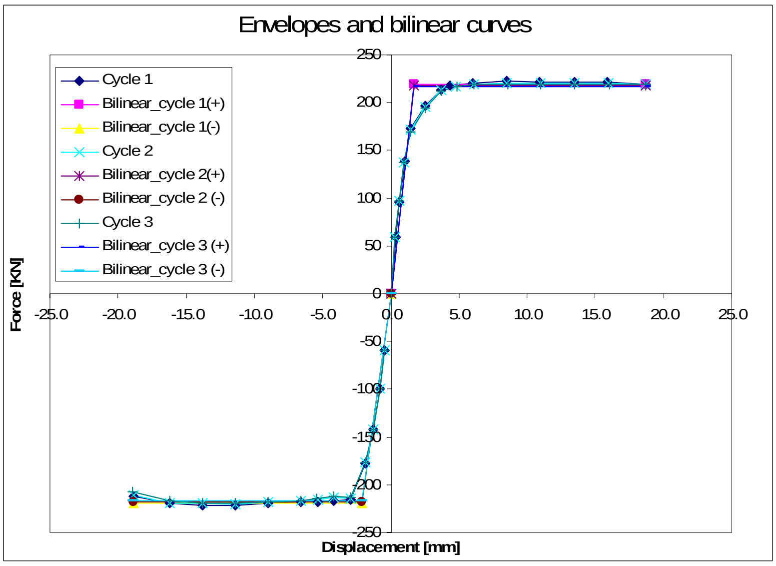
Envelopes and bilinear curves
Cycle 1
Bilinear_cycle 1(+)
Bilinear_cycle 1(-)
Cycle 2
Bilinear_cycle 2(+)
Bilinear_cycle 2 (-)
Cycle 3
Bilinear_cycle 3 (+)
Bilinear_cycle 3 (-)
Force [KN]
Displacement [mm]

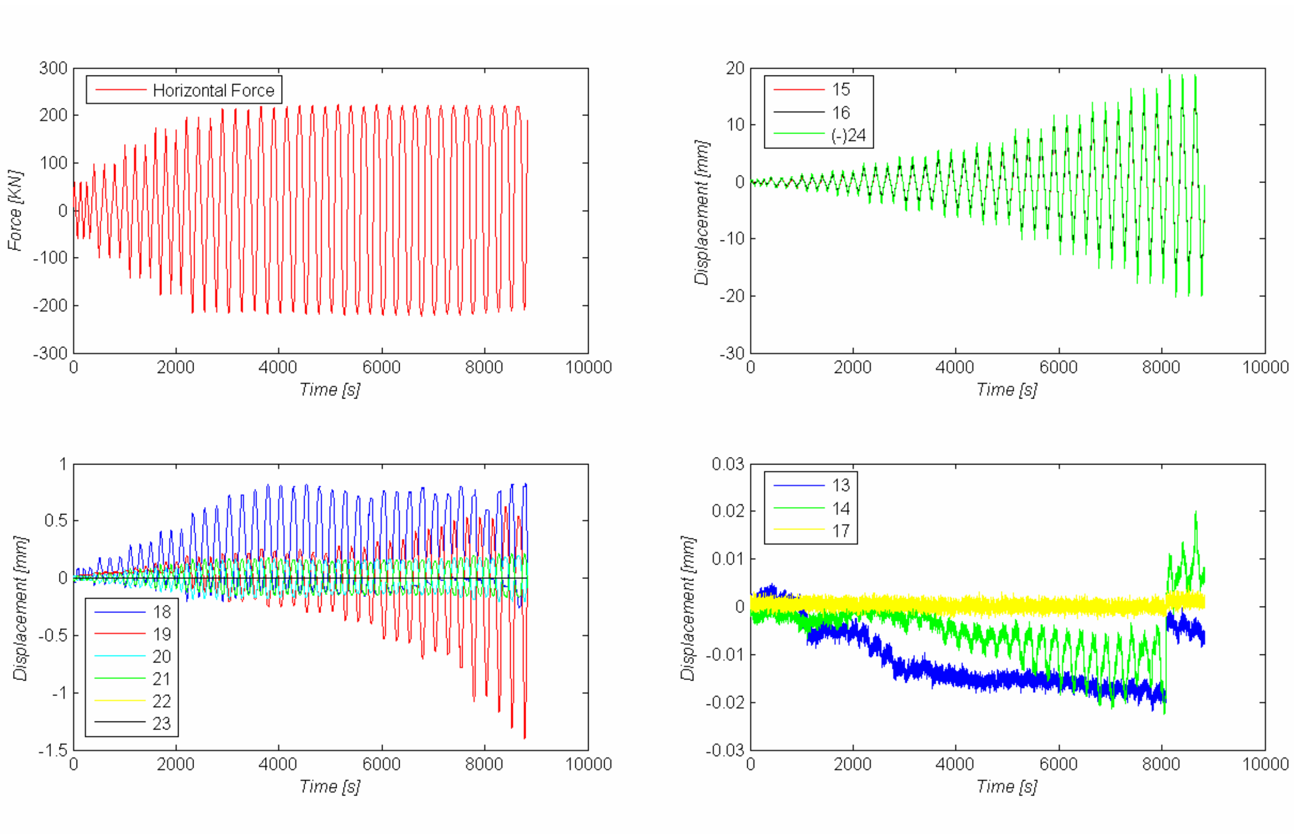
Horizontal Force
Force [KN]
Time [s]
15
16
(-)24
Displacement [mm]
Time [s]
18
19
20
21
22
23
Displacement [mm]
Time [s]
13
14
17
Displacement [mm]
Time [s]

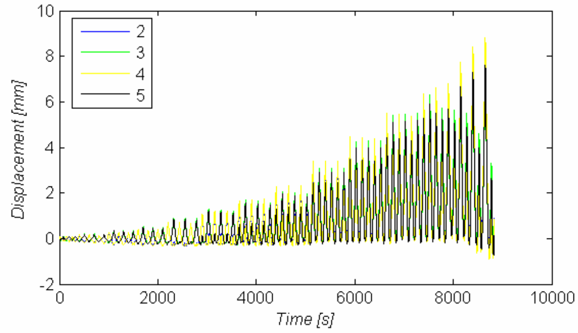
2
3
4
5
Displacement [mm]
Time [s]

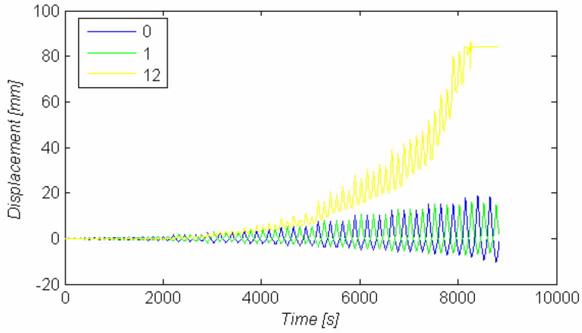
0
1
12
Displacement [mm]
Time [s]

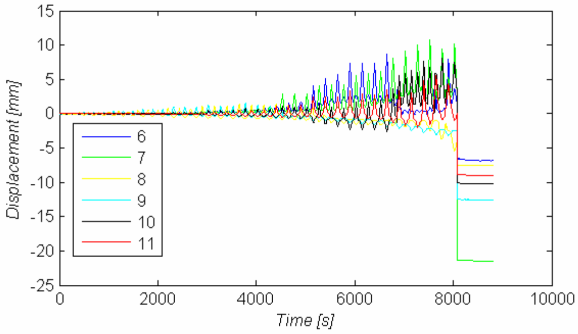
6
7
8
9
10
11
Displacement [mm]
Time [s]